THE MECHANICS OF LOCAL NICHES IN THE PRIMARY TUMOR REGULATE BREAST CANCER BRAIN METASTASIS

TANG KAI

PhD

The Hong Kong Polytechnic University

2023

The Hong Kong Polytechnic University

Department of Biomedical Engineering

The mechanics of local niches in the primary tumor regulate breast cancer brain metastasis

TANG Kai

A thesis submitted in partial fulfilment of the requirements for the degree of Doctor of Philosophy

Aug 2022

CERTIFICATE OF ORIGINALITY

I hereby declare that this thesis is my own work and that, to the best of my knowledge and belief, it reproduces no material previously published or written, nor material that has been accepted for the award of any other degree or diploma, except where due acknowledgement has been made in the text.

_____ (Signed)

TANG Kai (Name of student)

Abstract

Breast cancer cells disseminate to and colonize other organs not randomly, but rather have the preferred metastatic sites, including bone, liver, lung, and brain, which is defined as “organotropism”. Brain metastasis considerably deteriorates patient survival compared to the metastasis in other organs and thus requires urgent attention. Previous studies have indicated that tumor cells with the ability to metastasize to specific organs may pre-exist in the primary tumor, suggesting the significance of the primary tumor microenvironment and/or specific sub-clones with unique mutations. Accumulating evidence has demonstrated the importance of mechanical cues in tumor metastasis. However, it remains poorly understood whether and how local niche mechanics in the primary tumor influence breast cancer brain metastasis.

In this project, our study explored the effect of soft local niches in the primary tumor on breast cancer brain metastasis. We found that 1-month culture on soft matrices (soft niches-primed cells) remarkably increased the expressions of the genes related to brain but not bone metastasis, which was independent of ligand type and cell type. RNA-seq analysis showed that softness-primed cells exhibited molecular features of neuron, implying the promotive effect on brain metastasis. Soft niches-primed cells had enhanced the survival in circulation, cerebral endothelium adhesion and blood-brain barrier (BBB) transmigration *in vitro*. Further, these cells exhibited the mechanoadaptation to the soft matrix mimicking brain tissue and a high secretion level of Serpin B2 which might confer defense evasion ability to tumor cells to circumvent metastasis-suppressive effects in the brain. Moreover, soft niches-primed cells displayed unique biophysical properties and mechanical memory. *In vivo* animal experiments showed that the priming on soft matrices enhanced BBB transmigration and colonization ability of breast cancer cells in the brain. Importantly, soft niches-

primed breast cancer cells exhibited the ability to preferentially metastasize to the brain *in vivo*.

Mechanistically, the priming of single cell-derived progenies with low brain metastasis ability on soft matrices increased the expressions of brain metastasis-related genes expression, proliferation rate on brain-mimicking matrices, and BBB transmigration ability. Further, histone deacetylase (HDAC)-mediated chromatin condensation and remodeling were required in the softness-induced changes in brain metastasis gene expression. Among these HDACs, HDAC3 activity was highly upregulated in soft niches-primed cells, and necessary but not sufficient for the gain of brain metastatic phenotype. Brain metastasis formation was effectively antagonized *in vivo* by inhibiting HDAC3. Further, extended disruption of actin cytoskeleton increased HDAC3 activity and induced the acquisition of brain metastasis ability. In contrast, the increase of actin polymerization or contractility on soft matrices inhibited HDAC3 activity and prevented the up-regulation of brain metastasis ability.

Taken together, these findings demonstrate that soft niches in the primary tumor promote breast cancer brain metastasis, which depends on mechanotransduction-mediated HDAC3 activity, highlighting the significance of local microenvironmental mechanics in organotropism. This study unveils the regulatory role of local niche mechanics of the primary tumor in brain metastasis and provides new evidence to illustrate the importance of mechanics in tumor metastasis.

List of Publications

Journal articles

Chen, X., **Tang, K**., Li, X., Zhang, C., Xin, Y., Li, K., & Tan, Y. (2022). Biomechanics of cancer stem cells. Essays in Biochemistry.

Xu, Z., Li, K., Xin, Y., **Tang, K**., Yang, M., Wang, G., & Tan, Y. (2022). Fluid shear stress regulates the survival of circulating tumor cells via nuclear expansion. Journal of Cell Science, 135(10), jcs259586.

Chen, X., Fan, Y., Sun, J., Zhang, Z., Xin, Y., Li, K., **Tang, K**., ... & Tan, Y. (2021). Nanoparticle-mediated specific elimination of soft cancer stem cells by targeting low cell stiffness. Acta Biomaterialia, 135, 493-505.

Tang, K., Xin, Y., Li, K., Chen, X., & Tan, Y. (2021). Cell cytoskeleton and stiffness are mechanical indicators of organotropism in breast cancer. Biology, 10(4), 259.

Tang, K., Li, S., Li, P., Xia, Q., Yang, R., Li, T., ... Tan, Y. & Liu, Y. (2020). Shear stress stimulates integrin β1 trafficking and increases directional migration of cancer cells via promoting deacetylation of microtubules. Biochimica et Biophysica Acta (BBA)-Molecular Cell Research, 1867(5), 118676.

Jin, J., **Tang, K**., Xin, Y., Zhang, T., & Tan, Y. (2018). Hemodynamic shear flow regulates biophysical characteristics and functions of circulating breast tumor cells reminiscent of brain metastasis. Soft Matter, 14(47), 9528-9533.

Academic Award

2nd-Runner up of Hong Kong Medical and Healthcare Device Industries Association Student Research Award 2019

Acknowledgements

I am fortunate to have a good supervisor, friends and family to accompany me along the way and give me support and assistance. Drinking water and thinking of the source, I would like to express my sincere gratitude to them.

First of all, my chief supervisor, Dr. Youhua Tan, is my guide on the road of scientific research for the past three years. Dr. Tan gives me sufficient guidance, cultivates my critical thinking, and teaches me how to use scientific methods to solve problems encountered in the study. In the selection of research topics, the design and progression of studies, Dr. Tan has strict requirements, careful guidance, and the greatest support. Thus, I would like to express my heartfelt thanks and respect to my supervisor. At the same time, I would like to thank my co-supervisor, Professor Mo Yang, for his valuable support and help in this research.

Then, I would like to thank Professor. Lei Sun and his student Miss. Ting Zhu for their guidance and help in establishing intracranial injection models in mice. Professor. Sun generously provided the equipment and instruments required for the experiment. Miss. Zhu gave me a lot of support in this work and completed this part of the experiment with me. And I would like to express my thanks to Dr. Dexter Wong for his guidance and support in the preparation of hyaluronic acid hydrogel.

I sincerely thank lab members Ying Xin, Keming Li, Xi Chen, Pengyu Du, Cunyu Zhang, Bing Hu, Guanshuo Hu and Yufan Zheng for their assistance in work. I am also grateful to the staff from the University Research Facilities in Life Science, Centralised Animal Facilities and The University Research Facility in Behavioral and Systems Neuroscience of the Hong Kong Polytechnic University for their training and support in my study.

Last but not least, it is with great gratitude that I thank my parents, whose understanding and encouragement gave me the courage to move forward. My wife Shuting Huang deserves my sincere gratitude for our three years of mutual encouragement and support.

Table of Contents

List of Figures

List of abbreviations

AFM	atomic force microscope
BBB	blood-brain barrier
BLI	bioluminescence
BM	basement membrane
CAFs	cancer-associated fibroblast
CCP	chromatin condensation parameter
CK5/6	cytokeratin 5/6
CNS	central nervous system
Col-I	collagen I
COX2	cyclooxygenase 2
CSF	cerebrospinal fluid
CTCs	circulating tumor cells
CXCR4	C-X-C motif chemokine receptor 4
DEGs	differentially expressed genes
ECM	extracellular matrix
EGFR	epidermal growth factor receptor
ERs	estrogen receptors
EVs	extracellular vesicles
FN	fibronectin
GABA	γ-aminobutyric acid
GEO	Gene Expression Omnibus
GO	gene ontology
GRN	genetic regulatory network
GSEA	gene set enrichment analysis
HA	hyaluronic acid
HAT	histone acetyltransferase

HDAC	histone deacetylase
HER2	human epidermal growth factor receptor 2
HRs	hormone receptors
INM	inner nuclear membranes
LINC	the linker of the nucleoskeleton and cytoskeleton
LOX	lysyl oxidase
NE	nuclear envelope
NES	normalized enrichment score
NPCs	nuclear pore complexes
ONM	outer nuclear membranes
ORA	over-representation analysis
PA	polyacrylamide
PGE2	prostaglandin E2
pMLC	phosphorylation of myosin light chains
PMNs	pre-metastatic niches
PPIs	protein-protein interactions
PRs	progesterone receptors
RNA-seq	RNA-sequencing
SCPs	single cell-derived progenies
siRNA	small-interfering RNA
TCP	tissue culture plastic
TFs	transcription factors

Chapter 1: Introduction

Cancer patients die primarily from distant metastases which is a complex process involving many steps. Therefore, this makes treating metastatic tumors far more urgent and difficult than treating primary tumors. It is striking that the distribution of distant metastasis among organs is not random but has organ preference, which is termed metastatic organotropism [1]. Although the pattern of affected organs is remarkably variable depending on the cancer type, intrinsic properties of tumor cells and external cues from the microenvironment have been reported as vital regulators in organ-specific metastasis [2]. The "seed and soil" theory proposed by Steven Paget is commonly adopted to explain the mechanisms of organotropism [3]. "Seeds" are tumor cells that have the capacity to disseminate, whereas "soil" is any organ with a defined microenvironment. The match between tumor cells and the microenvironment of the distant organs is necessary for the survival or thriving of tumor cells. It is well-known that "secondary soil" features referring to the microenvironment of target organs, have a significant impact on the colonization and metastatic outgrowth of tumor cells in the progress of metastasis. Of note, a previous study shows that the biochemical microenvironment of the local niche preselects tumor cells with bone metastatic tropism, which highlights the crucial role of the local microenvironment in metastatic organotropism [4].

Metastatic brain lesions account for 90% of all primary tumors in central nervous system (CNS) [5]. Brain metastases from breast cancer have a dismal prognosis and are often accompanied by neurological dysfunction [6]. There is, however, a lack of understanding of the mechanisms behind brain metastasis derived from breast carcinoma. A better understanding of the underlying critical factors for brain metastasis is therefore essential for the development of new therapeutic strategies. Recently, most studies focus on investigating the role of the special biochemical microenvironment in the brain and the intrinsic genetic signature of cancer cells on brain metastasis. Besides the biochemical mechanisms underlying cancer metastasis, the mechanical microenvironment regulates many cellular functions and plays important roles in the orchestration of tumorigenesis and metastasis [7]. Mechanical stimulations affect

epigenetic modifications and induce chromatin remodeling, thereby changing gene expression patterns and cellular functions [8, 9]. Epigenetic modifications not only respond to mechanical signals but also promote cells to adapt to different mechanical microenvironments, including matrix stiffness [10]. Studies show matrix stiffness can affect HDAC activity and chromatin remodeling via mechanotransduction of cytoskeleton and nuclear mechanosensing, further regulating cell differentiation and fibroblast activation [10, 11]. Matrix stiffness as one of the important physical factors in the microenvironment has been proven to regulate a series of malignant behaviors of tumor cells, such as transformation, migration, invasion and proliferation [12, 13, 14]. It is a pity that few studies investigate the role of matrix stiffness on brain metastasis.

It is generally recognized that characteristics of cell mechanics, which are significant inherent features, are substantially connected with the malignancy of tumor cells. A unique alteration in cellular mechanical characteristics is associated with malignant transformation brought on by genetic alterations. Numerous earlier investigations demonstrate that tumor cells are less stiff than their matching normal cells [15, 16]. For instance, following transformation, normal breast epithelial cells soften considerably [17, 18]. Highly diverse tumor cell mechanical stiffness is substantially linked with malignant potential [19]. Low cell stiffness is a distinctive mechanical characteristic of tumor cells with high tumorigenesis and metastasis potential [20]. The softness of cancer cells can facilitate BBB transmigration in the metastatic steps [21]. The ability of tumor cells to self-renew can be increased by reducing the stiffness of tumor cells [22, 23]. There is still much to be explored about how cell stiffness influences biological processes, especially in malignant behaviors of tumor cells.

Knowledge gap and scientific questions

Recently, many studies have investigated the importance of intrinsic genetic features of tumor cells and the interactions between tumor cells and the biochemical

microenvironments of host organs in brain metastasis. One missing clue is the role of biomechanics, especially local niche stiffness and cell mechanics, in regulating brain metastasis of tumor cells.

Tumor cells experience highly heterogeneous stiffness of local niches within primary tumors and metastasized to different organs. Stiff matrix has been shown to promote osteolytic bone metastasis in breast carcinoma. Although the role of matrix stiffness in the malignant behaviors of tumor cells has been well identified, it is still unknown about the relationship between the local niche stiffness and breast cancer brain metastasis. In particular, whether matrix softness regulates the ability of breast cancer cells to preferentially colonize brain tissue is unknown. If matrix softness of local niches is involved in promoting brain metastasis, the molecular mechanisms, including epigenetic modifications, should be further investigated. The therapeutic role of the regulatory mechanism in targeting brain metastases and their clinical significance also needs to be further determined. In addition, in spite of the correlation between cell stiffness and tumor cell malignancy, the connection between cell mechanics and metastatic organotropism remains ambiguous. In this research, those unsolved questions will be explored.

Objectives and scopes

This project explores the metastatic organotropism of breast cancer cells from the perspective of biomechanics, investigates the role of the softness of primary niches in brain metastasis, explores the epigenetic mechanisms of microenvironmental softness inducing brain metastatic phenotype, and elucidates the role of cell mechanics in organotropism. The specific research contents are as follows:

(1) Reveal the effect of matrix softness on the ability of tumor cells to metastasize to the brain.

(2) Elucidate the role of HDAC-mediated chromatin condensation in matrix softness-

induced breast cancer brain metastasis.

(3) Investigate the mechanisms regulating HDAC3 activity in response to matrix softness and the therapeutic role of HDAC3 activity in breast cancer brain metastasis.

(4) Reveal the role of cell stiffness in organotropism and clarify the potential functions of cell stiffness acting as the indicator to reflect preferring metastatic site of tumor cells.

Scientific significance and values

A lot of intrinsic factors of tumor cells and microenvironmental factors of host organs have been proven to be involved in early metastatic seeding and outgrowth in the target organ. A more comprehensive evaluation of the interactions between the characteristics of the cancer cells and the microenvironment of local niches is needed to understand the organ-specific metastasis process. It remains to be identified whether biophysics factors in primary tumor play a key role in metastatic organotropism. Our research unveils the critical role of matrix softness and cell mechanics in specific-organic metastasis and facilitates the development of novel therapeutic strategies against brain metastasis. Moreover, research so far could not show whether the brain-targeted traits or brain metastasis-related gene signatures are pre-existing in the primary tumor or are the outcome of the effect of the brain microenvironment. We investigate whether the increased ability for brain metastasis is due to the survival advantage of some cells with special intrinsic properties or to the regulatory effects of the ECM stiffness. This study may provide insight into why tumor cells prefer to metastasize to the brain and the factors that enable tumor to thrive in the brain. In addition, our research unveils the mechanotransduction mechanism of breast cancer cells in response to tissue softness for the acquisition of brain metastatic phenotype, which underpins the preferential metastasis of breast cancer cells into soft brain tissue. Targeting this mechanism has highly prospective therapeutic significance in suppressing the brain metastasis of breast carcinoma. In addition, we explore the intrinsic cellular mechanical properties of cancer cells with different tropisms and investigate the role of mechanical properties of cancer

cells in organotropism, which may provide a powerful label-free marker for separating cancer cells with different tropisms for clinical diagnosis and an effective therapeutic target to prevent or cure organic metastasis. Overall, this project highlights the significance of tissue softness in metastatic tropism to the brain and may result in a paradigm shift in cancer therapy by targeting brain metastases based on mechanotransduction, which could be beneficial for cancer patients. As a result, it may be demonstrated that, despite biochemical factors, matrix softness also has a significant impact on brain metastasis. This project may help drive improvements in prevention, clinical diagnosis and treatment in patients who may suffer from brain metastasis.

Chapter 2: Literature Review

2.1 Breast cancer and metastasis

2.1.1 The overview of breast cancer

Human life expectancy has been seriously affected by cancer, the leading cause of death worldwide. According to the International Agency for Research on Cancer statistics, there were an estimated 19.3 million new cancer cases and 10.0 million people died of cancer in 2020 [24]. Breast cancer is a disease of breast dysplasia, which is characterized by heterogeneity and diverse inducing factors. Breast carcinoma has exceeded lung carcinoma as the most frequently diagnosed cancer, with around 2.3 million newly diagnosed cases (11.7%). It has been shown that breast cancer incidence rates in women are far higher than those of other cancers in not only transitioned (55.9 /100,000) but also transitioning countries (29.7 /100,000) [24]. There is one in six female patients died because of breast cancer. Chinese cancer statistics in 2015 show that breast cancer was the most common type of cancer and the fifth-ranking cause of cancer-related deaths among Chinese women [25].

Breast cancer is a very heterogeneous illness, with tumor cells that exhibit a variety of morphological characteristics, varying clinical outcomes, and responses to various treatment approaches. Therefore, in light of the fact that there are several ways to classify breast cancer, it is crucial to develop a classification system that is clinically relevant. For reflecting prognosis and dictating treatment, molecular classification based on immunohistochemistry and gene expression comes into greater use. Hormone receptors (HRs), estrogen receptors (ERs) and progesterone receptors (PRs), human epidermal growth factor receptor 2 (HER2), Ki67, cytokeratin 5/6 (CK5/6), and epidermal growth factor receptor (EGFR), in breast cancer cells are commonly used as markers to classify the subtypes of breast cancer. According to the expression levels of these HRs, breast cancer can be divided into various molecular subtypes including

luminal A (ER+ and/or PR+, HER2- and Ki67 low), luminal B (ER+ and/ or PR+, HER2- and Ki67 high), luminal-HER2 (ER+ and/or PR+ and HER2+), HER2-enriched (ER-, PR-, HER2+), basal-like (ER-, PR-, HER2-, and EFGR+ or CK5/6+), and triple-negative phenotype (TN) (ER-, PR-, HER2-) [26, 27, 28]. Additionally, based on the progression of cancer, clinical staging is a valuable standardized method to classify breast cancer. As soon as breast cancer is diagnosed, clinical staging is identified, which further determines how the patient will be treated. Breast cancer clinical staging is uniform across breast cancer subtypes based on the tumor, node, and metastatic (TNM) breast cancer staging system adopted by the American Joint Committee on Cancer (AJCC) and the International Union for Cancer Control (UICC): Stage 0, Stage I, Stage II, Stage III and Stage IV [29]. In Stage 0, abnormal cells exist but have not yet invaded the neighboring tissue. Ductal Carcinoma In Situ refers to the abnormal cells that are present at this stage inside breast ducts in the breast (DCIS). Breast cancer is apparent and becomes more prevalent in Stages I through III. The larger the cancer tumor is and the more it has spread to adjacent tissues, including lymph nodes, the higher the number of the stage level is defined. Stage IV denotes the spread of breast cancer to distant sites in the body. Clusters of tumor cells called micrometastases may still present in the body even after the original tumor has been removed, allowing the disease to recur.

2.1.2 The overview of metastasis

With 685,000 fatalities annually, cancer is the sixth most common mortality cause in the world [24]. Approximately 90% of cancer patients die from distant organic metastases, while between 20% and 30% of those with early breast cancer are diagnosed with distant metastases [24, 30]. Regardless of the subtype, currently, patients with metastatic breast cancer do not have viable treatment methods, and overall survival is typically 1 to 5 years [31]. To develop innovative therapeutics that target metastatic illness precisely, understanding the cellular and molecular pathways that allow cancer cells to escape the original tumor and expand and maintain at secondary sites is important [32].

2.1.3 The steps of metastasis

It is believed that the formation of metastases by carcinomas takes place after an intricate sequence of cellular and biological events, collectively referred to as the invasion-metastasis cascade (Fig. 2.1): (1) generate a local invasion by penetrating adjacent extracellular matrix (ECM) and stromal tissue. (2) intravasate into blood vessel lumens. (3) endure unfavored factors and survival in the transportation through the vascular system. (4) pass through the blood vessel after active arrest or passive trap and penetrate the tissue of distant organs. (5) successful survival in the hostile microenvironment of distant organs, escape from the dormancy and restart the progress of proliferation to form the secondary tumor (this progress is often termed as colonization) [33].

Local invasion refers to the penetration of cancer cells from a confined primary site through the stroma nearby, then getting into the parenchyma of the nearby healthy tissue. The basement membrane (BM), a specialized ECM, that is crucial in structuring epithelial tissues, including dividing epithelial and stromal into different compartments. The BM is a protective barrier, which must be breached before the invasion of cancer cells. In addition to its structural functions, the BM is also essential for biophysical signal transduction processes occurring inside of tumor via focal adhesion-mediated mechanosignaling, which regulates the invasive behavior and metastasis formation of tumor cells [34, 35].

Intravasation is known as locally invading tumor cells penetrating the lumina of lymph system or circulatory systems. The hematogenous distribution appears to be the primary route through which metastatic tumor cells spread, despite lymphatic dissemination of tumor cells being often seen in cancer patients and serving as a significant predictive sign for the progression of cancer [32]. Many biochemical factors secreted by tumor cells or stroma cells have been proven to enhance the capacity of tumor cells to transmigrate the endothelial cell barriers of blood vessels. Transforming growth factor-β (TGF-β), a

crucial cytokine for metastatic progression of cancer cells, promotes invasion by increasing transmigration through micro-blood vessels [36]. In addition, carcinoma cells can produce the vascular endothelial growth factors (VEGFs) to promote the generation of new microvessels which are prone to leakiness in contrast to the normal blood vessels, and then enter circulatory systems through those leaky neovessels [37].

As soon as carcinoma cells successfully penetrate into the blood vessel lumina, they can travel widely through the blood circulation and are called circulating tumor cells (CTCs). To arrive at distant organs, CTCs in the blood circulation must endure a range of stressors. They obviously lack, for instance, the integrin-mediated adhesion to the substrate that is typically necessary for cell survival. Anoikis, a kind of apoptosis driven by the absence of substrate anchorage, will happen when epithelial cells are in suspension [38]. In addition to anoikis, circulating tumor cells must tolerate shear forces caused by blood flow as well as immune surveillance by innate immune cells, notably natural killer cells, to survive [39].

A crucial stage in metastatic spreading is CTC arrest in distant organ sites. The issue of whether the process of CTCs arrest is an active seeking process through particular ligand-receptor interaction between CTCs and endothelium or just mechanical passive trapping by blood capillaries due to restricted blood vessel sizes is still up for debate [37, 40]. Extravasation is the process by which cancer cells, after arresting in the microvessels of distant organ sites, transmigrate vessel lumina and penetrate into the organ tissue by breaking through the barriers of endothelial cells and/or other cells [30].

If disseminated tumor cells survive in the early encounter with the microenvironment of the distant organs, this still cannot guarantee that tumor cells complete the process of metastatic colonization to finally develop large macroscopic metastatic lesions. In contrast, it appears that the vast majority of disseminated tumor cells either slowly disappear over weeks and months, or persist as micrometastasis in a markedly long-

term dormant state, remaining with relatively stable cells number [41]. Most disseminated tumor cells are dominantly dormant due to their poor compatibility with the surrounding microenvironment, resulting in their greatly weakened proliferation at distant organs [41, 42]. Furthermore, the capability of disseminated tumor cells to reinitiate proliferation in distant sites may depend on cell-nonautonomous mechanisms required to convert an unfavored microenvironment into a more hospitable niche [43, 44]. It can be deduced from the above information that the process of the metastatic cascade of tumor cells is extremely low efficient. For example, a high number of CTCs are present in the bloodstream of the vast majority of cancer patients, even those with unnoticed metastases [45]. However, approximately 0.01% of tumor cells that enter the blood circulation finally establish macrometastases, but this may be an overestimate [41]. In the complex progress of the invasion-metastatic cascade, colonization in the host organ typically stands for the utmost rate-limiting step [30, 46].

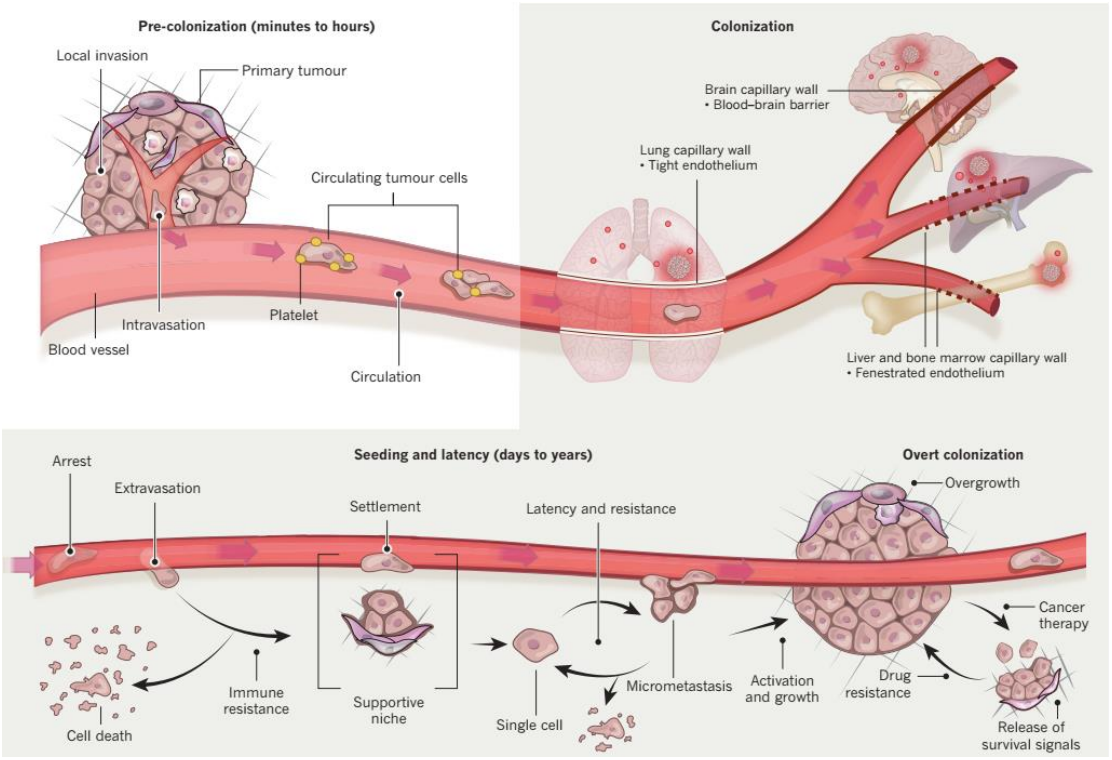

Figure 2.1 The Invasion-metastasis cascade [47]

2.2 Organotropism

2.2.1 The overview of organotropism

Metastatic organotropism refers to the non-random dissemination and metastases formation of metastatic cancer cells in different organs. Based on the specific types of cancer, the pattern of the targeted organs varies considerably. Metastatic organotropism refers to the non-random dissemination and metastases formation of metastatic cancer cells in different organs. Based on the specific types of cancer, the pattern of the targeted organs varies considerably. There are some cancer types that metastasize predominantly to one particular organ. For example, most prostate cancer primarily metastasizes to the bone, while pancreatic cancer and uveal melanoma choose the liver as their destination [48, 49]. Sequential metastasis from one metastatic site to other organ sites is observed in some cancer types. For example, colorectal cancer cells usually tend to form metastases in the liver and then metastasize to the lung [50]. Cancer cells, such as those from breast cancer and melanoma, can form metastatic sites in various organs sequentially or simultaneously [51]. There are many different kinds of cancer that often disseminate to the liver, lungs, bones, and brain as well as the lymph nodes.

The bone is the most frequent distant site with the second tumor in patients with breast carcinoma, occurring in 70% of those patients. The liver is the second most typical site for metastases, with a percentage of around 30, and the brain is the next typical site with a percentage of between 10 to 30 [52]. Diverse breast cancer subtypes have remarkably different overall survival rates and exhibit different preferences to disseminate to certain organs. Even while all subtypes of breast cancer tend to form bone metastasis, luminal subtype cancers show significantly higher incidence (~81%) for bone metastasis than that of basal-like (~42%) and HER2-like tumors (~55%) [53]. The luminal B subtype is linked to liver recurrence [54]. Breast tumors that are HER2-enriched, luminal-HER2, basal-like, and TN are more likely to form brain metastatic

tumors [55]. Numerous findings indicate that a number of factors, including circulatory patterns, intrinsic properties of tumor cells and the microenvironment of host organs, affect the organ-specific metastasis of cancer cells. Developing novel and effective clinical strategies and improving the prognosis of patients would be possible if we understood the mechanisms that underlie metastatic tropism.

2.2.2 “Seed and soil” theory

It has long been known that cancer cells have preferred organs to metastasize to and organic metastases are not incident. The hypothesis of “seed and soil” was suggested by Steven Paget in 1889. It was based on a review of 735 patients who died of breast cancer, each having an autopsy, as well as several additional cancer cases from other research [3]. The term "seed" refers to specific tumor cells with the ability to metastasize. The term "soil" refers to the distant organ or tissue that offers a milieu for the outgrowth of the seeds. The theory proposes that metastatic cells spread organ-specifically, rather than merely anatomically, and interact with the hosts. Only when the seed and soil were matched well, did metastases form.

This concept opposed Rudolf Virchow's prevalent mechanistic theory of metastasis, which considered metastasis is the result of tumor cells passively arrested in the arterial system [56]. The "seed and soil" theory of Paget was challenged by James Ewing in 1928, who hypothesized that metastatic dissemination occurs as a result of being mechanically trapped in the vascular system [57]. The idea of "seed and soil" faded into obscurity over the following many decades as a result of that viewpoint being the majority one. Although the structure of the vasculature and the specific circulation pattern of each organ undoubtedly have an impact on metastasis, this does not entirely account for the organ-specific metastasis clinically observed in the majority of cases. For instance, the brain, liver, and kidneys all get around 10% to 20% of the blood volume, yet each exhibits a totally distinct metastasis outcome [58]. Organs that get a

significant amount of blood, such as the heart, muscle, skin, kidney, and spleen, however, seldom suffer metastasis [59]. According to Sugarbaker in 1979, while regional metastases may be caused by anatomical or mechanical factors, such as lymphatic drainage, metastases in distant organ sites require a totally distinct mechanism [59]. Hart and Fidler's groundbreaking research from the 1980s validated Paget's "seed and soil" idea by demonstrating the preferred homing of B16 melanoma tumor cells in particular distant tissues. In spite of the fact that vasculatures in all organs contained metastatic tumor cells, their research definitely proved that metastases only formed in limited certain organs [60]. Despite the fact that CTCs are mechanically trapped at first in some organs, it is generally accepted that the compatibility and interactions between tumor cells and the microenvironment of the target organ determine the results of colonization.

2.2.3 Mechanisms involved in the organotropism

Our knowledge of the molecular and cellular mechanisms behind "seeds and soil" has significantly advanced over the past few decades as a result of related studies (Fig. 2.2). The process of metastasis is governed cooperatively by carcinoma cells and the microenvironment, in other words, both soil and seed cues are critical in promoting organic metastasis. Metastatic tropism is based on certain universal rules, despite the fact that each metastatic organ is distinctive.

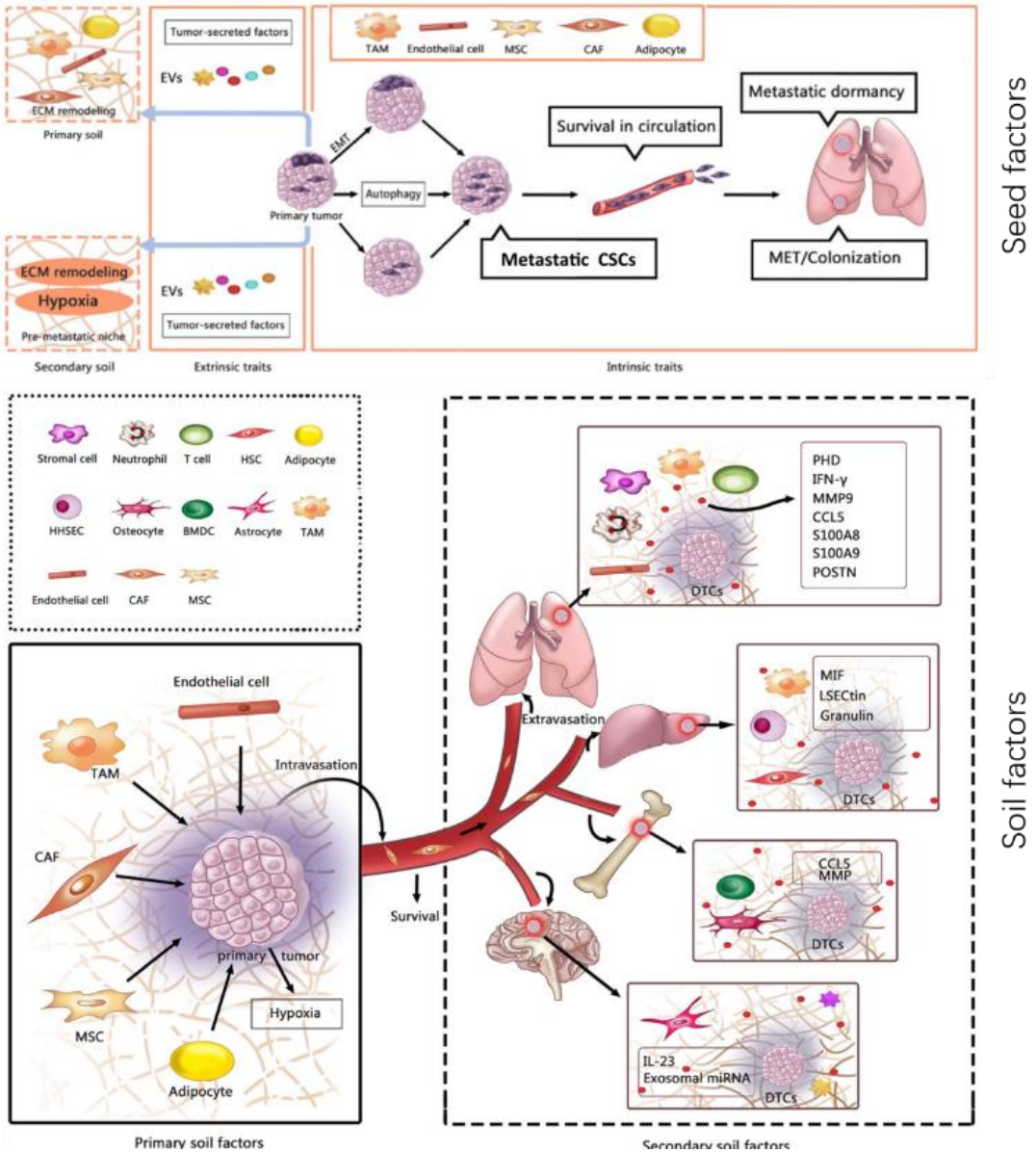

Figure 2.2 Seed and soil factors in organotropism [2]

Seed: tumor-intrinsic properties

The location preference and organotropism of metastatic tumor cells have been explained in a number of possible ways, including tumor cell surface properties, binding between tumor cells and the target tissue, and responsiveness to particular growth factors and specific chemokines from host organs. The interplay between tumor cells and the organ milieu, presumably in the form of unique adhesion to

endothelium, may explain the varied locations of metastasis development. Diverse surface receptors and secreted factors are generated by endothelial cells in various organs, which affects the generation of metastases. C-X-C motif chemokine receptor 4 (CXCR4) expression in the metastasis of breast carcinoma is the best-known example. CXCR4-expressing tumors tend to infiltrate organs with high levels of its ligand, CXCL12, particularly bone [61]. Similar to this, the CCL27/CCR10 chemokine receptor interaction is thought to attract melanoma cells to specific organs [62]. The permeability of lung blood microvessels was raised and tumor cell transendothelial migration was made easier by several of these intrinsic tumor factors that disrupt endothelial-endothelial connections. For instance, increased permeability and vascular penetration caused by melanoma-derived SPARC increased lung metastases in a way [63]. BBB separates the brain from external tissues and provides it with protection. The basement membrane, astrocytes, and pericytes maintain the BBB, which is a continuous, non-fenestrated endothelium held together by tight junctions [64]. The capacity of tumor cells to adhere to the endothelium and cross the BBB are both improved when the 2,6-sialyltransferase ST6GALNAC5 is expressed at high levels [65].

Tumor cells are prone to become imprisoned in a range of organs in equal measure, despite the fact that it has been confirmed that many of the characterizations they exhibit contribute to the selection of certain organs [66]. Therefore, the presence of cancer cells in a tissue alone cannot guarantee the development of a metastasis; rather, the development of new foci depends on the ability of metastatic tumor cells to survive and grow in the distant organ, which requires specific molecular traits to adapt to the microenvironment of the recipient organ. Specifically, CCL20 increases matrix metalloproteinase (MMP)-2/9 and RANKL/osteoprotegerin in breast cancer, which are key to the “vicious cycle” in bone metastasis [67]. It is noteworthy to note that the gene fusion of TMPRSS2-ERG has been correlated to specific bone metastasis of prostate cancer, which suggests that certain gene mutations are responsible for organic metastasis [68]. On one hand, DKK1 secreted by tumor cells inhibits lung metastasis; on

the other hand, it promotes bone metastasis, which plays distinct role in metastasis to different organs [69]. Gene profiling of metastatic cells has been used in studies to identify intrinsic drivers in tumor cells that facilitate specific metastasis to the target organs, including bone, lung, brain, and liver [54, 65, 70, 71]. Particularly, several single cell-derived subpopulations isolated from cell lines with heterogeneous genetical backgrounds exhibit various metastatic patterns, highlighting the function of inherent molecular characteristics of tumor cells in metastatic organotropism [72]. The ability of CTC lines generated from breast cancer patients to develop metastases in mice with a pattern that replicates the majority of metastatic sites in corresponding individuals further suggests that organotropic tumor cells may already be present in the primary tumor [73].

Soil: unique microenvironment of organs

The "seed and soil" hypothesis states that while particular genetic and phenotypic features of tumor cells unquestionably play a key role in successful formation of metastasis, microenvironmental conditions are also crucial in allowing malignant cells to survive and outgrowth after reaching their target organs. The specific habitats in the primary sites and metastatic sites, which are composed of certain resident cell types, ECM, soluble factors, and metabolic products, greatly influence the metastatic process to certain organs. Once tumor cells have entered the host organ, they must adapt to and survive in the diverse and unfavorable milieu that is produced by the distant organs in order to maintain growth. The perivascular microenvironment in the lung contains thrombospondin-1 (TSP-1) which can maintain the quiescence of breast carcinoma cells [74]. Plasmin derived from the stroma cells of the brain inhibits the cooption between tumor cells and blood vessels and also drives FasL-dependent death of tumor cells, which inhibits the formation of brain metastases [75]. It is worth noticing that, when it comes to the availability of energy, nutrients, and oxygen, different organs often exhibit diverse metabolic microenvironments. Bone resorption, which often happens in

osteolytic bone metastasis of breast cancer cells, produces numerous nutrients, such as glucose, glycerol, glycine and serine [76]. In contrast, the brain exhibits the greatest consumption of energy compared to other organs. Even though glucose is the predominant fuel source for tumor cells, when glucose is scarce, tumor cells in brain metastases can also utilize alternative forms of nutrients [77]. The lungs are respiratory organs, which means that the tissue in the lungs tends to receive oxidative stress. There may be a discrepancy between the oxygen-rich lung microenvironment and the oxygen-poor bone microenvironment [78].

Tumor cells shape the microenvironment

It is generally known that active reconstruction for niches is a common way for tumor cells to fit distant sites even before they reach, in addition to passive adaptation to the milieu. It is well known that tumor cells do not only passively adapt to the microenvironment, but can actively reconstruct the niches at the distant organ even before arrival. Pre-metastatic niches (PMNs), a favorable microenvironment, can be generated in distant sites by tumor cells even when these cells are in primary sites. Extracellular vesicles (EVs) released by the tumor and tumor-derived chemical factors work together to form PMNs, which shape the "soil" at distant locations to support the survival and proliferation of arriving tumor cells [79].

Lysyl oxidase (LOX) secreted by tumor cells in the primary site can promote osteoclastogenesis to form PMN and subsequently induce bone colonization of metastatic tumor cells [80]. Target cells that accept tumor-derived EVs are transformed or educated forward into a state with pro-metastatic and pro-inflammatory phenotypes by miRNA and proteins in EVs, resulting in the formation of PMN [81, 82]. Different compositions of surface proteins of tumor-derived EVs lead to the establishment of PMNs in distinct organs. In tumor-derived EVs, a high expression level of integrin α6β4 on the surface assists the targeting of the lung, while integrin

α6β4 directs EVs to localize in the liver. And then EVs-containing S100 family proteins increase inflammatory levels in the target organs to generate supportive niches for metastatic tumor cells [83].

Tumor cells continue to actively remodel the microenvironment once they have reached the target organs. One of the best-known cases is the interaction between osteolysis and metastatic tumor in the bone, which is termed the "vicious cycle". Tumor cells homing to the bone can induce the differentiation of osteoclasts and thus enhance osteolysis, which depends on tumor-secreted various kinds of factors, such as OPN, PTHrP and IL-1. [84, 85]. As the result of osteolysis, a series of growth factors are released from bone matrix to promote the growth of bone-metastatic tumor cells [86]. Not only does bone resorption increase, but also tumor outgrowth is fertilized by this vicious cycle.

Microenvironment selects and/or converts resident tumor cells

On one hand, increasing evidence points to organic metastasis as a Darwinian selection process where tumor cells with inherent features that allow them to pass through bottlenecks in the metastatic process are selected from a tumor cell population with diverse genetic and epigenetic backgrounds [87, 88]. On the other hand, under the pressure of unique microenvironments in certain organs, tumor cells can evolve as a result of epigenetic changes (cell plasticity) [88, 89, 90]. Bone-metastatic tumor cells tend to evolve to acquire the features of bone cells and exhibit osteoblast-specific markers, such as ALP, OPN, PTHrP, RANKL and Runx2, which facilitates the maturation of osteoclasts without the help of osteoblasts and refers as the osteomimimcry [91, 92, 93, 94] As mentioned before tissues in the lungs receive a high level of oxygen and lung-metastatic tumor cells with increasing PPARγ and PGC-1a to upregulate the mitochondrial biogenesis which assists antioxidant and protect against oxidative stress and damage [95]. In colonization progress, tumor cells change to replicate the metabolic pattern of the relevant distant organs. As glucose is scarce during brain metastasis,

tumor cells exhibit metabolic adaptability that allows them to take use of locally accessible nutrients such acetate, amino acids, and glutamine [77]. Neuronal mimicry of brain-metastatic tumor cells utilizes γ-aminobutyric acid (GABA) as a fuel source via upregulating GABA receptors and transporters [96]. According to previous research, cancer-associated fibroblasts can generate a microenvironment similar to the bone marrow, thus pre-select the tumor cells that are compatible with the bone, which suggests metastatic preference may pre-exist when tumor cells are in their primary sites. According to previous research, cancer-associated fibroblasts can generate a microenvironment similar to the bone marrow, thus pre-select the tumor cells that are compatible with the bone microenvironment, which suggests metastatic preference may pre-exist when tumor cells in their primary sites. This process is called 'seed pre-selection' and provides insight into why bone metastasis can be predicted by the gene signature of primary tumors [4, 97].

Is the mechanism of metastatic organotropism the consequence of selection or conversion (adaptation)? If organotropism is the consequence of selection, its driving forces most likely come from mutations, abnormalities in copy number, and other genomic alterations. As a result, a number of studies using extensive metastatic cancer genome resequencing are attempting to uncover the genes responsible for phenotypic alterations in the metastatic preference of tumor cells [98]. If the mechanisms of specific-organic metastasis are dependent on conversion, the role of environmental cues in reversible mechanisms that contribute to the acquisition of the phenotypes is likely related to epigenetic mechanisms. Consequently, the microenvironment may cause epigenetic modifications that alter the preference for organic metastasis before or during the process. In contrast to mutations, epigenetic alterations are quick and reversible, suggesting that they are more adaptable and widespread. It does not imply, however, that there are no mutations driven by the microenvironment that support metastasis. Although clones present in early tumors and their corresponding brain metastasis had a common ancestor, researchers discovered distinctive evolutionary

patterns happening at the metastatic location by sequencing primary tumors and paired brain metastases from a range of human tumors [99]. Further research will be needed in the future to provide a conclusive answer to the question of what mechanism governs organotropism. Additionally, a lot is still unknown regarding how the heterogeneous microenvironments in the primary site affect metastatic organotropism.

2.3 brain metastasis and brain microenvironment

The brain is the central organ of the nervous system and controls most of activities of the human body. On one hand, the skull protects the brain mechanically, and on the other hand, the blood-brain barrier prevents the entry of harmful substances by selectively separating the brain from the blood circulation. There are two main sources of brain metastases, which are lung and breast tumors [100]. Patients with CNS metastases make up 10–30% of the cases with breast tumor [101]. The current treatment for brain metastases only can stabilize the disease in a short period of time, but cannot significantly prolong the survival of patients, and the one-year survival rate of patients with brain metastases is less than 20% [102]. Brain metastases not only exhibit an overwhelmingly poor prognosis but often lead to neurological damage that seriously affects cognitive and sensory functions [6]. Consequently, brain metastases pose a significant public health threat, and despite extensive research, little effective treatment has been found for patients.

Brain metastasis caused by breast carcinoma exhibits two different patterns, which are leptomeningeal and parenchymal metastases. About 80% of the total brain metastasis cases are brain parenchymal metastasis [103]. Hematogenous origin is assumed to be the main cause of metastatic lesions to the brain parenchyma [104]. And breast tumor is a leading cause of leptomeningeal metastasis [103]. The cerebrospinal fluid allows the cancer cells to further disseminate after cancer cells have reached leptomeninges [104].

Research to date has shown that brain-specific tropism in certain types of cancer is caused by the interplay of the following factors (Fig. 2.3): (1) The distinctive genetic characteristics of cancer cells enable them to invade, disseminate, and penetrate the BBB [65, 105, 106, 107]. (2) Disseminated cells evolved from clonal evolution exhibit specific transcriptomes as a result of genetic mutations and epigenetic modifications, which help them colonize the brain [107, 108, 109]. (3) A brain milieu that is conducive to metastasis resulting from the interplay of tumor cells and brain stroma, including promoting inflammatory responses, attracting suppressive cells derived from myeloid, and metabolic reprogramming [77, 96, 110, 111]. (4) Inhibition of immunity leads to the immune system failing to detect or eliminate tumor cells within brain [110, 112].

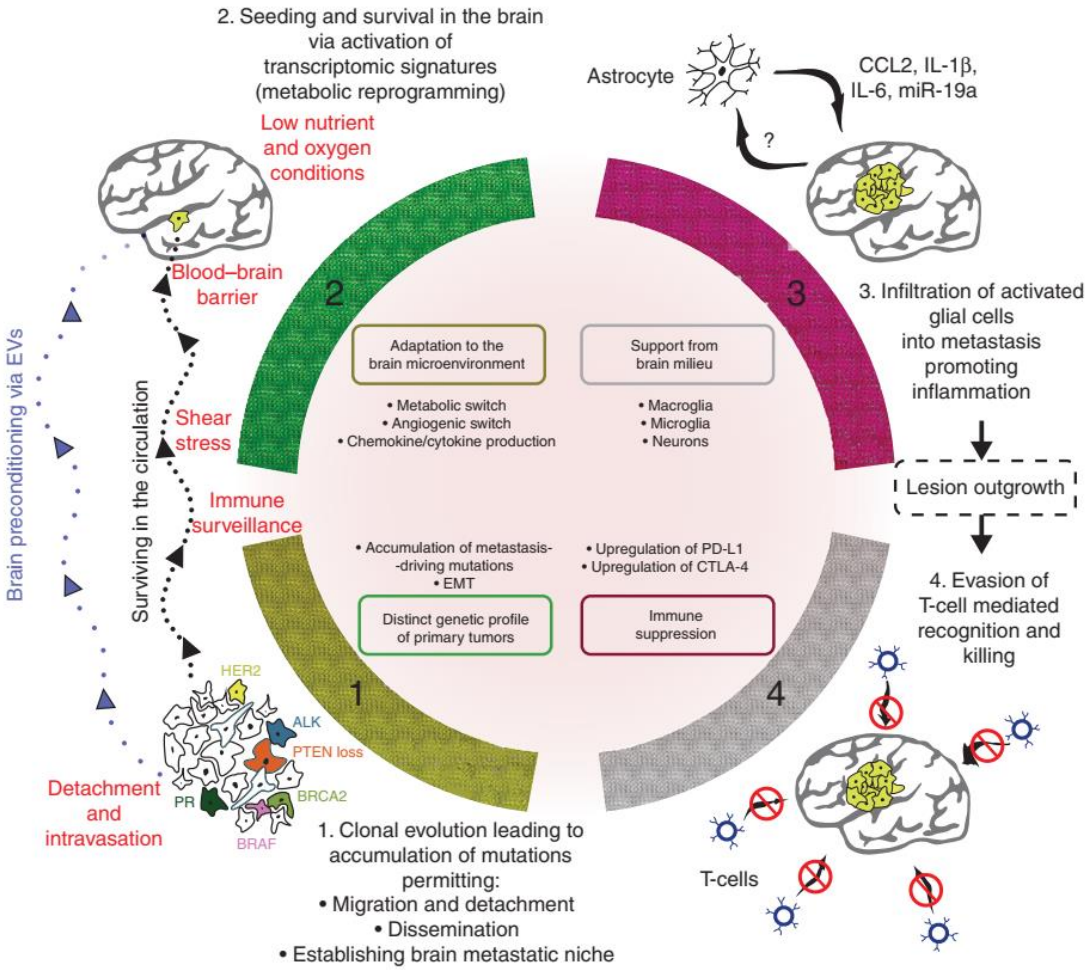

Figure 2.3 An illustration of key factors in different stages that enable brain organotropism of cancer cells [113].

The different noncellular components and special resident cell types, like neurons, glials and astrocytes, co-consist in the unique brain microenvironment. On the one side, metastatic tumor cells tend to attract activated astrocytes to enhance the various proinflammatory factors which facilitate the proliferation of tumor cells [114]. miR-19a, a miRNA that can downregulate PTEN, is uptake by tumor cells landing on the brain via astrocyte-generated EVs, which activate NF-κB and enhance the CCL2 to promote the formation of brain metastasis [115]. On the other side, reactive astrocytes secrete plasmin in response to extravasating tumor cells [75]. Overall, astrocytes may exert both a promoting and a suppressing function in brain metastasis depending on the context.

By co-opting brain blood vessels, tumor cells acquire the supports to proliferate, migrate and penetrate the brain parenchyma[116]. The ECM in the brain parenchyma supports organizational patterns in the brain regions and provides a habitat that is vital for cell survival, plasticity, and survival [117, 118]. Recent evidence strongly suggests that the ECM plays an important role in the successful metastatic seeding and metastasis formation of brain-metastatic tumor cells [119, 120]. The ECM in the brain consists of a variety of components, mainly including hyaluronic acid (HA), a non-sulfated glycosaminoglycan [121, 122]. In contrast, there is a relatively low amount of fibrillar proteins such as collagen type I, fibronectin, and vitronectin in the ECM microenvironment, and these in addition to basement membrane proteins, such as laminin, are largely restricted to the vascular and perivascular spaces in the brain [123]. Contrarily, the ECM microenvironment contains a few fibrillar proteins like collagen I and fibronectin and they are mostly constricted to the vascular and perivascular areas in the brain [123]. HA is rather soft and takes up a significant portion of the ECM amount of the brain. HMMR, one of HA receptors, has been demonstrated to associate with brain metastasis derived from lung cancer and to promote colonization in the brain *in vivo* experiments [124].

For the goal of developing novel, powerful targeted treatments for brain metastasis, the continuous and intricate interaction between the brain microenvironment and metastatic cells has not yet been extensively investigated.

2.4 Biomechanics in metastasis

Numerous research has emphasized genetic and biochemical features as the driving forces for malignancy. Physical properties, however, have usually been disregarded. Microenvironmental alterations have a substantial impact on the behaviors of tumor cells since tumor cells are restricted to a particular microenvironment, such as surrounding ECM. In the tumor microenvironment, anomalies in biology and physiology coexist. The importance of the mechanics, which includes solid stress, interstitial fluid pressure, shear stress, matrix rigidity and cell stiffness is becoming recognized more and more recently in terms of how tumors form, progress, metastasize, and respond to therapy. Novel medications and treatment methods have been made available by investigating the connections between cancer biology and mechanics.

The unrestrained growth of tumor cells leads to the continued expansion of the tumor tissue, compression of the tumor core, and distention of the paracancerous tissue. Solid stress refers to the force generated by the expansion of tumor tissue and the resistance force of the paracancerous tissue to the deformation [125]. Usually, solid stress increases with the development of tumor progress and then causes the compression and even collapsing of blood vessels and lymphatic tubes, which leads to the hypoxia of tumor core and impairs drug delivery as well as the efficacy of various therapies [126, 127, 128, 129, 130]. It is also possible that solid stress can exert direct impacts on tumor development, such as enhancing tumor cell invasion [131] and inducing tumorigenesis in colon epithelium [132].

Most organs have arteries and veins for blood entry and exit, while lymphatic tubes drain any extra tissue fluid. Interstitial fluid pressure (IFP) in the majority of healthy organs is kept around zero as a result of maintaining fluid homeostasis. Tumor anomalies, such as leaky blood vessels and solid stress-induced impairment of the drainage system, disrupt this homeostasis. IFP-induced flow stresses influence several aspects of cancer biology [133], such as the increases in MMP activity, migration ability and invasiveness in tumor cells [134, 135, 136].

Tumor cells are subjected to shear stress when they leave the original tumor site and travel into the circulatory. Viscosity and rate of blood flow determine hemodynamic shear force, occurring as blood flows over the exterior of cells [13]. Tumor cells need to survive in travelling through the blood circulation for metastasis to take place, and surprisingly, studies have revealed that tumor cells show a higher resistive ability to shear force than normal cells [137]. The surviving capacity of cancer cells depends on how long they circulate and how much shear force they endure [138]. Under physiological resting levels of shear force, the proliferation of tumor cells is inhibited and the adhesion and motility of tumor cells are enhanced, whereas the death of tumor cells occurs at levels of shear force comparable to exercise conditions [139, 140, 141]. Therefore, tumor cells required ongoing adaptation in order to be able to endure the numerous mechanical pressures which they will experience when they depart from the primary sites and form secondary tumors.

2.4.1 Matrix stiffness

Stiffness, also term as rigidity or modulus of elasticity, means the resistant ability of a material to displacement caused by slow force application, which is an inherent property of tissue. Significantly stiffness of the tissue is the most obvious and easily recognized mechanical phenomenon in tumors and has traditionally served as a useful marker for tumor diagnosis [142] and recently as a marker for prognosis [143, 144]. Malignant

tumors show higher tissue stiffness than these benign tumors in a variety of cancer types, such as carcinomas in breasts, pancreas, livers and prostates [144, 145, 146, 147]. Deposition and cross-linking of the ECM contribute to ECM stiffening. Tumors are usually fibrotic and stiff, dues to cancer-associated fibroblast (CAFs) producing collagen fiber and generating greater contractile force by polymerization of actin stress fiber, high expression of α-smooth muscle actin and formation of focal adhesion [148, 149]. LOX promotes the cross-linking of collagen, which contributes to the mechanical strength of the matrix. Transglutaminase 2 shows abundant expression in pancreatic tumor and also improves collagen cross-linking, which increases the activation of fibroblasts [150]. Enhanced ECM stiffness and TGF-β signaling induce fibroblasts to transit to CAFs, further enhancing ECM stiffness in a positive feedback manner.

There is a wealth of research demonstrating how the material characteristics, especially tissue stiffness, exert dominant functions in many malignant traits of tumor cells, such as proliferation, blood vessel formation, metabolism, motility and metastasis [12, 13, 14, 151, 152, 153, 154, 155]. Several types of cancer, which include breast, pancreas, colon, and brain, progress faster when the matrix is stiffened [156, 157, 158, 159]. Furthermore, by enhancing the stiffness of the matrix alone, breast epithelial cells can be driven to a malignant transformation [160]. However, there has been some debate over the importance of matrix stiffness in the progression of tumors because several studies have demonstrated that a soft matrix, rather than a stiff one, is crucial for the development of tumors. A mechanics-based theory has been presented to account for the role of heterogenous stiffness of tumor in invasion progress: secreted collagen stiffens the matrix, maybe as a defensive measure to restrict the development of the tumor [161]. Optimal soft fibrin gel generates a metastatic population of melanoma cells with high tumorigenesis ability [162]. Thus, mechanical properties are likely to affect metastatic phenotype to produce or opt for a particular subpopulation of tumor cells [163]. Actually, the matrix with homogeneously high stiffness suppresses the outgrowth of tumor and induces the stem-like soft tumor-repopulating cells into the dormancy state [164]. Dormancy of breast tumor

cells is induced by rigid fibronectin matrix and inhibited by MMP-2-dependent degradation [165]. Additionally, research shows that tumor-derived type III collagen is more abundant in the tumors of patients without lymph node metastasis and is necessary to maintain tumor cell dormancy [166]. These results support the stiffness matching model [167], which states that intrinsically soft stem-cell-like tumor cells show low intracellular forces and grow in a soft 3D microenvironment, whilst stiff differentiated tumor cells have high intracellular forces and thrive in a stiff 3D microenvironment inside primary tumor. This model suggests that the stiff ECM acts as a physical barrier to restrict tumor development [34]. Furthermore, the survival time of patients with liver cancer shows a positive correlation with the levels of collagen1, supporting the idea that ECM proteins like collagen are barrier protection and not motivators to solid tumor progression [168]. Additionally, a recent study demonstrates that reducing tissue stiffness in pancreatic cancer metastases in the liver speeds up tumor development and decreases overall survival [169]. These data emphasize the significance of matrix softness in the metastasis of tumor cells.

Inspiring work shows that tumor tissues tend to have a bimodal distribution of stiffness, as opposed to healthy tissue with unimodal distribution. Moreover, cells under hypoxia corresponding to the soft peak of the bimodal distribution have a high risk of metastatic spread [19]. The invasive zone of the stroma has notably stiffer tissue than the tumor center or the nearby normal tissue. Additionally, it was discovered that mechanical heterogeneity within tumors correlated positively with more malignant breast cancer [170]. Various tissue stiffness is crucial for promoting the invasion of tumor cells in an embryo, which is in line with previous statement findings [171]. In light of durotaxis, heterogeneous stiffness in tissue may act as a driving force for the invasion behavior of tumor cells [172].

Overall, this is still an incomplete study illustrating how matrix mechanical properties affect tumor growth. The exact roles of matrix rigidity in cancer metastasis need to be

determined in the future, especially in distant-organ metastatic colonization.

2.4.2 Cell stiffness

In addition to the biophysical factors from the microenvironment, mechanical properties of tumor cells can also have an impact on the malignancy. Contrary to popular opinion, malignant tumor cells are usually soft compared to healthy counterparts, despite the fact that tumors are typically stiffer than corresponding healthy tissue [18, 156, 173]. An effective indicator of tumor cells with high tumorigenic and metastatic potential is cell softness [20]. The relationship between cellular stiffness and the propensity for migration and invasion is inverse. Additionally, some therapies, such as pharmacological myosin II antagonists, decrease cell stiffness, which causes cancer cells to acquire invasive phenotype [15, 174]. Low cell mechanics and less F-actin of tumor cells enhance their efficiency of extravasating the blood vessels, while the transmigration ability was suppressed by cytoskeleton activator in zebrafish model [21], which is in line with the high blood vessel penetration ability in soft tumor-repopulating cells. Moreover, tumor stem cells exhibit low cell stiffness than their differentiated counterparts, and this mechanical characteristic can be used as an effective target to eliminate CSCs by nanoparticle [20, 162, 175].

The prospect of tumor treatment is greatly enhanced by the role of cell mechanics in regulating interactions between immune cells and tumor cells. When combined with anti-PD-1 antibody therapy, increasing the cell stiffness of tumor-repopulating cells restores T cell-mediated cytolysis of tumor-repopulating cells and significantly increases the efficiency of killing tumor-repopulating cells in mice [176]. Because of the stresses generated at the synapse, promotes cytolysis by T-cells is enhanced by tumor cell stiffening [177]. It has been shown that macrophages swallow stiff target cells more eagerly than soft target cells, hence the effect of cell softness in limiting T cell death also extends to macrophages [178]. By increasing tumor cell stiffness, MRTF renders

cancer cells more susceptible to lymphocytes [179].

Overall, cell softness cannot be regarded as a minor side effect of other alterations but a potentially vital physical feature in tumor cells. Additionally, additional research is needed to determine the possible functions of cell stiffness in metastasis.

2.4.3 Biomechanics in brain metastasis

Numerous studies conducted over the past 10 years have shown the significance of the ongoing dynamic interaction between cells and their surroundings. These findings have outlined how mechanical tissue characteristics can affect how cells behave. The involvement of brain microenvironmental tissue biophysics in infiltrative cells may be one of the missing pieces of the puzzle. Exploring the origin of brain metastases and enhancing therapy choices can both benefit from an understanding of the function of unique tissue biophysics.

Interstitial spaces in the brain, where metastatic tumor cells may disseminate, contain the cerebrospinal fluid (CSF) [180]. Within the microenvironment containing the liquid, tumor cells are subject to below 1 kPa shear stress caused by CSF [181]. Although the effects of blood shear flow on tumors have received substantial research, little is known about how tumor cells that come into contact with the CSF perceive and react to shear stress.

In contrast to other tissues, the mammalian brain is compliant, of which the stiffness can vary from 0.1 to 6.1 kPa depending on the approach, spatial and temporal dimensions [182, 183]. The characteristics of neural stem cells (NSC), progenitors, neurons, and glia are guided by the rigidity of the brain tissue in accordance with a mechanical instruction [184, 185, 186]. For instance, NSCs differentiation and growth are affected by tissue stiffness. While differentiation toward oligodendrocyte was improved on stiff

matrix, neuronal differentiation was boosted when adult NSCs were cultured on compliant substrates [185].

It has been extensively studied how tissue stiffness affects primary brain tumors. GBM cells stiffen the matrix around them, which strengthens their migration capacity [187]. The proliferation of GBM cells, cell motility, and the localization and activation of the EGFR at focal adhesions were all boosted by high matrix stiffness surrounding GBM cells [188]. There have been few research looking at the impact of the stiffness of brain niches on cancer cells entering the brain, despite the fact that tissue mechanics have been examined in relation to malignancies that arise in the brain. Through the suppression of DNMT1 expression, compliant matrix causes dormancy and improves the survival of metastatic breast cancer cells in the brain [10].

2.5 Mechanotransduction

When cells are in response to biophysical factors in the microenvironment, there is the conversion of mechanical force into biochemical signals, which is known as mechanotransduction. This transduction consists of mechanosensing, force transmission and mechanoresponses relying on mechanosensors, cytoskeletal networks, molecular motors and nuclear (Fig 2.4).

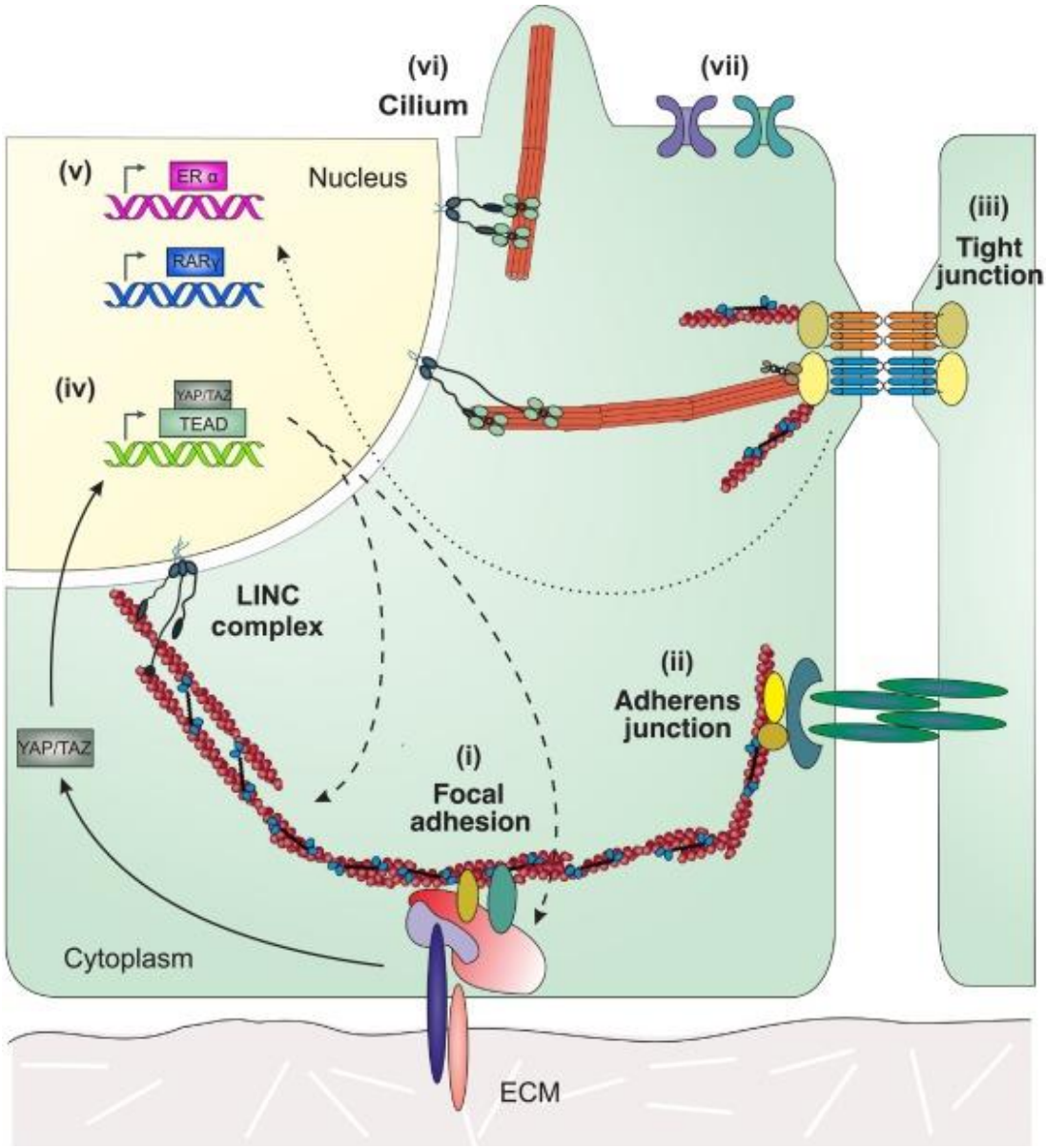

Figure 2.4 Mechanotransduction progress in cells [189]

Mechanical signals are typically sensed by mechanosensing molecules at the cell membrane, including integrins and cadherins at cell-matrix adhesions and cell junctions, tyrosine kinases, and ion channels [190]. By myosin-mediated contractility and cytoskeleton rearrangement, cells respond to and offset external biophysical stresses [191]. Tensioned cytoskeletal elements, including F-actin stress fibers, transduce mechanical forces from the cell surface to the nuclear envelope (NE) and the nuclear lamina through

the linker of the nucleoskeleton and cytoskeleton (LINC) complex [192], which in turn affects chromatin remodeling and epigenetic modifying and finally regulates gene expression pattern [193, 194, 195]. In parallel, mechanical forces have the ability to activate pathways of intracellular signalings that include transcription factors (TFs), such as YAP, MRTF and other molecules, that translocate into the nucleus [193, 196].

2.5.1 Nuclear mechanotransduction

The biggest and toughest organelle in a cell is the nucleus which may be generically divided into the NE, nuclear matrix (including the nuclear lamina) and nuclear interior (containing chromatin) [197, 198]. Both the outer and inner nuclear membranes (ONM and INM, respectively) and the nuclear pore complexes (NPCs) which regulate the importation and exportation of big molecules shuttling between the nuclear interior and cytoplasm, make up the NE [199, 200]. The LINC complex, consisting of proteins with SUN- and KASH- domains, links the nuclear lamina and NE with the cytoskeleton and mediates force transmission between the cytoskeleton and nuclear interior (Fig 2.5) [201, 202]. LINC complex proteins across the nuclear envelope anchor to the nuclear envelope via interacting with Lamins, NPCs, and chromatin [202]. SUN1 and SUN2 make up the SUN-domain proteins in mammal cells, whereas nesprin1 -4 make up the KASH-domain proteins. SUN at INM engage with the lamina at nuclear interior and with nesprin in the perinuclear space [203]. Nesprin spanning ONM connects to the cytoskeleton including F-actin, microtubules and intermediate filaments via direct binding or mediator molecules [204]. The LINC complex exerts an essential role in mechanotransduction progress in turn to regulate a series of cellular functions, such as gene expression, nuclear deformation and chromatin remodeling [205, 206]. When the association of nuclear Lamins and LINC complex proteins are disrupted, nucleo-cytoskeletal coupling, cytoskeletal reorganization, and nuclear stiffness are compromised [207]. Mechanisms of nuclear mechanotransduction can be divided into three non-exclusive parts: 1. Applied force to the nucleus can result in nuclear envelope-

related proteins being partially unfolded and nuclear proteins being phosphorylated, such as Lamins, SUN-domain proteins, and Emerin [208, 209 210]; 2. NPCs and ion channels on the cytoplasmic side are opened when the nuclear membrane stretches in response to force, promoting the entry of molecules into the cell nucleus. Gene expression patterns may change as a result of an altered import/export of TFs into/out of nucleoplasm [211, 212, 213]; 3. in response to mechanical forces, chromatin can be stretched, opened, and compacted, DNA and histones modifications are altered, which affect transcription factor accessibility at their promoter and result in gene expression changes [194, 214, 215, 216, 217].

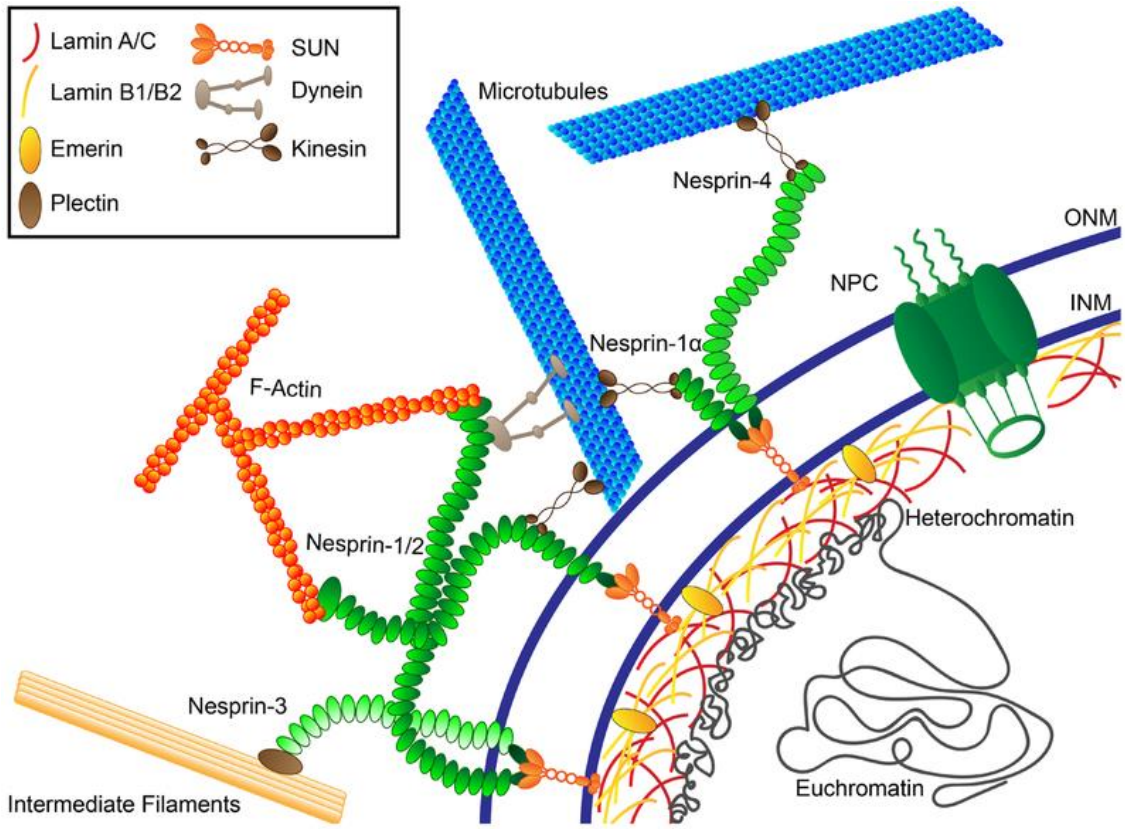

Figure 2.5 LINC complex [218]

2.5.2 Chromatin organization and epigenetics shaped by force

In order to control transcriptional regulation and eventually cell fates, epigenetics,

which alters gene expression without modifying the DNA sequence, is crucial [219]. It is widely known that the transmission of external mechanical stress from the cell membrane to the nucleus may alter nuclear chromatin architecture and epigenetic patterns, which in turn can affect transcription of genes [220]. When cells are grown on the matrix with linear changes of stiffness, the expression levels of tissue-specific TFs become maximum at a certain stiffness [221]. Histone modifications including acetylation and methylation are altered by the topography of substrate as epigenetic regulators [222]. Study have demonstrated that human mesenchymal stem cells expanded on rigid matrices go through chromatin remodeling, which is reflected in elevated levels of histone acetyltransferase (HAT) and decreased levels of histone deacetylase (HDAC) [195]. Matrix stiffness-induced chromatin and histone changes are dependent on the LINC complex, supporting nucleo-cytoskeletal coupling as a key regulator of chromatin remodeling in response to mechano-stimulation [195, 223]. It is interesting to note that long-term cell culture on stiff surfaces prevents cells from changing their chromatin state in response to matrix softness, highlighting the significance of physiology-relevant matrix stiffness for cell culture [223]. When cells are stretched mechanically, emerin translocates from the INM to the ONM and then promotes the methylation of H3K27me3 and demethylation of H3K9me2,3, leading to transcriptome silence eventually [224]. Emerin binding with actin in the ONM promotes the perinuclear actin cap assembly and remodeling of F-actin networks, which reduces G-actin levels and downregulates Pol II activity [210, 215]. In addition, nuclear softening that is caused by the force-induced loss of H3K9me3-marked heterochromatin enables cells to release strain energy and thus preserve the genome [225]. Geometric cues influence nuclear architecture, chromatin remodeling, and transcriptional regulation. In comparison to fibroblasts grown in elongated rectangular shapes, those cultured on tiny circular islands have higher nuclear HDAC3 levels, altered chromosomal contacts, and enhanced chromatin and NE dynamics [226, 227, 228]. Fibroblasts cultured on elongated rectangular platforms undergo dedifferentiation and reprogramming [229]. These studies imply that mechanical factors that come in distinct forms can differently affect the epigenetic state in a cell

type-specific way, which has crucial implications for physiology, applications and treatments.

Chapter 3: Materials and Methods

3.1 Cell Culture

MDA-MB-231 (231 for short) and its brain metastatic derivative MDA231-BrM2-831 (231-BrM for short), bone metastatic derivative MDA-BoM-1833 (231-BoM for short) cell lines were purchased from Memorial Sloan Kettering Cancer Center. The cells were maintained in Dulbecco's Modified Eagle Medium (DMEM; HyClone) supplemented with 10% fetal bovine serum (FBS; HyClone) and 1% penicillin/streptomycin (Gibco). The human cerebral microvascular endothelial cell line hCMEC/D3 (FuHeng Biology) was cultured with EndoGRO-MV complete culture media kit (Sigma-Aldrich) supplemented with 200ng/mL human basic fibroblast growth factor (bFGF; Sigma-Aldrich) and 1% penicillin/streptomycin. The human umbilical vein endothelial cells (HUVECs) and human astrocytes isolated from human brain (cerebral cortex) were generous gifts from Prof. YANG Mo (The Hong Kong Polytechnic University) and maintained in Astrocyte Medium (ScienCell) and Endothelial Cell Medium (ScienCell) respectively. HEK-293T cell line was received as a gift from Dr. RUAN Yechun (The Hong Kong Polytechnic University) and cultured with DMEM supplemented with 10% FBS and 1% penicillin/streptomycin. 4T1 cells purchased from ATCC were cultured in RPMI-1640 medium (Gibco) with 10% FBS and 1% penicillin/streptomycin. All cell lines were cultured in 5% CO_2 incubator at 37 °C

3.2 Polyacrylamide Hydrogels (PA gels) Preparation

According to the previous description, hydrogels were manufactured [230]. Briefly, 30 mm circular amino-silanated coverslips and chloro-silanated glass slides were prepared in advance following the instruction. 40% (w/v) acrylamide (Bio-rad) and 2% (w/v) bis-acrylamide (Bio-rad) were mixed to their desired concentrations in distilled H_2O according to Table 1. 1/100 total volume of 10% (w/v) ammonium persulfate (APS; Sigma-Aldrich), and 1/1000 total volume of tetramethylethylenediamine (TEMED; Sigma-Aldrich) was added and mixed gel solution quickly. 240 μl (for 6-well plate) of

the gel solution was quickly pipetted onto the treated side of the chloro-silanated glass slide and amino-silanated coverslip with the treated side was covered. After the gel was fully polymerized, the hydrogel was immersed in phosphate-buffered saline (PBS; Hyclone) and stored at 4 ℃. The gel surface was coated with Sulfosuccinimidyl-6-(4'-azido-2'-nitrophenylamino) hexanoate (Sulfo-SANPAH; Sigma-Aldrich) with 365-nm UV light. After washing with PBS 3 times, the gel was coated with 0.2 mg/mL rat-tail collagen type I (Sigma-Aldrich) or 10 μg/ml human plasma fibronectin (Sigma-Aldrich) at 4 ℃ overnight. The gel was placed in the cell culture cabinet for 30 min under UV for sterilization. After that 1 ml full medium was added and the gel was placed in the incubator for at least 30 min before usage.

Table 1 The composition for polyacrylamide Hydrogels preparation

Acrylamide %	Bis-acrylamide %	40% acrylamide stock solution (ml)	2% bis-acrylamide stock solution (ml)	Water (ml)	E (kPa)
3	0.06	0.75	0.3	8.95	0.6
10	0.3	2.5	1.5	6	35

3.3 Quantitative RT-PCR Analysis

Following the manufacturer-recommended methods, total mRNAs were harvested utilizing E.Z.N.A.® Total RNA Kit (Omega) and cDNAs were prepared to utilize RevertAid First Strand cDNA Synthesis Kit (Thermo Fisher). Utilizing the Forget-Me-Not EvaGreen qPCR Master Mix with Rox (Biotium) and CFX96 Real-Time System (Bio-Rad), quantitative RT-PCR was performed. The National Center for Biotechnology Information (NCBI) database was used to construct all primer sequences, which are all shown in Table 2. Utilizing 2-ΔΔCT approach, relative gene expression was assessed and standardized to the expression level of human glyceraldehyde 3-phosphate dehydrogenase (GAPDH).

Table 2 List of primers

Gene name	**Forward (5' - 3')**	**Reverse (5' - 3')**
ADAMTS1	TCCGTCATAGAAGATGATGGTTT	GCATGTTAAACACGTGGCCTA
ANGPTL4	TCCGTACCCTTCTCCACTTG	AGTACTGGCCGTTGAGGTTG
B4GALT6	CTCATTCCTTTCCGTAATCGCCA	GCCCACATTGAAAAGCATCGCAC
COL13A1	GCTGCTGCCTCTCCTCAATTCAG	TGGATGCTGGCCTGGCTCTG
COX2	TTCAACACACTCTATCACTGGC	AGAAGCGTTTGCGGTACTCAT
ST6GALNAC5	GATTACTCGCCACAAGATGCTGC	GATCCTGTCACAGAGCTCCAGT
CTGF	CTCCTGCAGGCTAGAGAAGC	GATGCACTTTTTGCCCTTCTT
CXCR4	GGTAGCGGTCCAGACTGATGA	CCTATGCAAGGCAGTCCATGT
EREG	CTGCCTGGGTTTCCATCTTCT	GCCATTCATGTCAGAGCTACACT
FGF5	CCCGGATGGCAAAGTCAATGG	TTCAGGGCAACATACCACTCCCG
FST	ACCTGAGAAAGGCTACCTG	ACTGAACCTGACCGTACACAACCTTGAAATCCCATAAA
FYN	AAGAGCCCCAGAAATTCACA	CGCCAACGATCACAAACTT
GAPDH	GCGACACCCACTCCTCCACCTTT	TGCTGTAGCCAAATTCGTTGTCATA

HBEGF	GGACCCATGTCTTCGGAAAT	CCCATGACACCTCTCTCCAT
HDAC1	AACCTGCCTATGCTGATGCTGG	TCGTCTTCGTCCTCATCG
HDAC2	CAACGCAGCCCATTCACC	GCAAGTTATGGGTCATGCGG
HDAC3	AGTTCTGCTCGCGTTACACA	CAGAAGCCAGAGGCCTCAAA
HDAC8	GGCTGCGGAACGGTTTTAAG	GCTTCAATCAAAGAATGCACCATAC
IMPG1	GGCTGTAGTCCTGCCAGAAG	GTTGAGGCCTGATGAGTGGT
ITGAV	CTCGGGACTCCTGCTACCTC	AAGAAACATCCGGGAAGACG
ITGB3	CCGTGACGAGATTGAGTCA	AGGATGGACTTTCCACTAGAA
LAMA4	GAGATGACTCTCTGCTGGACCT	AGTTCCAGGCAGCCAACAAAGC
LTBP1	CTTCCCCTGCCCGGTCT	CTGCATCTTTATAGTTCTCACCACCA
FSCN1	GACACCAAAAAGTGTGCCTTCCG	CAAACTTGCCATTGGACGCCCT
OPN	TCCAACGAAAGCCATGACCA	CTGTGGGGACAACTGGAGTG
PELI1	AGATGGATGGCTTGACCACT	TGCTGCATTGATTTCCTGTC
PIEZO2	GACGGACACAACTTTGAGCCTG	CTGGCTTTGTTGGGCACTCATTG
PLOD2	CATGGACACAGGATAATGGCTG	AGGGGTTGGTTGCTCAATAAAAA

PTHLH	CTCGGTGGAGGGTCTCAG	TGGATGGACTTCCCCTTGT
RGC32	TCTCTGCCACTGTCACTCCTCA	GATGAAAGGACCCAGAACTTCTTG
SERPINE1	CTCATCAGCCACTGGAAAGGCA	GACTCGTGAAGTCAGCCTGAAAC
SERPINB2	GTTCATGCAGCAGATCCAGA	CGCAGACTTCTCACCAAACA
SERPINI1	CTACCCAGAAAGAAATCCGCCAC	TGGCTCTCTTTAGCAGTTACCATG
OCT4	CCTGAAGCAGAAGAGGATCACC	AAAGCGGCAGATGGTCGTTTGG
SOX2	GCTACAGCATGATGCAGGACCA	TCTGCGAGCTGGTCATGGAGTT
NANOG	CTCCAACATCCTGAACCTCAGC	CGTCACACCATTGCTATTCTTCG
CD44	CCAGAAGGAACAGTGGTTTGGC	ACTGTCCTCTGGGCTTGGTGTT
CD133	CACTACCAAGGACAAGGCGTTC	CAACGCCTCTTTGGTCTCCTTG
BMI1	GGTACTTCATTGATGCCACAACC	CTGGTCTTGTGAACTTGGACATC
For Mus musculus		
Angptl4	CTGGACAGTGATTCAGAGACGC	GATGCTGTGCATCTTTTCCAGGC
Cox2	GCGACATACTCAAGCAGGAGCA	AGTGGTAACCGCTCAGGTGTTG
Gapdh	CATCACTGCCACCCAGAAGACTG	ATGCCAGTGAGCTTCCCGTTCAG
Itgb3	GTGAGTGCGATGACTTCT	CAGGTGTCAGTGCGTGTAGTAC

	CCTG	
Ltbp1	TGCCTGTGGAAGTAGCTC CTGA	AGTGTCCTGCTCCGCAAATGTC
Piezo2	GCACTCTACCTCAGGAAG ACTG	CAAAGCTGTGCCACCAGGTTCT
Serpinb2	ACCCAGAGAACTTCAGTG GCTG	GAGAGAGGAGAAGGCTGAATG G

3.4 RNA-seq and bioinformatic analysis

For RNA-seq, 231 cells were cultured for 30 days on tissue culture plastic (TCP), 0.6 kPa PA gels (mimicking the tissue stiffness in high cellularity and low matrix density regions of breast tumor.) and 35 kPa PA gels (mimicking the tissue stiffness in low cellularity and extremely high matrix density regions of breast tumor.), respectively. Cells were passaged every 3 days and total RNAs of 3 biological replicates for each condition were extracted using the RNeasy Mini kit (QIAGEN). Sample quality control, including quantitation, integrity and purity, was performed using Agilent 5400 to ensure the samples meet the requirement of library construction.

Messenger RNA was purified from total RNA using poly-T oligo-attached magnetic beads. After fragmentation, the first strand cDNA was synthesized using random hexamer primers, followed by the second strand cDNA synthesis. The library was checked with Qubit and real-time PCR for quantification and bioanalyzer for size distribution detection. Quantified libraries will be pooled and sequenced on Illumina platforms, according to effective library concentration and data amount. The clustering of the index-coded samples was performed according to the manufacturer's instructions. After cluster generation, the library preparations were sequenced on NovaSeq PE150 platform (Novogene) and paired-end reads were generated.

All the downstream analyses were based on the clean data with high quality provided by Novogene. FPKM, expected number of Fragments Per Kilobase of transcript sequence per Millions base pairs sequenced, was calculated based on the length of the gene and reads count mapped to this gene and differential expression analysis of two conditions was performed using the DESeq2R package (1.20.0). Genes with an adjusted P-value (padj) <=0.05 found by DESeq2 and |log2(Fold Change) | >=1 were assigned as differentially expressed. In addition, RNA-seq data of SUM159 breast cancer cells cultured on 0.5 kPa and 8 kPa substrates for 14 days was acquired from GSE127887 in Gene Expression Omnibus (GEO) database (https://www.ncbi.nlm.nih.gov/geo/).

In bioinformatic analysis of RNA-seq data, over-representation analysis (ORA) of enriched terms and pathways in gene ontology (GO), DisGeNET and PaGenBase database was performed by Metascape (https://metascape.org/gp/index.html#/main/step1). Padj <=0.05 was set as the threshold of significant levels for terms and pathways. Gene set enrichment analysis (GSEA) was performed by easyGSEA (https://tau.cmmt.ubc.ca/eVITTA/easyGSEA/). Default parameters (minimum gene set size:15, maximum gene set size:200, and the number of permutations:1000) were chosen to conduct GSEA. Padj <0.25 and normalized enrichment score (NES) >1 were set as the threshold of significant levels for terms and pathways. Generic Protein-Protein Interactions (PPIs) network and Gene Regulatory Network (GRN) were analyzed using data obtained from the STRING database (version 10) and the ENCODE ChIP-seq database respectively. The networks were visualized using NetworkAnalyst (https://www.networkanalyst.ca/). Volcano plots, bubble plots and heatmaps were generated using ImageGP (http://www.ehbio.com/Cloud_Platform/front/).

3.5 *In vitro* circulation system

Fluid shear force was generated by the *in vitro* circulation system which consists of a peristaltic pump (Harvard Instruments, P-230), a 10 ml syringe (to store the medium containing tumor cells) and a silicone microtube with 0.51 mm in diameter and 1.5 m in length. The wall shear stress is regulated by flow rate according to Poiseuille's law, $\tau = 4\mu Q/(\pi R3)$, where Q is the flow rate and μ= 0.01 dyne/cm^2 is the liquid dynamic viscosity of cell culture media, R=0.255mm is the radius of the tube. Before the assembly, the whole components of the system were exposed to UV for 15min. The tube and syringe were sterilized with 75% ethanol for 5min and then washed with PBS for 5min and finally pretreated with 1% bovine serum albumin (BSA; VWR Life Science) in PBS for 5min to avoid the unspecific adhesion of suspended cells to the

walls of the channel. 4×10^5 cells (in 2 ml) suspended cells were plated into the circulation device and applied with 20 dyne/cm^2 for 6 h and 12 h in 5% CO_2 incubator at 37 °C.

3.6 MTS assay

The MTS method was used to assess cell viability. In brief, a sample of 100 µl cell suspension was taken from the *in vitro* circulation system and placed in one well of a clear 96-well cell culture plate for 12h incubation. In the next step, 20 µl of 5 mg/ml working solution from CellTiter 96 aqueous One Solution Reagent (Promega) were pipetted into each well, and the plate was left for incubation at 37 °C. After 4 h incubation, analyzing the absorbance of the cell solution at 490 nm was performed using LEDETECT 96 microplate reader (Labexim Products).

3.7 Cell adhesion assay

For endothelial adhesion assay, Endothelial cells were grown into confluency in 6-well cell culture plates and tumor cells were labelled by CellTracker Green CMFDA Dye (Invitrogen) or PKH26 red fluorescent cell linker kit (Sigma-Aldrich). Before tumour cells seeding, Endothelial monolayers were washed two times with 0.5% BSA in PBS. 1 ml 1×10^5 suspended tumor cells were added into each well and allowed to attach for 15 min or 30 min. Then the medium was disposed and plates were washed with PBS 3 times for 5 min. Under the inverted fluorescent microscope, adherent cancer cells were quantified. (Nikon).

For substrate adhesion assay, 100 µl 1×10^5 suspended tumor cells were added to the corresponding functionalized surface of PA gels and incubated for 15 min or 30 min at the cell incubator. Following this, the wells were rinsed 3 times using PBS for 5 minutes each. Adherent tumor cells were counted under the inverted microscope.

3.8 *In vitro* blood-brain barrier transmigration assay

The human cerebral microvascular endothelial cells hCMEC/D3 were cocultured with human primary astrocytes on opposite sides of a poly-lysine-treated, gelatin-coated tissue culture transwell insert for 3 days. In brief, transwell inserts with 3 μm pore size (Corning, cat. no. 3415) were treated with 1 μg/ml poly-l-lysine (Sigma-Aldrich) overnight, washed with PBS four times, and treated with 0.2% gelatin (Sigma-Aldrich) for 30min. Inserts were put upside down in a 12-well plate, and 1×10^5 primary human astrocytes were resuspended in 30 μl culture medium and plated on the membrane surface. Astrocytes were fed every 15 min for 5 h, and the inserts were then flipped and placed in 24-well plates. 5×10^4 endothelial cells were added to the upper chamber of the inserts, and the plate was placed in the incubator for 3 days without any perturbation before use. 1×10^5 cancer cells were collected and labelled with CellTracker Deep Red Dye (Invitrogen) following the instruction. After being labelled with the cell tracker, cells were resuspended with serum-free medium and added to the upper chamber of the transwell inserts. After being incubated for 48h, non-invading cells were removed. The chambers were washed with PBS and fixed with 4% paraformaldehyde (PFA) and then stained with DAPI. Immunofluorescence pictures of multiple fields from 3-6 inserts per experiment were taken, and the number of transmigrated cells was counted.

3.9 Cell Morphology Analysis

Cells after treatment were seeded on corresponding substrates for 24 hours. Then images were captured by using an inverted microscope (Nikon) or fluorescence microscope (Nikon), from which cell boundary was identified and the parameters of cell morphology, including area, circularity, and aspect ratio, were then analyzed using the software ImageJ (NIH).

3.10 Western blotting analysis

The total protein samples were extracted from cells after treatment by using Radioimmunoprecipitation assay (RIPA) buffer (Thermo Fisher, cat. no. 89901) added with protease inhibitor cocktail (Thermo Fisher, cat. no. 78430) and phosphatase inhibitor cocktail (Thermo Fisher, cat. no. 78420). After being separated by SDS-PAGE gel electrophoresis, proteins were transferred to PVDF membranes (Millipore) using Trans-Blot Turbo (Bio-Rad). After electrotransfer, the PVDF membranes were blocked with the blocking buffer (Beyotime, cat. no. P0252) for 1 h incubation to prevent nonspecific binding. Then the PVDF membranes were incubated with primary antibody (diluted in blocking buffer) for 12 h at 4 degrees. After being washed with TBST 3 times (5 min/time), the membranes were incubated with corresponding HRP-conjugated secondary antibody (diluted in blocking buffer at 1:2000) at room temperature for 1 h. Antibodies against COX2 (1:1000; Abcam, ab188183), HDAC3 (1:5000; Abcam, cat. no. ab32369), GAPDH (1:2000; Abcam, cat. no. ab8245), Goat Anti-Rabbit Antibody Conjugated to HRP (1:2000; Bio-rad, cat. no. 1662408EDU), Goat Anti-Mouse IgG (H + L)-HRP Conjugate (1:2000; Bio-rad, cat. no. 1706516) were used. The membranes were washed with TBST 3 times (5 min/time) following the secondary antibody incubation and then incubated with Clarity Western ECL Substrate (Bio-rad, cat. no. 1705061) and imaged by ChemiDoc imaging system (Bio-rad). Densitometry of immunoreactive bands was quantified by Image J and normalized to the density of GAPDH.

3.11 Enzyme-linked immunosorbent assay (ELISA) for Prostaglandin E2 (PGE2)

Cancer cells were cultured at a density of 3×10^5 cells/well on tissue culture plates or PA gels with different stiffness. After 24h, the supernatants were collected and quantified for the level of PEG2 by using PEG2 ELISA kit (Abcam, cat. no. ab133021)

in accordance with manufacturer's instructions. The colorimetric signal of samples was measured by LEDETECT 96 microplate reader.

3.12 Proliferation assay

The proliferation of cells was measured by the EdU proliferation kit (Beyotime cat. no. C0078L) following the instruction. Simply, the complete culture medium was mixed with EdU stock solution at a ratio of 500:1 to obtain the 2x working reagent. Until use, the working reagent was prewarmed to 37 °C and supplied together with an equivalent amount of complete culture media to each well. Following a two-hour incubation period at 37 °C, the cells were collected, treated with 4% PFA, and permeabilized with 0.3% Triton X-100. Next, click reaction buffer was prepared following the instruction before use and added to stain the cells for 30 min at room temperature in dark. The cells were stained with DAPI solution and rinsed with PBS. The percentage of EdU-positive cells was measured by fluorescence microscope or flow cytometry.

3.13 Live/dead staining assay

The survival of cells was examined by Calcein/PI live/dead viability assay kit (Beyotime, cat. no. C2015L) following the instruction. Briefly, Cells were plated to corresponding matrix and incubated for 24 h. Calcein AM/PI detection working solution was prepared following the protocol provided by manufacturer. The culture medium was disposed and 1ml Calcein AM/PI detection working solution was added into each well of 6-well plate. After 30min incubation, images of Live/dead staining were captured by fluorescence microscope and the ratio of dead cells to live cells was analyzed by Image J.

3.14 Wound healing assay

The ibidi Culture-Insert 2 Well (ibidi, cat. no. 80209) was used to perform wound healing assay. Adjust the cell suspension to a cell concentration of 3×10^5 cells/ml and add 70 µl cell suspension into each well of the Culture-Insert 2 Well. After Incubating cells at 37 °C and 5% CO_2 for at least 24 hours, gently remove the Culture-Insert 2 Well with sterile tweezers. Wash cell layer with PBS to remove cell debris and non-attached cells and then add 2 ml medium with 2% FBS. The microscopic pictures were obtained for the indicated time and the healing degree was calculated by dividing the healing area at the end timepoint by the wound area at the start time point. The area of wound and healing was measured by Image J.

3.15 Transwell invasion assay

Matrigel was polymerized in the upper chamber of the transwells with 8.0 µm pore polycarbonate membrane inserts (Corning, cat. no. 3422). By varying concentrations of Matrigel (BD Biosciences), Matrigel was liquefied on ice and then reconstituted with the serum-free medium according to the manufacturer's instructions at final concentrations of 2 mg/ml, 3 mg/ml, and 4 mg/ml. The full-length FN was added to the gels prior to the polymerization at the final concentration of 10 mg/ml. After gels of varying rigidities were prepared, 30 µl Matrigel was pipetted into the upper chamber of the transwell insert and solidified in a 37°C incubator for 15-30 minutes to form a thin gel layer. The bottom of the lower chamber was coated with 10 mg/ml FN to facilitate the adhesion of the invaded cells. 1×10^5 Cells suspended with the serum-free medium were plated on top of the gels and the down chambers of transwells were filled with 500 µl full culture medium. After 48h incubation, the cells on the upper side as well as the Matrigel were gently removed by a cotton swab. The remaining cells on the other side of the chamber were stained with 0.1% crystal violet solutions. The number of invaded cells was counted using the 20× objective and the minimum of 5 representative

fields was counted for each condition.

3.16 Collagen gel invasion assay

70 µl cell suspension (3×10^5 cells/ml) was added into the each well of the ibidi Culture-Insert 2 Well to produce a scratch in 24-well plate after 24h incubation. Type I rat tail collagen (Corning)was diluted with 10% 10×DMEM and distilled deionized water. The pH of collagen was neutralized using NaOH. Gently remove the Culture-Insert 2 Well with sterile tweezers, and cover the cell layer with 500 µl different concentrations of neutralized collagen solution (0.5mg/ml, 1mg/ml, 3mg/ml). Cell culture medium with 2% FBS was added to the top of gels after collagen solidification. Photos were taken to measure the healing degree of the scratches after 24h.

3.17 Soft agar assay

3% low melt temperature agarose was melted and stored in 42°C water bath. To prepare the base agar layer, 3% agarose was diluted in 1% agarose with DMEM and 2 ml 1% agarose was pipetted into each well of the 6-well cell culture plate and allowed to solidify at room temperature for at least 30min. For the top agar layer containing cells preparation, 0.8% agarose was prepared by mixing the full cell culture medium, 3 % Agarose and FBS at a 6.3:2.7:1 ratio and stored in 42°C water bath. And then 2.5×10^3 cells/ml cells were resuspended in full culture medium and mixed with 0.8% agarose at equal volume. 2 ml reagent was gently pipetted into each well precoated with base agar and the plate was incubated at 4℃ for 15min for solidification. Finally, after 300 µl full culture medium was added on the top of agar, the plate was incubated at 37°C in the humidified incubator with 5% CO_2. 200 µl full culture medium for each well was supplied every 3 days. After incubation for 28 days, the plate was stained with 0.5 ml 0.1% crystal violet (dissolved in 10% ethanol) for 1 h and then washed with dH_2O rinses. Colonies were imaged with the ChemiDoc imaging system and the number of colonies

was counted by Image J. Each condition was analyzed by preparing and analyzing three wells of soft agar.

3.18 AFM measurements

Atomic force microscope (AFM; BioScope Catalyst, Bruker) was combined with the inverted microscope (Nikon) equipped with 20×objective to provide the view of the probe which is available for controlling tips and sample position. Cells were seeded on the PA gels or TCPs for 24h and grew at ~50% confluent before measurement. Silicon cantilevers (MLCT, Bruker) with spring constant k at 0.02 N/m were chosen for stiffness measurement [231]. Setup and calibration of AFM were carried out following user manual. Briefly, the contact model and ScanAsyst in Fluid model were selected for detecting the stiffness of cells in liquid media. Following, the laser positioning, AFM positioning and cantilever calibration were processed in sequence. Young's modulus E of the cell was obtained by analyzing the force, F, produced by the indentation between probe and cell. For quantification of the force F, formula $F= k \times \delta$ was used, where k is the spring constant of the cantilever, δ is the indentation which equals to sample height subtracting the deflection. Sneddon's modification of the Hertzian model was adapted to fit force-indentation curves generated by AFM for cantilever with a pyramidal indenter. The Young's modulus value of cells was calculated following the formula $F=2/\pi \times \tan(\alpha) \times E/(1-v2) \times d2$, in which d means the depth of indentation, α means the half of tip angle, and v equals 0.5. To avoid cell damage, d was set up below 500 nm. The elastic value of cells was obtained in the perinuclear area, since the outliers may be collected at the cell periphery of well-spread cells resulting from the potential effect of substrate. At least 100 force curves collected from randomly selected cells without cell-cell contact were used to evaluate the cell stiffness of each group.

3.19 Hyaluronic acid (HA) hydrogel preparation

For synthesis of methacrylated hyaluronic acid (MeHA), the solution of sodium hyaluronate at the ratio of 1 wt % was prepared with deionized water (DI water). Dropwise addition of methacrylic anhydride (MA) (2 mL per gram HA) at 4 °C was performed with stirring and maintained at pH 8.5 through the continuous addition of 2 M NaOH solution for ~8 h. Next, followed by further addition of MA (2 mL per gram HA) was added and pH was maintained at pH 8.5 for ~4 h and then overnight at 4 °C. After dialyzing against NaCl solution and DI water for 2 days, MeHA was frozen at -80 °C, subsequently lyophilized and finally stored at -20 °C as powder.

For cell encapsulation, HA hydrogel solution was prepared to a final concentration of 2 wt % MeHA and 0.5% wt Lithium phenyl-2,4,6-trimethyl-benzoyl phosphinate (LAP) photo-initiator in PBS. And cells were harvested and resuspended in full culture medium at 2×10^6 cells/ml. HA hydrogel solution was mixed well with the medium containing cells at a 1:1 ratio, following exposure to the 365-nm UV light for 1 min. The polymerized HA gel was placed on 96 well culture plate and soaked with the full culture medium.

3.20 Dot blot assay

Cells were seeded at a density of 2×10^5 cells per well in a six-well plate and allowed to grow for 24 h, at which time 100 μL of supernatant medium was used to place on a nitrocellulose membrane (Millipore) with a 0.45-μm pore size and allowed to adsorb for 1 h at room temperature. After aspiration of the remaining liquid, the membrane was blocked for 1 h with 5% dry milk in 0.1% Tween-TBS (TBST) followed by overnight incubation with an anti-SERPINB2 antibody (1:500 in blocking solution; Abcam, cat. no. 47742) at 4 °C. After washing thrice with TBST for 5 min, the membrane was incubated with an anti-rabbit horseradish peroxidase-coupled IgG (1/2000 in blocking

solution) for 1 h, and repeated the washing steps. After that, ECL solution was used to detect signal.

3.21 Animal experiments

Cell Preparation

Cells were trypsinized at 80-90% confluence and then mixed with 10 ml ice-cold DMEM containing 10% FBS, centrifuged at 200 x g for 5 min. The cells were resuspended 10 ml ice-cold PBS and counted. After being Centrifuged, cells were resuspended at 1×10^6 cells /ml (intracardiac injection) or at $2x10^4$ cells /3 µl (intracerebral injection) in 1% bovine serum albumin (IgG-free) in ice-cold PBS. The mixture was incubated on ice and mixed gently by finger flicking before injection. Female BALB/c nude mice aged 6-8 weeks were used in the experiments.

Intracardiac injection

Mice were anesthetized by intraperitoneal injection with (8.7 mg of ketamine + 1.3 mg of xylazine)/100 g. Each mouse was placed on its back with the chest facing up. The chest was washed with iodine swabs and then 70% ethanol, repeat 2 times. The injection site was chosen in the middle between the sternal notch and the top of the xiphoid process, and on the left side of the sternum (anatomical position) and marked with a sterile marker. A small bubble was drawn up in a 1 ml 27 g½ insulin syringe to create a space between the plunger and the meniscus for observing the heartbeat, and 100µl of cells was drawn up. The needle was kept upright and inserted while holding the skin of the mouse with the other hand. Successful insertion into the left ventricle should produce a distinct bright red pulse in the syringe. At this depth, the plunger of the syringe should be carefully pressed without moving the needle significantly, so as not to pierce the heart or spill cells into the chest cavity. After injection, the needle was

pulled straight out of the chest while making sure to avoid tilting the needle during removal. The chest was applied light pressure at the injection site to reduce bleeding. The mouse was moved to the heating pad until fully conscious.

Intracerebral injection

All surfaces of the surgical area were sprayed with 2% chlorhexidine solution for disinfection. The mouse stereotaxic frame, the alignment console and the micro-syringe pump (Harvard Apparatus, 11 Elite Nanomite), the heating pad, the fiber optic work light and the variable speed rotary drill are all installed and disinfected. The 26 G precision micro-syringe (Hamilton) is rinsed with sterile deionized water (diH_2O) and 70% ethanol (EtOH) several times, and finally rinsed with diH_2O. Mice were anesthetized by intraperitoneal injection with (8.7 mg of ketamine + 1.3 mg of xylazine)/100 g. After anesthetizing the mouse, the mouse was placed in the stereotaxic frame and fixed. During the operation, eye ointment should be used to keep the mice's eyes moist enough. The scalp was wiped several times with a sterile gauze soaked in chlorhexidine solution. Using a sterile scalpel, a sagittal incision over the parieto-occipital bone was completed approximately 1 cm long. The exposed skull surface was then cleaned using a cotton swab soaked in a 3% hydrogen peroxide solution. The micro-syringe was positioned directly over the bregma after the micro-syringe was secured onto the micro-pump. And then the coordinate settings on the calibration console were zeroed. Prior to tumor cell injection, control knobs on the stereotaxic unit and a sterile variable speed rotary drill were used to puncture the skull at 2 mm to the right of the bregma and 1 mm anterior to the coronal suture, thereby creating an opening for the injection of tumor cells. With the use of a cotton swab dipped in PBS, the bone powder was cleaned. To verify position, the needle was lowered vertically down to the hole for the injection. The hole was made larger with the drill if the hole was not centred with the needle. The cell suspension was gently mixed and drawn into the syringe using the pump controller while avoiding bubbles and clumps. The needle was inserted slowly

into the depth of 4mm. The injection parameters (Injection volume: 3µl, Injection rate: 0.25 µl/min) were entered into the pump controller and the "RUN/STOP" button was pressed to auto-inject cells. After being in the brain for one to two minutes, the needle was gently removed from the tissue (over the course of three to four minutes). Using forceps, the scalps were drawn together over the skull and sutured.

Imaging

Mice were injected intraperitoneally with 300µl 25 mM D-luciferin sodium salt (Abcam) in DPBS (Hyclone), anesthetized, and imaged at 20 min after injection using IVIS Lumina Series III pre-clinical *in vivo* animal imaging system (Perkin-Elmer). For ex vivo imaging of bioluminescence signals in the brain, mice were injected intraperitoneally with 300µl 25 mM D-luciferin and then sacrificed with sodium pentobarbital. Brains were removed and placed in separate wells of 12 well-plate. Images were captured at 1 min after 1ml 300 µg/ml D-luciferin was added into each well to cover the tissue.

3.22 Immunofluorescence staining

Cells were fixed with pre-cold 4% PFA for 20 min at room temperature, followed by permeabilization with 0.3% Triton X-100 in PBS for 20 min. After being washed with PBS, cells were blocked with 1% BSA, 22.52 mg/mL glycine in PBST (PBS+ 0.1% Tween 20) for 1 h at room temperature. Cells were then incubated with diluted primary antibodies in 1% BSA in PBST overnight at 4°C, washed 3 times with PBST for 5 min each time and incubated with diluted second antibodies in 1% BSA in PBST at room temperature. After decanting the solution and washing cells 3 times with PBST, nuclei were stained with DAPI. The imaging of cells was performed with the confocal microscope (Leica, TCS SPE) at 40× and 63× objectives. For F-actin staining, CytoPainter F-actin labeling kit (Abcam, cat. no. ab112125) was used following the

user guidebook. Images were taken using the confocal microscope or the inverted fluorescence microscope. Quantification of fluorescence intensity was analyzed with ImageJ software.

For the staining of brain slice, mice were sacrificed after anaesthetized and then immediately perfused with PBS and 4% PFA and fixed overnight at 4℃. The section of the brain into 40 μm or 80 μm was performed using vibrating microtome (Leica, VT1200S). The prepared brain slices were treated with blocking buffer (0.3% Triton X-100, 5% goat serum in PBS) for 1 h at room temperature. After then, the brain slices were incubated with primary antibodies diluted in blocking buffer overnight at 4℃ with or without 10 μg/ml Lectin-DyLight 649 (ThermoFisher, cat. no. L32472). Following extensive washing 3 times with PBS, the fluorophore-conjugated second primary antibodies were diluted in blocking buffer and incubated for 2 h at room temperature. After nuclei were stained, the brain sections were scanned or visualized with the inverted fluorescent microscope and confocal microscope utilizing 10×, 20× and 40× objectives. For 3D reconstruction, confocal images were captured every 2-μm interval for a total of 60 μm maximum at depth. Image J was used to analyze images. Imaris was used to generate 3D reconstruction images.

The primary antibodies used in the study are listed below: p-MLC (1:50; Cell Signaling Technology, cat. no. 3671), HDAC3 (1:500; Abcam, cat. no. ab32369), ki67 (1:200, Abcam, cat. no. ab15580), The second antibodies used in the study are listed below: Alexa Fluor 594 Goat Anti-Mouse IgG H&L (1:400, Abcam, cat. no. ab150116), Alexa Fluor 647 Goat Anti-Mouse IgG H&L (1:400, Abcam, cat. no. ab15011).

3.23 Traction force microscope

The traction force of cells was measured following the protocol reported by previous studies[162, 232]. Briefly, amino-silanated glass bottom of the confocal dish (NEST

Scientific) and PA gel solution were prepared referring to PA gel preparation and 0.2-μm diameter red fluorescence microspheres (Invitrogen, cat. no. F8763) were embedded into the top layer of PA gel. Cells were implanted on the PA gels and incubate for 24 h. The prestressed state of PA gel was captured by the inverted fluorescence microscope with a 20× magnitude at the red fluorescence channel and the boundary of cells was recorded by changing the imaging model to bright-field without moving the microscope stage. After that, cells were lysed by adding TRK lysis buffer (Omega, cat. no. PR021) carefully and gently and then the image of microspheres beneath the cell was captured to stand for the null-stress state of PA gel. Images of prestressed and null-stress states were utilized to confirm the displacement maps of microspheres due to cellular contractility. According to the displacement map, the value of cell traction force was computed using the inverse Boussinesq mathematical model-based MATLAB algorithm.

3.24 Chromatin condensation parameter (CCP) measurement

To assess chromatin condensation, cells seeded on the corresponding substrate for at least 24h were fixed in pre-cold 4% PFA for 15min at room temperature. After being washed three times with PBS, nuclei were visualized by DAPI and imaged at their mid-section using confocal microscopy with 63× objectives. The gradient-based Sobel edge detection algorithm in MATLAB was used to process images to produce an edge map and calculate edge density standing for the CCP, as described in the previous study [233]. In order to reduce the impact of different fluorescence intensities of each nuclear image, after converting the image to an 8-bit image, the intensity of each pixel of the image was divided by the highest intensity of the image and multiplied by 255. Gradient-based Sobel edge detection algorithm was conducted to find the hasty reduction in intensity or strong edges associated with the degree of chromatin condensation. The thinning morphological algorithm was processed to count the number of sharp edges in the nucleus. The CCP of nuclear was calculated by dividing the number of edges by the

area of nuclear. The images of heterochromatin regions in the nucleus were obtained following the adjusted threshold method reported by the previous study [234]. The formula: Mean of (0.4× max) and min + (0.35 (max-min)) was used to compute the adjusted threshold of heterochromatin, where max and min stand for the maximum and minimum value of the pixel intensity of images respectively. After being processed, images of heterochromatin were converted into green color and then stacked with nuclear images converted into red color. All the image processing was conducted by Image J.

3.25 HDACs activity measurement

HDACs activity of cells was measured using in situ HDAC activity fluorometric assay kit (EPI003, Sigma-Aldrich) following the provided technical bulletin. 5×10^4 cells/well were seeded in a 24-well plate with or without PA gels. After 24 h incubation, the spent medium was deposited and 300 μl reaction mix was added to each well. Once 2-hour incubation at cell incubator was completed, 300 μl developer solution was added following incubation for 30 min at cell incubator. The supernatant was transferred to the black plate with transparent bottom and the fluorescence at Ex/Em = 368/442 nm was detected using the Varioskan LUX multimode microplate reader (Thermo Fisher).

3.26 Pharmacologic Treatment

For the pharmacologic treatment of cells, cells grew to 50~70% of confluency and were then treated with 2 or 6 μM Y-27632 (Selleck Chemicals), 2 or 6 μM blebbistatin (Sigma-Aldrich), 2 μM Vorinostat (SAHA; Selleck Chemicals), 50 μM anacardic acid (ANA; Selleck Chemicals), 100 nM trichostatin A (TSA; MedChemExpress),0.1 or 0.3 μM cytochalasin D (CytoD; Tocris Bioscience), 5, 10 or 50 nM narciclasine (Narci; Selleck Chemicals), 30 or 100 nM jasplakinolide (Jas; Selleck Chemicals), and 1μM or 10 μM RGFP966 (MedChemExpress) for indicating time. In accordance with the

manufacturer's recommendations, all of the compounds were dissolved in DMSO to obtain the stock solution, which was then adjusted with the full culture medium to get the working solution. DMSO as the vehicle was chosen for the treatment of the control group.

For the invention trial, mice were inoculated with 231-0.6 kPa cells via cardiac injection and treated every two days from day 0 with the vehicle, 10 mg/kg or 40 mg/kg of RGFP966 intraperitoneally. RGFP966 was dissolved in the vehicle (10% DMSO, 45% PEG 400 in H_2O).

3.27 siRNA, plasmids and transfection

Small-interfering RNA (siRNA) and plasmids were transfected using Lipofectamine 3000 based on the kit-supplied protocol (Invitrogen). In general, cells were trypsinized and seeded to be 70%-80% confluent on the day of transfection. Lipofectamine 3000 reagent was mixed well with Opti-MEM reduced serum medium (Gibco) at a suggested ratio. Next, siRNA or plasmid was diluted in Opti-MEM reduced serum medium with or without P3000 reagent following the protocol. The diluted siRNA or plasmid was mixed with prepared lipofectamine 3000 at equal volume and added to cells after incubation for 15 minutes at room temperature. All the siRNAs were designed and produced by General Biosystems, and the efficiency of siRNA was verified by qPCR. HDAC3-Flag plasmid (#13819) was purchased from Addgene.

3.28 Lentiviral transduction and stable cell line establishment

For lentivirus packing and production, 293T cells were cotransfected with the target plasmid， 2nd generation lentiviral packaging plasmid psPAX2 (Addgene, cat. no. 12260) and VSV-G envelope expressing plasmid pMD2.G (Addgene, cat. no. 12259)

by using Lipofectamine 3000. Culture supernatant containing virus was collected at 48 h and 72 h post-transfection. Then, the collected supernatant was filtered by a 0.45 μm polyethersulfone filter and concentrated with the universal virus concentration kit (Beyotime, cat. no. C2901S). Tumor cells were transduced via adding concentrated lentiviruses reagent into the completed medium supplied with 8 μg/mL polybrene overnight. After 48 h, stable cell lines were selected with 500 μg/ml G418 (Sigma-Aldrich) or 2 μg/ml puromycin (MedChemExpress) according to the target plasmid and then further sorted by using FACSAria III Cell Sorter (BD).

Plasmids: pLV-mCherry: T2A: Puro-EF1A>hHDAC3 (VectorBuilder), pLV-mCherry/Puro-EF1A>ORF (VectorBuilder), pinducer 20 DN-KASH (Addgene, cat. no. 125554), pinducer 20 DN-KASHΔPPPL (Addgene, cat. no. 129280).

3.29 Statistical Analysis

All the data are reported as mean ± SEM of at least 3 independent repeats. Statistical analysis was carried out using the unpaired two-tailed Student's t-test for comparisons between the two groups. To analyze the comparisons among multiple groups, one-way ANOVA with a relevant post hoc test was adopted. Statistical differences in the Kaplan-Meier curves were analyzed utilizing the log-rank test. All statistical analyses were conducted by using GraphPad Prism 8.0 software and statistical significance was defined as a P value less than 0.05.

Chapter 4: The influence of matrix softness on breast cancer brain metastasis

4.1 Introduction

Cancer is the leading cause of human mortality. Globally, there were approximately 19.3 million new cancer cases and 10 million cancer-related deaths in 2020 [24]. Breast cancer accounted for approximately 2.3 million new cases, making it the most prevalent type of cancer in 2020 and causing approximately one in six deaths in women with cancer [24]. Metastasis is the cause of more than 90% of cancer deaths, and the process involves cancer cells spreading through the circulatory system after shedding from the initial lesion, arresting at blood capillaries, penetrating through vascular endothelium, and colonizing distant organs to develop into metastases [33]. Clinical studies indicate that carcinoma cell metastasis has metastatic tropism. Different cancer types and subtypes prefer to metastasize to specific distant organs, which is known as metastatic organotropism. For example, prostate cancer mainly metastasizes to bone, uveal melanoma metastases to the liver, and major target organs of breast cancer include bone, lung/liver, and brain [52, 235, 236]. Brain metastases are present in around 20% of cancer patients, more frequently in those with breast, lung, colorectal, and skin cancers [237], and 90% of tumors in the CNS are brain metastases, which occur in 10- 30% of patients with metastatic breast cancer [5, 101]. Neurological dysfunction and poor outcomes are frequently caused by brain metastasis. The median survival (MTS) of patients with brain metastases is 11 months, much lower than those with bone metastases (31 months), lung metastases (20 months), and liver metastases (19 months) [238]. The poor survival and outcome necessitate improved prevention and therapy for patients with brain metastasis. However, little is known about the mechanisms underlying brain metastasis derived from breast cancer. Therefore, identifying underlying critical factors of brain metastasis is vital for the development of novel therapeutic strategies to prevent and target brain metastasis.

Tumor metastasis requires the synergistic encounter between tumor cells and the microenvironment of the target organ, of which underlying mechanisms refer to the "seed-soil" theory [3]. As the seeds of metastasis, tumor cells are vital to the development

of metastasis. Cancer cells in primary lesions are heterogeneous, which means not all cancer cells can metastasize, and different subpopulations of cancer cells may prefer to metastasize to different organs, such as breast cancer cells with specific gene expression signatures that specifically metastasize to the brain [52, 65]. The target organ microenvironment, as the soil of metastatic cells, plays a double-edged role in metastasis. In the target organ, there are both favorable factors that promote metastasis, such as fibroblasts, growth factors, and chemokines, as well as unfavorable factors inhibiting colonization of tumor cells, such as immune cells [239]. The target organ microenvironment is crucial for tumor brain metastasis, including the BBB, plasmin, exosomes, microglia, and the hypoxia and hypoglycemia characteristics of the brain [113].

In addition to these biochemical factors, the role of matrix stiffness, as a key component of the mechanical microenvironment, has become increasingly prominent in cancer development and metastasis [7]. The transformation process of reprogramming normal cells into tumor precursor cells requires high matrix stiffness [240]. Matrix stiffness stimulates the expression of migration-related genes by the transcriptional regulator YAP/TAZ, resulting in the promotion of tumor metastasis [196]. As a result of Netrin-4 decreasing the stiffness of the basement membrane, tumor cells are less likely to penetrate the membrane and metastasize, indicating that the stiffness of the basement membrane determines the generation of metastatic tumors [35]. These findings demonstrate that matrix rigidity enhances tumor cell metastatic potential and facilitates tumor metastasis. Notably, a number of other studies report a link between low tumor stiffness and tumor recurrence and metastasis [241]. Soft fibrin gels enhance tumorigenicity and metastatic properties of melanoma [162]. Soft matrices enable ovarian cancer cells to migrate and invade [242]. Therefore, microenvironment stiffness affects the metastatic capacity of tumor cells. Meanwhile, the influence of matrix rigidity is less well understood on metastatic preference and brain metastatic ability. Through Iβ3/TGF-β, the rigid matrix impacts gene expression and promotes transition of tumor cells to an osteoclastic phenotype [243]. Exposed to stiff substrate induces RUNX2-

mediated mechanical memory and promotes osteolytic bone metastasis of breast cancer cells [244]. Moreover, Breast cancer cells with metastatic tropism exhibit enhanced cell proliferation and migration on correspondingly substrates with the stiffness of the targeted organ [245]. Breast cancer cells experience mechanically heterogeneous primary tumor tissues with local stiffness up to dozens of kilopascal and disseminate into the brain with low tissue stiffness (0.1-1 kPa) compared to bone (25-40 kPa), lung, and liver (2-7 kPa) [19, 230]. Rarely has the effect of low brain tissue stiffness on brain metastases been reported: soft brain tissue inhibits DNA methyltransferase 1, thereby promoting tumor cell survival, but inhibits their proliferation, and low stiffness of brain tissue can induce tumor cells to enter a dormant state [10, 246]. In summary, it is suggested that microenvironmental stiffness affects the metastatic ability of tumor cells and is associated with metastatic tropism, but the effects of matrix softness of local soft niches within breast tumor and brain tissue on breast cancer brain metastasis remain not well understood. In this chapter, we investigated the effect of matrix softness on brain metastasis of breast cancer cells, demonstrating a direct role of the mechanical microenvironment in regulating metastatic organotropism.

4.2 Results

4.2.1 Long-term culture on soft substrates induces a gene expression profile reminiscent of brain metastasis in breast cancer cells

In primary breast tumor, the distribution of tissue stiffness is highly heterogeneous, ranging from 0.4-50 kPa, even though the average stiffness is around 4 kPa [19, 156, 247]. To investigate the effect of matrix softness on the brain metastasis ability of breast cancer cells, 0.6 kPa and 35 kPa collagen I (Col-I)- coated polyacrylamide (PA) hydrogels were adopted to mimic the regions in breast tumor with extremely low stiffness (close to brain tissue) and high stiffness (close to bone matrix) [230]. Parental MDA-MB-231 cells (denoted as 231) and the derivatives with the preference to

metastasize to the brain (MDA231-BrM2-831, denoted as 231-BrM) and bone (MDA-BoM-1833, denoted as 231-BoM) were used as negative control and positive control cell line, respectively [65, 70]. Recent studies have reported mechanical memory, which indicates some cells retain information about matrix stiffness and maintain some gene expression patterns and behaviors for a long period against acute changes caused by substrate switching [244, 248]. To avoid the potential mechanical memory induced by TCP, plastic-tolerant 231 cells were cultured on 0.6 kPa and 35 kPa PA gels for 10 passages (3 days per passage, 30 consecutive days). After more than 10 passages prior to adaptive treatment on 0.6 kPa and 35 kPa PA gels, 231 cells were named as 231-0.6 kPa and 231-35 kPa respectively (Fig. 4.1A). The expression levels of genes associated with brain or bone metastasis that have been reported previously were measured at 1 passage (P1), P2, P5 and P10 [65, 70, 75, 249]. The data showed that most genes that are positively correlated with brain metastasis were not changed significantly after 231 cells were cultured on soft substrates for one or two passages. Intriguingly, the majority of brain metastasis-related genes (13/18) were gradually up-regulated at P5 and P10 in cells on the soft but not stiff matrix (Fig. 4.1B). To further validate the founding, we conducted transcriptomic profiling in 231, 231-0.6 kPa and 231-35 kPa cells by RNA-sequencing (RNA-seq). Similarly, RNA-seq data showed that the expression levels of most genes associated with brain metastasis were higher in 231-0.6 kPa cells than in 231 or 231-35 kPa cells (Fig. 4.1C and D). Moreover, not only qPCR data but also RNA-seq data showed that the expressions of most bone metastasis-related genes were down-regulated at 231-0.6 kPa cells compared with 231 or 231-35 kPa cells (Fig. 4.1E, F and G). The expression levels of brain metastasis-associated genes were not further increased by 60 days of priming on soft matrices as compared to 30 days of priming on soft matrices. (Fig. 4.2A).

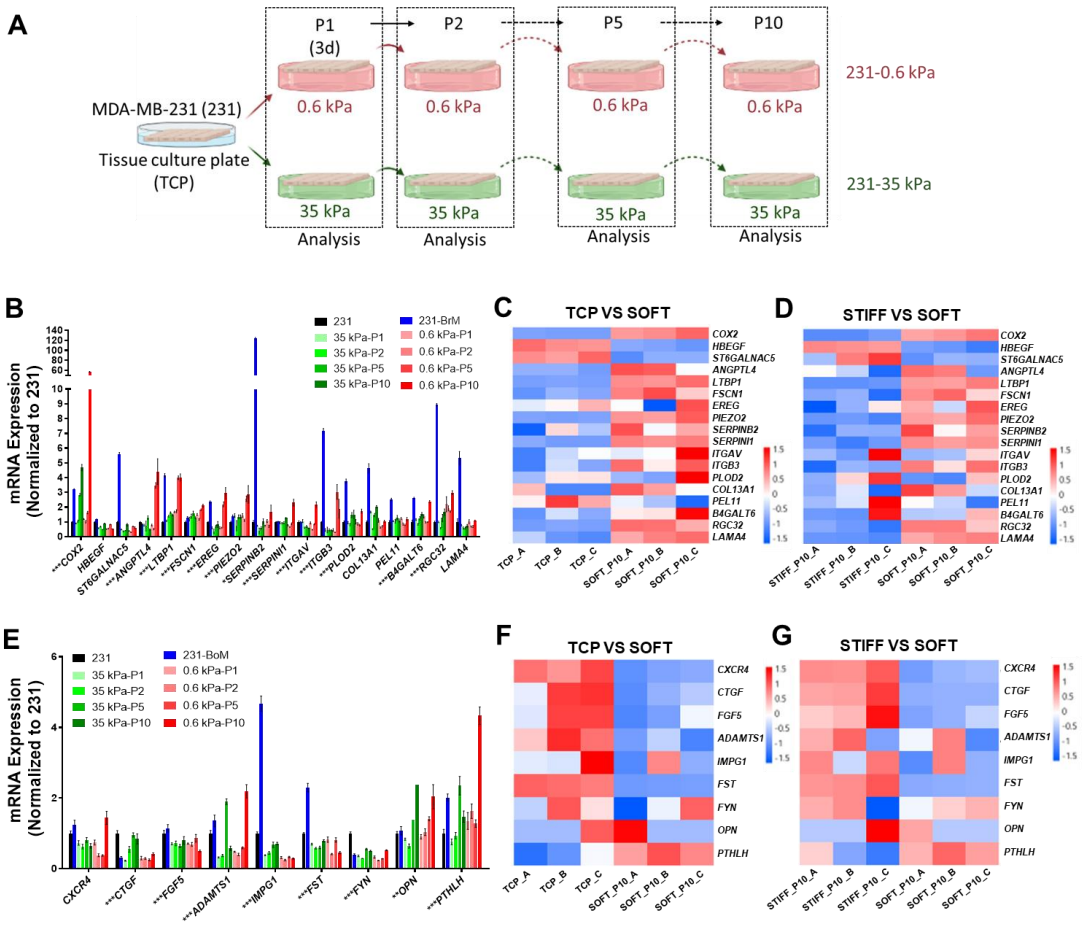

Figure 4.1 Long-term soft substrate culture increases the expression of brain metastasis-related genes in breast cancer cells. (A) Scheme of the mechanical priming set-up. MDA-MB-231 (231) cells were cultured on 0.6 kPa and 35 kPa polyacrylamide (PA) gels coated with collagen for 10 passages (3 days/passage, 30 consecutive days). Total RNA samples were collected at P1, P2, P5, and P10 after priming, and the expression levels of (B) the brain metastasis-related genes and (E) the bone metastasis-related genes were measured by quantitative PCR (qPCR). The cells after long-term culture on corresponding PA gels were termed as 231-0.6 kPa and 231-35 kPa, respectively. The RNAs extracted from 231, 231-0.6 kPa and 231-35 kPa cells were analyzed by RNA-seq. (C-D and F-G) Heatmaps of RNA-Seq analysis show the expression of genes associated with brain metastasis and bone metastasis. The gene expression levels from low to high are represented by pseudo-colors ranging from blue to white to red. N=3; the data = mean ± SEM. Significance of 231 group versus 0.6 kPa-P10. *, $p < 0.05$; **, $p < 0.01$; and ***, $p < 0.001$.

Then we tested whether the changes in gene pattern were dependent on ligand type for coating substrate, fibronectin (FN)-coated PA gels were used to precondition 231 cells up to P10. Soft-primed cells at P10 also showed the gene expression pattern favoring

brain metastasis, which was similar to cells on Col-I coating soft PA gels at P10 (Fig. 4.2B). To further exclude the possibility that the observed transcriptional changes are driven simply by random genetic drift, we compared the expression of brain metastasis-related genes of 231 cells at P10 and P0 on TCPs. The data showed that the changes in gene profile related to brain metastasis were not similar to the changes on soft/stiff substrates and few of these genes were increased, suggesting that the enhanced expression of genes associated with brain metastasis was induced by matrix softness rather than the genetic drift following long-term culture on the soft matrices (Fig. 4.2C). Furthermore, we examined whether the increase in expression levels of brain metastasis-related genes is cell line-dependent. 4T1 cells, the murine mammary carcinoma cells, were preconditioned on 0.6 kPa and 5 kPa PA gels for 10 passages. A significant increase in the expression of genes involved in brain metastasis was also observed in 4T1 cells following long-term priming on soft matrices (Fig. 4.2D). Collectively, these data suggested that long-term culture on soft matrices induced the gene expression pattern favoring brain metastasis, which was independent of ligand type, gene drift and cell type.

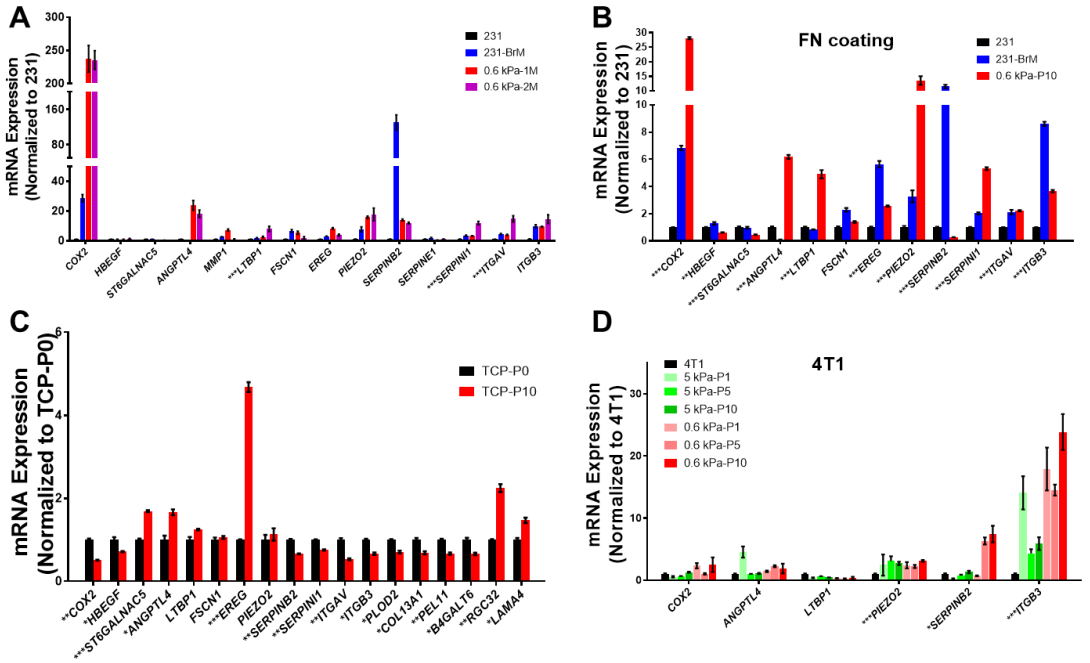

Figure 4.2 Soft matrix-induced expression pattern of brain metastasis-associated genes is independent of ligand type, gene drift and cell type. (A) 231 cells were

cultured on 0.6 kPa PA gels for 1 month (1M) and 2 months (2M), which were termed 0.6 kPa-1M and 0.6 kPa-2M cells respectively. Statistical differences between 0.6 kPa-1M group and 0.6 kPa-2M group are shown. (B) 231 cells were cultured on PA gels coating with fibronectin (FN) for 10 passages. Statistical differences between 231 group and 0.6 kPa-P10 group are shown. (C) 231 cells were cultured on the TCPs and the RNA was extracted (TCP-P0). After consecutive cultures on TCPs for 10 passages (TCP-P10), the RNA was collected. (D) 4T1 cells were cultured on 0.6 kPa and 5 kPa PA gels for 10 passages. Total RNA samples were collected at P1, P5 and P10. The total RNA samples from corresponding cells were analyzed by qPCR to measure the expression levels of brain metastasis-related genes. Statistical differences between 4T1 group and 0.6 kPa-P10 group are shown. N=3; the data = mean ± SEM; *, $p < 0.05$; **, $p < 0.01$; and ***, $p < 0.001$.

4.2.2 Transcriptomic profile of soft niches-primed breast cancer cells displays neural characteristics

To ascertain the changes of transcriptional signature in 231-0.6 kPa cells, we conducted a comprehensive transcriptomic analysis based on RNA-seq data. Comparing 231-0.6 kPa cells to 231 or 231-35 kPa cells, differential expression analysis identified upregulated and downregulated differentially expressed genes (DEGs) by more than two-fold at a 0.05 adjusted P value (Padj) (Fig. 4.3A and F). Brain metastatic tumor cells usually exhibit neuronal mimicry, which means tumor cells can gain some neural signatures to survive and outgrow in brain tissue [96, 250, 251]. Notably, gene ontology (GO) over-representation analysis (ORA) of upregulated DEGs were enriched in neuronal-like pathways, such as ‘cell morphogenesis involved in neuron differentiation’, ‘axon development’ and ‘regulation of neuron projection development’ (Fig. 4.3B and G). Overall gene set enrichment analysis (GSEA) also showed diverse biological process pathways associated with the CNS were enriched significantly (Fig. 4.3C and H). Moreover, PaGenBase enrichment analysis showed up-regulated DEGs in 231-0.6 kPa cells were mainly enriched in brain cell (cell-specific) (Fig. 4.3D and I). DisGeNET was then utilized to assess upregulated DEGs for their approximate association in disease-gene networks. Strikingly, enrichment of upregulated DEGs in 231-0.6 kPa cells could be linked to the gene features of diverse brain tumors, even brain metastatic

tumor (Fig. 4.3D and J). Taken together, these results indicated that matrix softness induced the transcriptomic characteristic of neuronal mimicry and imply that preconditioning on soft matrices might confer brain metastasis ability to tumor cells.

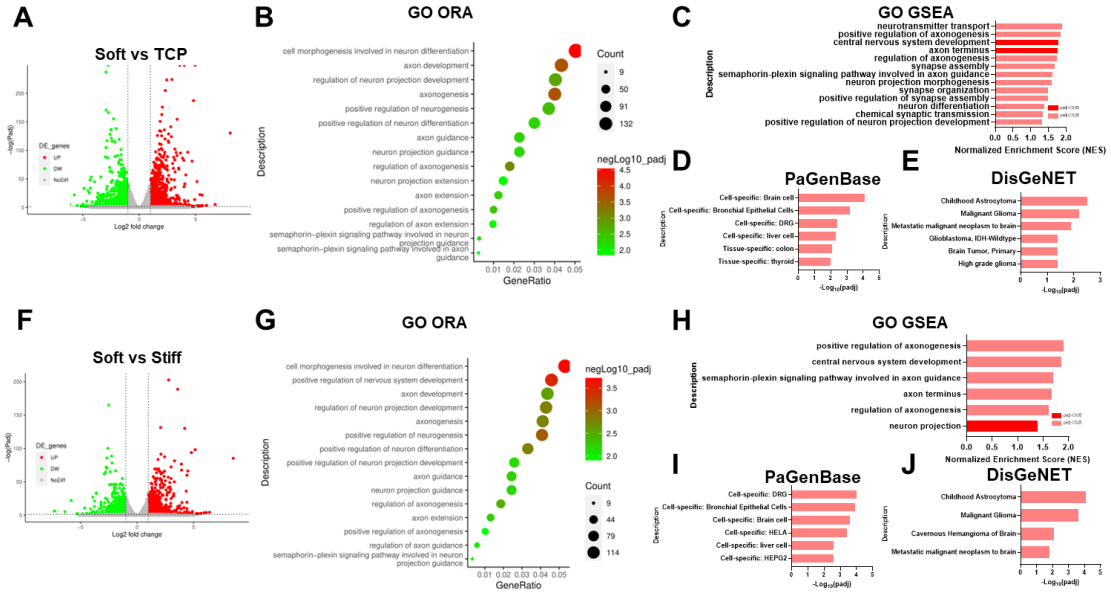

Figure 4.3 Molecular Features of 231 cells cultured on the soft matrices for long term. Volcano plots for differentially expressed genes (DEGs) in 231-0.6 kPa cells versus (A) 231 cells on TCPs or (F) 231-35 kPa cells, as determined by RNA-seq. DEGs were filtered by Padj < 0.05 and |log2fold change| > 1. Genes are colored, with red indicating high expression and green indicating low expression in 231-0.6 cells. The Grey color represents all genes not changing between two groups. Cleveland plot for gene ontology (GO) over-representation analysis (ORA) of up-regulated genes in 231-0.6 kPa cells versus (B) 231 cells on TCPs or (G) 231-35 kPa cells. Significantly enriched neuronal-like pathways are shown in the diagram (Padj < 0.05). Gene set enrichment analysis (GSEA) of DEGs in 231-0.6 kPa cells versus (C) 231 cells on TCPs or (H) 231-35 kPa cells. Significantly enriched neuronal-like terms from GO are shown (normalized enrichment score (NES > 1), Padj < 0.25). Significantly enriched terms associated with brain tumors are shown (Padj < 0.05). PaGenBase enrichment analysis of up-regulated genes in 231-0.6 kPa cells versus (D) 231 cells on TCPs or (I) 231-35 kPa cells. DisGeNET enrichment analysis of up-regulated genes in 231-0.6 kPa cells versus (E) 231 cells on TCPs or (J) 231-35 kPa cells. Top enriched terms are shown (Padj < 0.05).

To further confirm whether adaptive transcriptomic signature induced by soft matrix was cell-type dependent, we obtained RNA-seq data from data set GSE1278887

uploaded in Gene Expression Omnibus (GEO), in which SUM159 breast cancer cells were preconditioned for 2 weeks on 0.5 kPa and 8 kPa hydrogel coated with Col-I before RNA extraction [244]. Analogously, global gene expression in 231-0.6 kPa cells was significantly different from that in soft niches-primed cells (Fig. 4.4A). Similar results were obtained in ORA analysis and GSEA, which show significant enrichment in CNS-associated pathways (Fig. 4.4B and C). SUN159 cells preconditioned by soft matrix also showed gene characteristics similar to brain cell (Fig. 4.4D). In addition, upregulated DEGs were preferentially enriched in the terms associated with brain tumors (Fig. 4.4E). In light of these findings, we prioritized brain metastasis as a matrix softness-induced consequence of cancer cells capable of metastasizing.

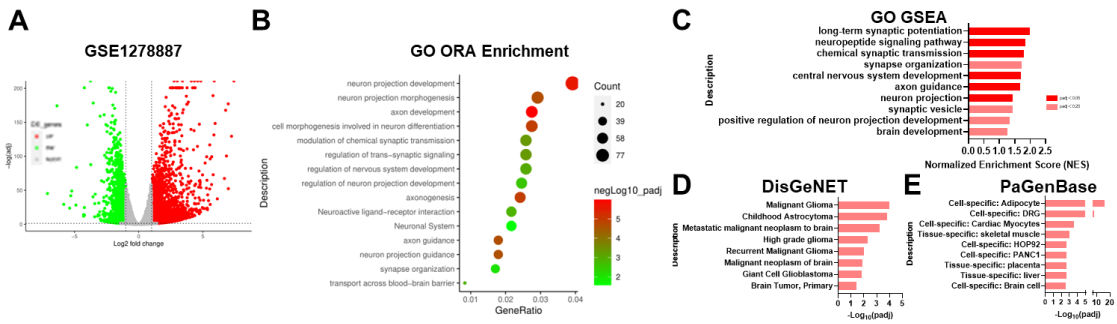

Figure 4.4 Molecular Features of SUM159 cells cultured on the soft matrices for long term. The RNA-seq data of GSE1278887 was queried from the Gene Expression Omnibus (GEO). In this study, breast cancer SUM159 cells were cultured on 0.5 kPa or 8 kPa collagen I-coated hydrogels for 2 weeks. The extracted RNAs were analyzed by RNA-seq. (A) Volcano plots for differentially expressed genes (DEGs) in cells on 0.5 kPa versus cells on 8 kPa. DEGs were filtered by Padj < 0.05 and |log2fold change| > 1. Genes are colored, with red indicating high expression and green indicating low expression in cells on the soft matrices. The Grey color represents all genes not changing between the two groups. (B) Cleveland plot for gene ontology (GO) over-representation analysis (ORA) of up-regulated genes in cells on 0.5kpa versus cells on 8 kPa. Significantly enriched neuronal-like pathways are shown in the diagram (Padj < 0.05). (C) Gene set enrichment analysis (GSEA) of DEGs in cells on 0.5 kPa versus cells on 8 kPa. Significantly enriched neuronal-like terms from GO are shown (normalized enrichment score (NES) > 1, Padj < 0.25). (D) DisGeNET enrichment analysis of up-regulated genes in cells on 0.5kpa versus cells on 8 kPa. Significantly enriched terms associated with brain tumors are shown (Padj < 0.05). (E) PaGenBase enrichment analysis of up-regulated genes in cells on 0.5 kPa versus cells on 8 kPa. Top enriched terms are shown (Padj < 0.05).

4.2.3 Soft niches-primed cells show advantages in the survival within circulation system, adhesion on brain endothelium, and transmigration through brain-blood barrier

To establish overt brain macrometastases, disseminated tumor cells must overcome each of the necessary metastatic steps, including survival in the circulation system, intravascular arrest in the brain, penetration through the BBB and outgrowth in the brain microenvironment [237]. To investigate whether matrix-softness priming induced brain metastasis, we systematically examined the influence of matrix softness on the whole brain-metastatic processes of tumor cells *in vitro*. After intravasation into the circulation, circulating tumor cells are required to resist anoikis under a suspension state and survival in shear force caused by blood flow. 20 dyne/cm^2 hemodynamic shear flow produced by a microfluidic circulation system was used to mimic the shear stress level in brain capillaries [252]. The data showed that the viability of 231-0.6 kPa cells was significantly higher than 231 cells not only under suspension but also under shear stress (Fig. 4.5A and B). 231-BrM cells also showed resistance to shear force, whereas 231-35 kPa cells exhibited similar cell viability to 231 cells under both statuses.

Then, we evaluated the adhesion ability of tumor cells on the endothelial layer consisting of the human cerebral endothelial cell line. The results showed that compared to 231 cells, cell adhesion on brain endothelium only was increased in 231-0.6 kPa cells but decreased in 231-35 kPa cells at the time point of 15min. Extending the incubation time to 30min, all the cells showed a similar brain endothelium adhesion outcome except 231-35 cells showed a worse adhesion outcome (Fig. 4.5C-E). Then the cell spreading on the brain endothelial layer was measured at 30min. We found 231-BrM cells exhibited significantly higher cell spreading area than other cells, indicating their better cooperation with brain blood vessels (Fig. 4.5C and F). In contrast, soft matrix priming had no influence on cell spreading and even decreased the aspect ratio of tumor cells on human brain microvascular endothelial cells (Fig. 4.5C, F and G). Of note, the results showed that soft priming did not affect the adhesion ability on the human umbilical vein endothelial cell layer, which implied that the soft preconditioning

specifically enhanced brain endothelial adhesion ability of tumor cells (Fig. 4.5H and I).

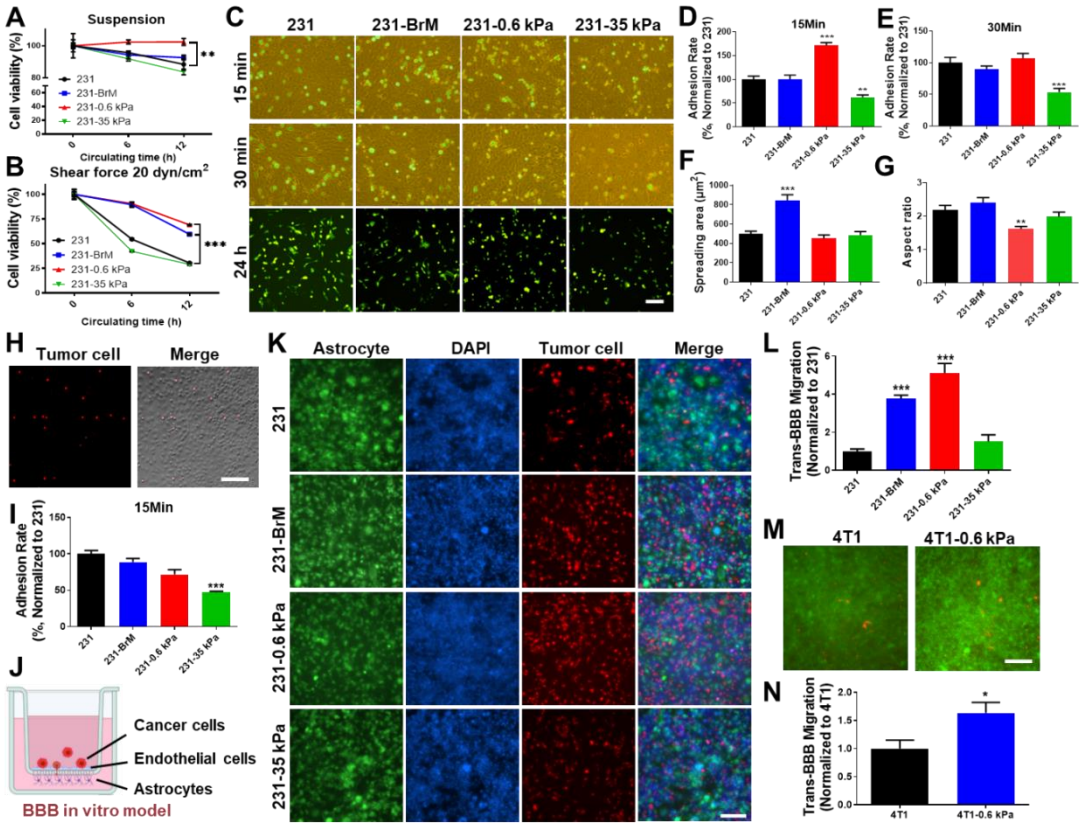

Figure 4.5 Soft priming enhances survival in circulation, cerebral endothelium adhesion and blood-brain barrier transmigration of 231 cells *in vitro*. The viability of suspended cells under suspension (A) or 20 dyne/cm^2 shear flow (B) for different times were measured by MTS assay. (C) Tumor cells were stained with cell tracker (green) and seeded on cerebral endothelial layer. After 15 min, 30 min and 24 h, the wells were washed with PBS for 3 times and imaged. The representative images were presented. Scale bar, 100μm. (D-E) Quantification of the tumor cell adhesion rate on human cerebral endothelial layer at 15 min and 35 min. (F-G) Tumor cell spreading area and aspect ratio were measured after seeding cells on cerebral endothelial layer for 24 h. (H) Tumor cells were stained with cell tracker (red) and seeded on human umbilical vein endothelial layer. After 15 min, the wells were washed with PBS 3 times and imaged. The representative images are presented. Scale bar, 200 μm. (I) Quantification of the adhesion rate in (H). (J) Schematic diagram demonstrating blood-brain barrier (BBB) *in vitro* model constructed from human cerebral endothelial cells and EGFP-labeled human astrocytes for tumor cell transmigration assay. (K) Tumor cells were labeled with red cell tracker and imaged after seeding in the upper chamber for 48 h. Representative pictures of human astrocytes and transmigrated tumor cells are shown. Scale bar, 200 μm. (L) Transmigrated cells were visually counted using a fluorescent microscope. The number of transmigrated cells relative to 231 cells is

plotted. (M) 4T1 and 4T1-0.6 kPa cells were labeled with red cell tracker and BBB transmigration assay was performed. Representative pictures of human astrocytes and transmigrated tumor cells are shown. Scale bar, 200 μm. (N) The number of transmigrated cells relative to 4T1 cells is plotted. N=3, isolates; mean ± SEM; *, $p < 0.05$; **, $p < 0.01$; and ***, $p < 0.001$.

BBB transmigration is necessary for the initiation of brain metastases formation [65]. Therefore, we further developed an *in vitro* model of the BBB that consisted of brain microvascular endothelial cells on the upper side and astrocytes on the downside of a transwell and assessed the BBB transmigration ability of tumor cells (Fig. 4.5J). Consistent with the previous studies [65, 253], 231-BrM cells penetrated the BBB more efficiently than their corresponding parental 231 cells (Fig. 4.5K and L). Moreover, the BBB transmigration ability of soft-primed 231 cells was enhanced. We extended these results with 4T1 cell lines and, similarly, increasing BBB transmigration was observed in 4T1-0.6 kPa cells (Fig. 4.5M and N). It has been well demonstrated that cyclooxygenase 2 (COX2) is profoundly increased in 231-BrM cells and COX2-induced prostaglandins can promote dissemination of tumor cells to the brain by tampering with BBB [65, 253]. Our results showed that long-term culture on soft substrates remarkably increased the expression of COX2 in mRNA and protein level (Fig. 4.1B and 4.6A). Additionally, the amount of prostaglandin E2 (PGE2), the end product of COX2, in the supernatant was also significantly increased in 231-0.6 kPa cells (Fig. 4.6B). To further test the role of COX2 in matrix softness-induced BBB transmigration, NS398, COX2 inhibitor, was used to pretreat the cells. As shown in Fig. 4.6C, NS398 pretreatment significantly abrogated BBB transmigration ability of 231-0.6 kPa cells. Together, these data strongly suggested long-term culture on soft matrices confers tumor cells the ability to reach the brain via improvements in survival in blood flow, endothelial adhesion in brain and BBB transmigration.

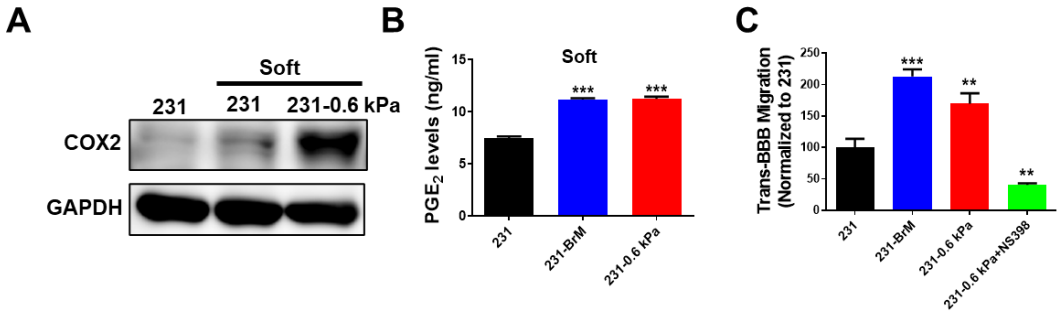

Figure 4.6 Matrix softness induces BBB transmigration via the increased expression of COX2. (A) After cells were seeded on TCPs or 0.6 kPa PA gels for 24 h, the total protein samples were extracted. The expression levels of COX2 protein were analyzed by Western blotting. (B) The cells were seeded on 0.6 kPa PA gels and cell culture supernatants were collected after 24 h. The secretion levels of PEG2 were detected by ELISA. (C) The cells were pretreated by DMSO or COX2 inhibitor NS398 (3 μM) for 24 h and then the BBB transmigration assay was performed. N=3, isolates; mean ± SEM; **, $p < 0.01$; and ***, $p < 0.001$.

4.2.4 The extended priming on soft matrices alters the mechanoadaptation ability of breast cancer cells

Tumor cells that successfully infiltrate into brain need to adapt to not only biochemical microenvironments but also mechanical microenvironments in order to survive and outgrowth [254]. Thus, we further examined the mechanoadaptation ability of tumor cells on soft matrices, including spreading, adhesion, proliferation, survival, mechanoresponse, migration and invasion. Spreading and morphological parameters of cells are usually associated with cell growth and motility, which can be employed as useful indications to assess if the microenvironment is favorable to tumor cells [255, 256]. We found that soft priming significantly enhanced both spreading area and aspect ratio of the cells on soft matrices and reduced the circularity (Fig. 4.7A-D). Compare to other cells, cells that were prolonged passaging on soft matrices had smaller spreading areas, lower aspect ratio, and higher circularity on stiff substrates and TCPs. We further examined adhesion ability of the cells on soft, stiff substrates, and TCPs. The data showed the adhesion abilities of 231-0.6 kPa and 231-BrM cells were higher than that of 231 and 231-35 kPa cells on soft substrates, whereas 0.6 kPa and 231-BrM cells

showed limited adhesion abilities on TCPs (Fig 4.7E). Moreover, the proliferation of 231-0.6 kPa cells was significantly higher than that of other cells on soft matrices. Interestingly, both 231-0.6 kPa cells and 231-35 kPa cells showed lower proliferation rates on TCPs compared to 231 and 231-BrM cells which are plastic-tolerant. There is no significant difference in proliferation among these cells on TCPs (Fig. 4.7F-I). In addition, matrix softness had no influence on cell survival among these cells (Fig. 4.7J). The mechanoresponse was assessed by comparing three parameters on TCPs with those on soft matrices, including spreading area, proliferation, and CTGF expression which is a downstream target gene of well-known mechanosensitive transcription factor YAP. Although all of cells showed increased response on TCPs compared to soft matrices, 231-0.6 cells showed lower combined mechanoresponse, indicating the long-term soft matrix culture induces mechano-insensitivity of tumor cells (Fig. 4.7K). 4T1-0.6 kPa cells also showed a higher proliferation rate than their parental 4T1 cells on soft matrices (Fig. 4.7L and M).

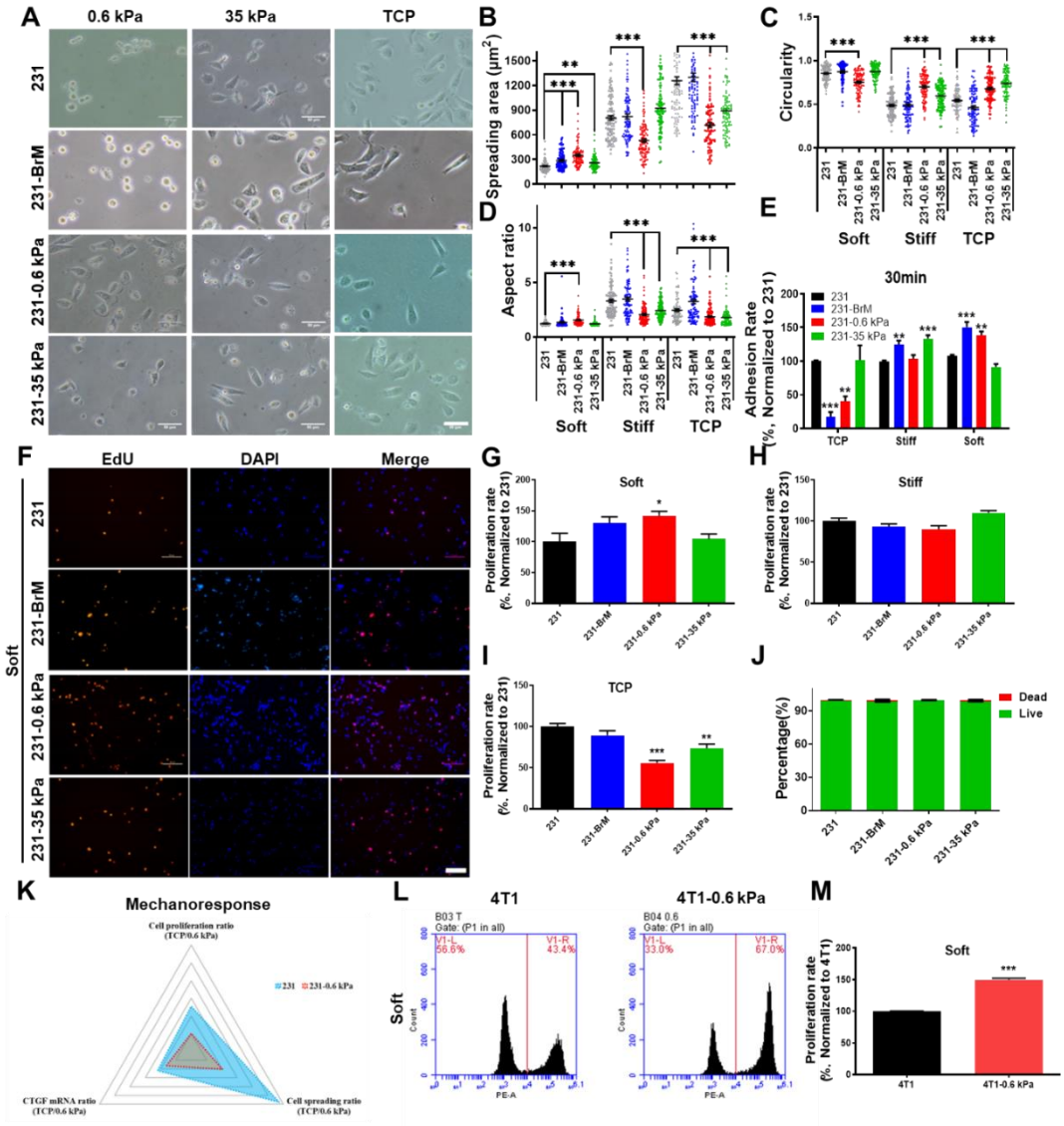

Figure 4.7 Continued soft priming increases mechanodapation of breast cancer cells on soft matrices. (A) Cells were seeded on 0.6 kPa, 35 kPa PA gels and TCPs for 24h. The representative images were presented. Scale bar, 50 μm. Tumor cell spreading area (B), circularity (C), and aspect ratio (D) were measured. (E) Tumor cells were seeded on 0.6 kPa PA gels for 30 min and then the cells were washed with PBS 3 times and imaged for counting. Quantification of the tumor cell adhesion rate. (F) Cells were seeded on 0.6 kPa, 35 kPa PA gels and TCPs for 24h and then cell proliferation was measured by EdU proliferation assay. The representative images of EdU-positive cells on 0.6 kPa gels were presented. Scale bar, 50 μm. (G-I) Quantification of EdU incorporation for cells adhering to corresponding substrates. (J) Cells were seeded on 0.6 kPa, 35 kPa PA gels and TCPs for 24h and then cell survival was measured by Live (Calcein AM) /dead (PI) assay. (K) Mechanoresponse readouts for 231 cells and 231-0.6 kPa cells. (L) 4T1 and 4T1-0.6 kPa cells were seeded on 0.6 kPa PA gels for 24 h and cell proliferation was measured by EdU proliferation assay. N=3, isolates; mean ± SEM; *, $p < 0.05$; **, $p < 0.01$; and ***, $p < 0.001$.

Then we assessed the motility of cells on the different matrices using wound healing assay. The migration ability was enhanced on the soft matrices but decreased on the stiff matrices and TCPs after cells experienced prolonged passages on the soft matrices. 231-BrM also showed low migration ability on stiff substrates and TCPs (Fig. 4.8A-D). Invading the surrounding tissues is curial for establishing distant metastases. To evaluate the invasion ability under different stiffness conditions, different concentrations of Matrigel (soft: 2 mg/ml, intermediate: 3 mg/ml, and rigid: 4 mg/ml) mixed with 10 μg/ml full-length FN were applied to obtain gels of varying rigidities, which were used to coat transwell chambers. 231-BrM, 231-0.6 kPa cells showed higher invasion ability in the soft condition than 231 and 231-35 kPa cells (Fig. 4.8E and F). Interestingly, the invasion ability of 231-BrM and 231-0.6 kPa cells in the rigid condition were also increased, despite both of them showing a lower invasion rate compared to 231 cells in the intermediate condition. The invasion ability in varying rigid conditions was further confirmed by the 3D collagen gel invasion assay through the modification of collagen concentration. Embedding tumor spheroids into a 3D collagen gel is a well establish method for invasion assay. Since 231 cells cannot form spheroid via hanging drop culture[257], we adopted the modified method to evaluate the 3D invasion as shown in chapter 3. We found that soft priming increased the invasion rate of 231 cells in the soft condition but decreased the invasion rate in the rigid condition (Fig. 4.8G and H). Overall, these results demonstrated that soft matrix priming enhances the mechanoadpation abilities of cells on soft substrates but impairs the adaptation in the rigid condition.

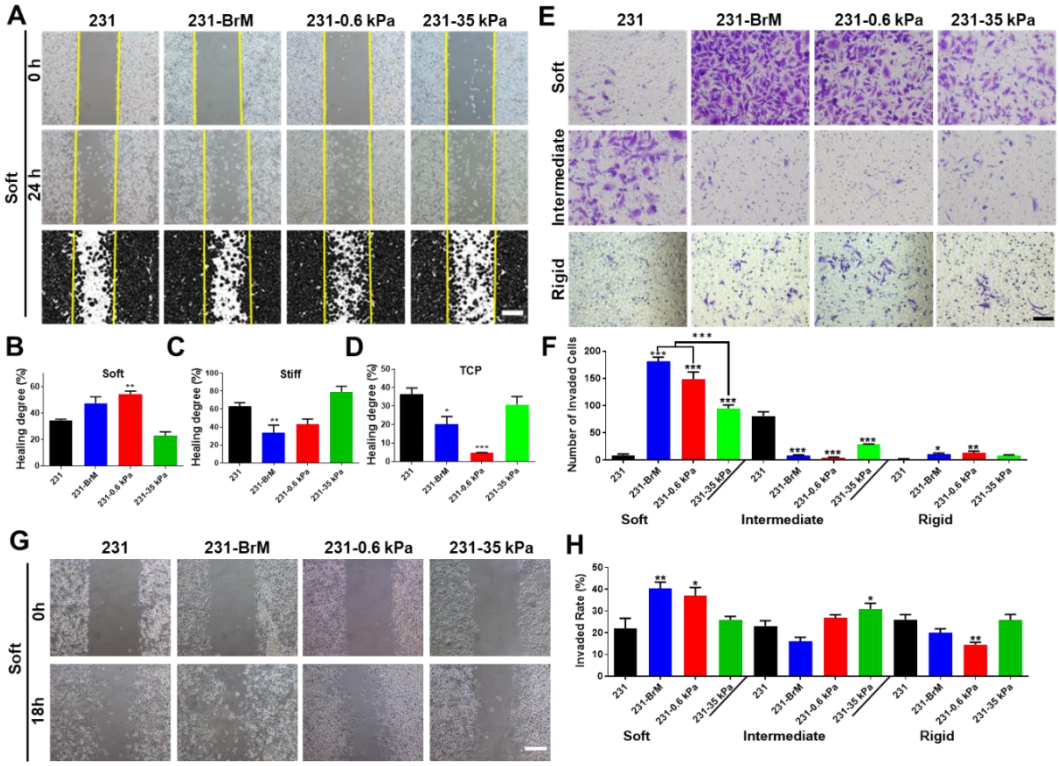

Figure 4.8 Matrix softness enhances the migration and invasion ability of breast cancer cells on soft matrices. (A-D) Cells were seeded on 0.6 kPa, 35 kPa PA gels and TCPs for 24h and then cell migration ability was measured by wound healing assay. The representative images of wound healing on 0.6 kPa matrices (A) and quantification (B-D) were presented. Scale bar, 100 μm. (E and F) Transwell system used consists of the upper chambers containing a thin layer of FN-enriched Matrigel, perforated membrane, and the lower chamber coated with FN. Cells were plated in Matrigel with different rigidities. Invaded cells stained with crystal violet were imaged (E) and their transwell invasion rates were quantified (F) after 72 h incubation. Scale bar, 100 μm. (G and H) Cells were seeded on TCPs and scratched areas were made after 24 h. Then cells were covered by collagen gel with different rigidities and their invasion rates were quantified after 48 h incubation. Representative images (G) and corresponding quantification (H) of invasion in collagen. Scale bar, 100 μm. N=3, isolates; mean ± SEM; *, $p < 0.05$; **, $p < 0.01$; and ***, $p < 0.001$.

4.2.5 Continued soft priming confers tumor cells with the increase of stemness, growth in 3D hyaluronic acid (HA) hydrogels and Serpin B2 secretion

To explore whether matrix softness enhanced the stemness properties of tumor cells which facilitates early colonization in the brain, qPCR was carried out to identify the expression levels of stemness genes. There was no gradual increase in stemness-related

genes following culture on soft matrices, except for *OCT4* and *CD133* (Fig. 4.9A). Moreover, the results of colony formation assay showed that the colony numbers were significantly increased in 231-0.6 kPa cells and 231-35 kPa cells compared to parental 231 cells, whereas no quantitative difference in colony formation ability was detected between 231-0.6 kPa cells and 231-35 kPa cells (Fig. 4.9B and C). These results suggested that long-term priming on soft/stiff had a similar effect on stemness of tumor cells. Brain ECM is largely composed of nonsulphated glycosaminoglycans called hyaluronic acid (HA) [258]. To better examine the brain metastatic capacities of tumor cells *in vitro*, a synthetic 3D HA hydrogel platform with low stiffness was applied to mimic the physiological ECM in the brain. The stiffness of HA gels was ~1 kPa (Fig. 4.9D). Compared to parental 231 cells, 231-0.6 kPa cells exhibited enhanced survival ability and proliferation rate in 3D HA gel (Fig. 4.9E-G). The proliferation of 231-BrM cells was increased while survival ability was not changed. In addition, both survival and proliferation of 231-35 kPa cells were impaired. Four serpins, including serpin B2, D1, E2 and I1, show high expressions in brain metastatic derivatives but not in bone or lung metastatic derivatives [75]. As a result of secreting plasminogen activator inhibitory serpins, brain metastatic cells prevent reactive stroma in the brain from releasing the lethal plasmin and survival in the defense of the brain microenvironment. The data of RNA-seq showed that the expression levels of all of these four serpins were elevated in 231-0.6 kPa cells (Fig. 4.9H and I). Thus, we further tested whether soft priming participated in the regulation of Serpins release. Compared to 231 and 231-35 kPa cells, 231-BrM and 231-0.6 kPa cells presented increased Serpin B2 protein secretion (Fig. 4.9J). These data supported that soft priming increases functions *in vitro* that favor brain metastasis in tumor cells.

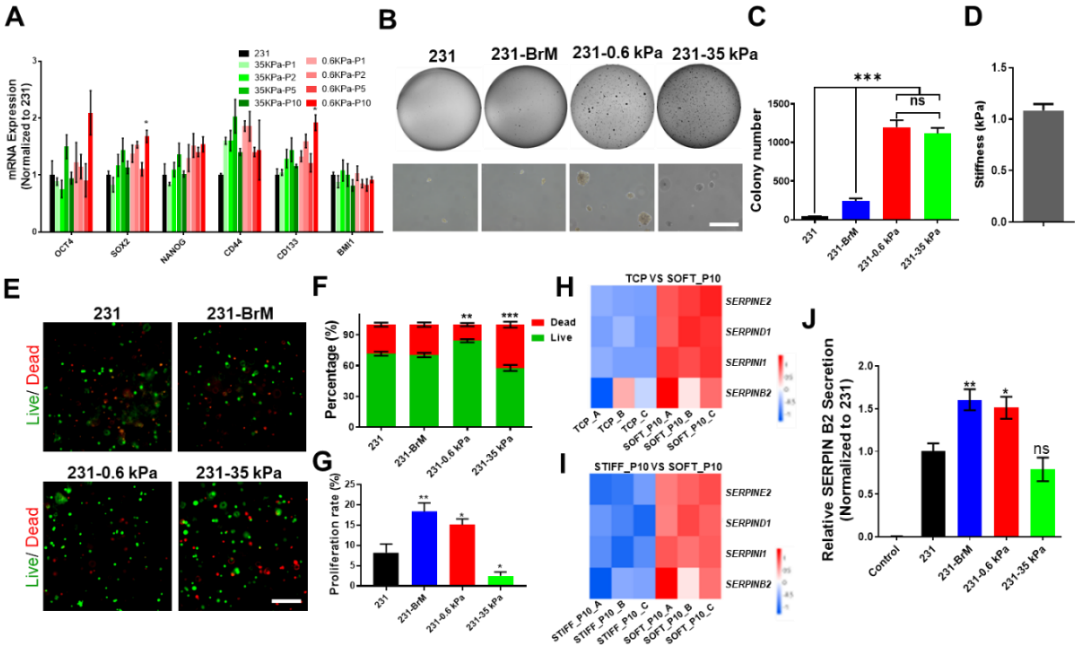

Figure 4.9 Matrix softness conditioning enhances stemness, growth in 3D hyaluronic acid (HA) hydrogels and Serpin B2 secretion of tumor cells. (A) The RNAs were extracted from cells seeded on corresponding substrates. The expression levels of stemness-related genes were measured by qPCR. The soft agar assay was applied for the detection of the colony formation ability of cells. (B) Representative images of formed colonies were shown. (C) Quantification of the numbers of formed colonies in (B). Scale bar, 100 μm. (D) HA-methacrylate functionalized with RGD peptide was crosslinked to form HA hydrogels by lithium phenyl-2,4,6-trimethylbenzoylphosphinate (LAP). The stiffness of HA hydrogels was measured by the atomic force microscope. Cells were plated into HA gels for 24 hours. (E) Live (Calcein AM)/dead (PI) staining was performed to detect the cell survival. Representative images of the live/ dead staining assay were shown. Scale bar, 200 μm. (F) Quantification of the live/ dead staining assay in (E). (G) The proliferation of cells in HA hydrogels was measured by EdU proliferation assay. (H-I) Clustering of serpin mRNA levels measured by RNA-seq and heatmaps were normalized by Z-score. The gene expression levels from low to high are represented by pseudo-colors ranging from blue to white to red. (J) Cells were seeded on 0.6 kPa PA gels and supernatants were collected after 48h. Dot blot of collected supernatants detected with anti-SERPIN2 B2 antibody. N=3, isolates; mean ± SEM; ns, $p > 0.05$; *, $p < 0.05$; **, $p < 0.01$; and ***, $p < 0.001$.

4.2.6 Soft niches-primed breast cancer cells exhibit enhanced abilities to transmigrate BBB *in vivo* and proliferate in the brain

We next utilized experimental metastasis in *vivo* models to validate the metastatic

abilities of tumor cells in several stages of brain metastasis, including arrest, extravasation and colonization in the brain. BBB transmigration is crucial in the initiation of brain metastasis. Therefore, we examined the effect of soft priming on tumor cell arrest in the brain at the initial stage (1-3 days) after inoculating the tumor cells into the arterial circulation of immunodeficient mice via intracardiac injection (Fig 4.10A). By monitoring the bioluminescence in the brain, we found the soft/stiff priming did not enhance the arrest ability of 231 cells in the brain (Fig. 4.10B and C). In contrast to parental 231 cells, 231-BrM cells showed increased initial cerebral seeding. Note that arrest of tumor cells in the brain does not necessarily mean they will eventually reach the parenchyma of the brain. Thus, we further investigated whether long-term priming on the soft matrices affects the ability of breast cancer cells to cross the BBB and infiltrate the brain parenchyma. Due to the fact that cancer cells that later successfully proliferated into macrometastases left blood vessels by day 3 [259], we fixed and sectioned brain tissue to count tumor cells that were trapped in brain capillaries, processed or completed BBB extravasation, on day 3 (Fig. 4.10D and E). In parental 231 and 231-35 kPa cells, more cells were trapped in brain microvessels (Fig. 4.10F). 231-BrM cells showed a significantly increased incidence of penetrating cells and extravasated cells (Fig. 4.10G and H). Although no significant increase in extravasating cells was observed, 231-0.6 kPa cells showed more extravasated cells, which was consistent with our previous *in vitro* BBB transmigration study.

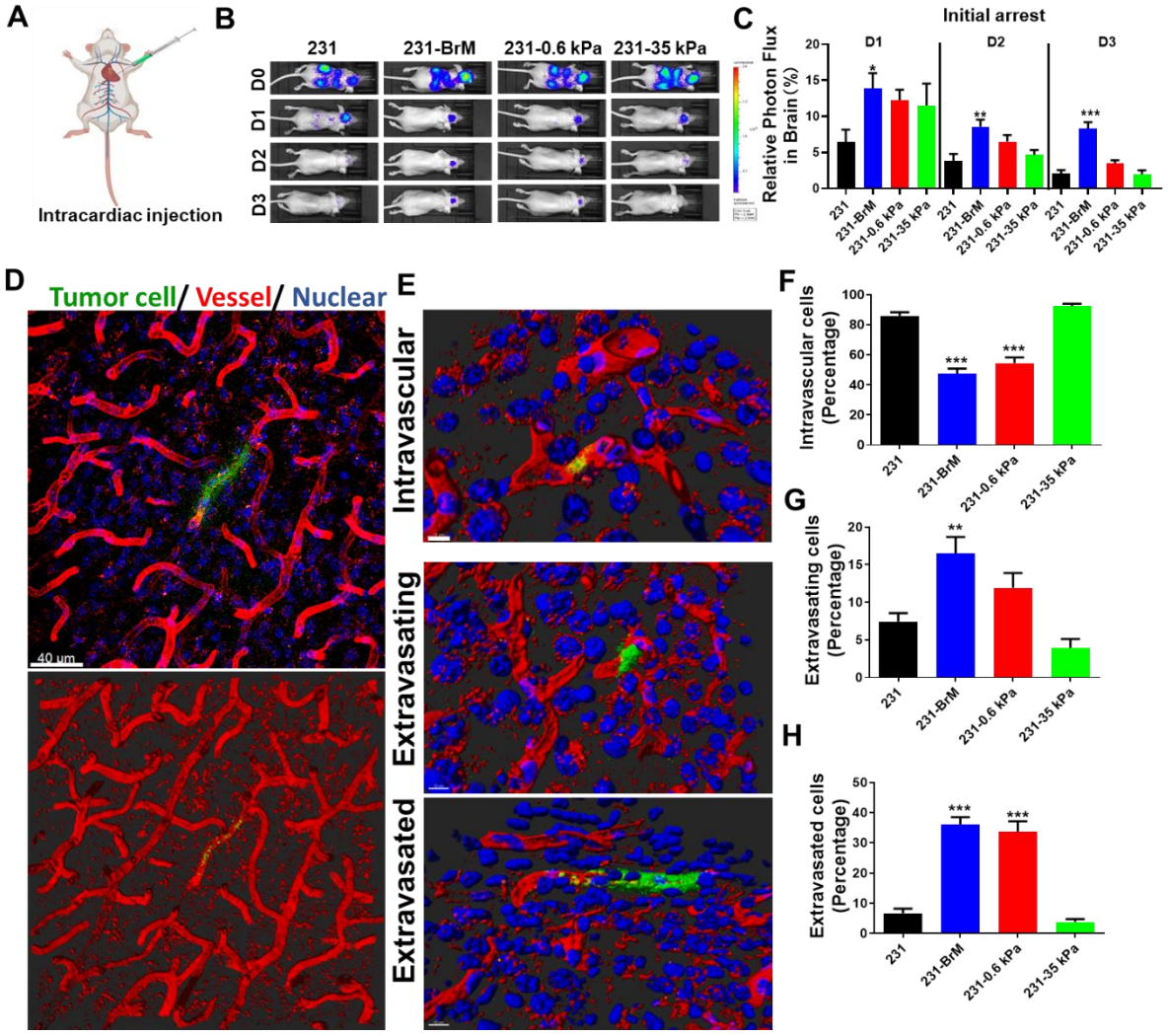

Figure 4.10 Matrix softness conditioning enhances BBB transmigration of breast cancer cells but not the initial arrest in vivo. (A) Schematic diagram of intracardiac injection. (B) Cells were implanted into nude mice through intracardiac injection and bioluminescence (BLI) photon flux signals were measured on day 1, day 2 and day 3. Representative images of whole-body BLI photon flux signals are presented. (C) Quantification of BLI photon flux signal in brains from (B). 231 n=10, 231-BrM, n=11; 231-0.6 kPa, n=12; 231-35 kPa, n=10. (D) Representative confocal image and 3D reconstruction image showing metastatic breast cancer cells (green) were trapped in the brain capillaries (red) on day 3 post-injection. Scale bar, 40 μm. (E) Confocal analysis of cells being under each extravasation step on day 3 post-injection, including intravascular, extravasating and extravasated cells. Scale bar, 10 μm. Quantification of (F) intravascular, (G) extravasating and (H) extravasated tumor cells on day 3 after tumor cell injection. n = 2 mice per condition. The data = mean ± SEM. *, $p < 0.05$; **, $p < 0.01$; and ***, $p < 0.001$.

To evaluate the effect of soft priming on intracranial growth of tumor cells, we inoculated tumor cells directly into brain parenchyma of female athymic mice using

intracranial implantation (Fig. 4.11A). The results showed that 231-0.6 kPa cells exhibited high tumorigenesis property in brain (Fig. 4.11B). Brain metastases of 231-BrM and 231-0.6 kPa cells were much larger than these of 231 and 231-35 kPa cells (Fig 4.11C). Notably, brains of mice bearing brain metastasis of 231-BrM and 231-0.6 kPa cells were visibly vascularized (Fig. 4.11D). We further examined tumors via immunostaining on brain slices. Breast cancer brain metastases of 231-BrM and 231-0.6 kPa cells were larger and showed more proliferative in contrast to 231 and 231-35 kPa xenografts (Fig. 4.11E-G). Taken together, these results indicated that soft priming promoted BBB transmigration and intracranial growth of breast cancer cells.

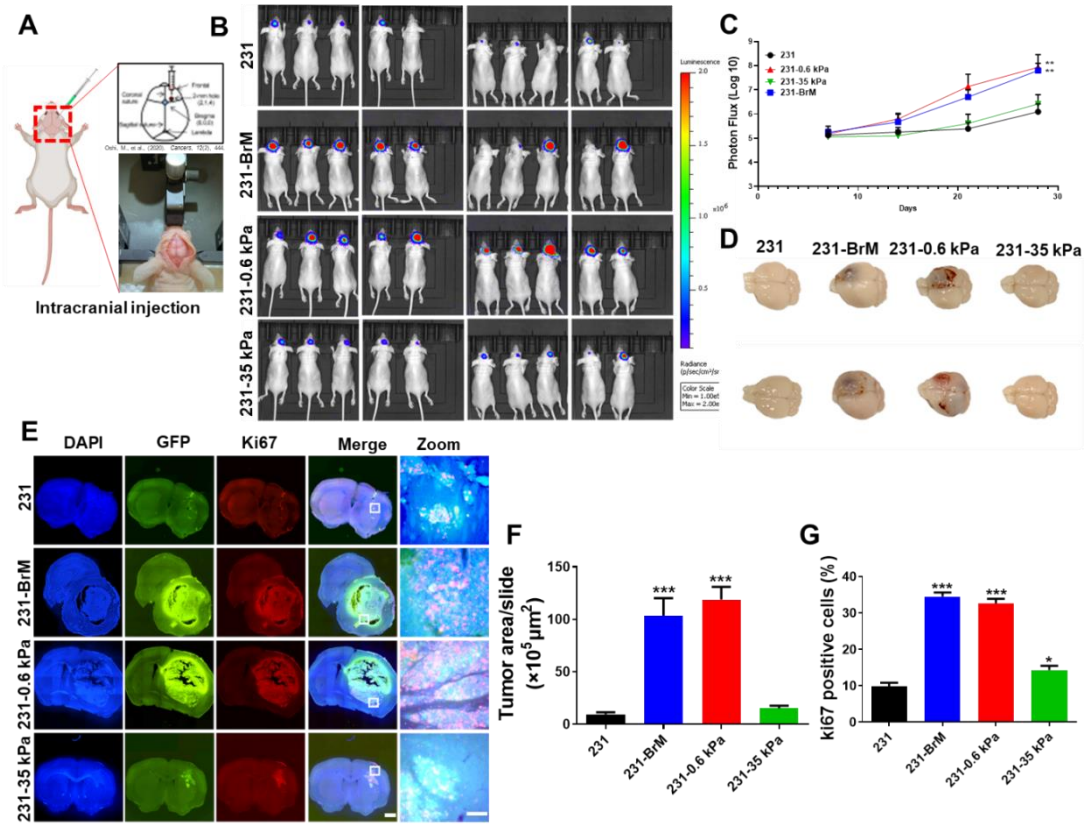

Figure 4.11 Matrix softness conditioning promotes the cerebral outgrowth of breast cancer cells. (A) Schematic diagram of intracranial injection and representative images of the experiment. (B) Cells were implanted into the cerebrums of nude mice through intracranial injection and the BLI photon flux signals in brains were measured weekly. Mice were sacrificed on day 28 and the brains were fixed for further experiments. Representative images of brain BLI photon flux signal are presented. (C) Quantification of BLI photon flux signal in brains. n=10 in each group. (D) Representative mouse brains ex vivo on day 28 are shown. (E) Immunofluorescence of

ki67 (red) in coronal brain sections. Tumor cells were labeled with GFP (Green) before injection, nuclei were stained with DAPI (blue), respectively. Representative images of coronal brain sections are shown. Scale bar, 1 mm and 100 μm in Zoom panel. (F) Quantification of lesions in brain based on the size in (E). (G) Quantitation of ki67-positive tumor cells in (E). The data = mean ± SEM. *, $p < 0.05$; **, $p < 0.01$; and ***, $p < 0.001$.

4.2.7 Soft niches-primed breast cancer cells exhibit metastatic tropism to brain *in vivo*.

To further validate the effect of long-term soft priming on brain metastasis and organotropism, we used an experimental metastasis model to mimic several stages of metastasis including evasion of anoikis, intravasation, and colonization to distant organs. For this, 231, 231-BrM, 231-0.6 kPa and 231-35 kPa cells were injected into nude mice by intracardiac injection respectively and the mice were imaged weekly using the *in vivo* imaging system (IVIS) for 4 weeks. Consistent with previous studies, 231-BrM showed a high preference for brain metastasis. Remarkably, 75% of mice after 231-0.6 kPa cells injection developed brain metastasis compared to 20% in 231 cells group and 40% in 231-35 kPa cells (Fig. 4.12A). Representative bioluminescent images and *in vivo* signals showed that soft priming but not stiff priming significantly enhanced brain metastasis compared to 231 cells on TCPs (Fig. 4.12B and C). 231-BrM and 231-0.6 kPa cells also showed a higher incidence of brain metastasis (Fig. 4.12D). To confirm the bioluminescent signals were strictly from the brain, but not surrounding tissues, we imaged the brain ex vivo and data showed that soft priming increased brain metastasis and the number of tumor foci in the brain (Fig. 4.12E-G). These results demonstrated that soft priming changed organotropism and promoted brain metastasis of circulating breast cancer cells.

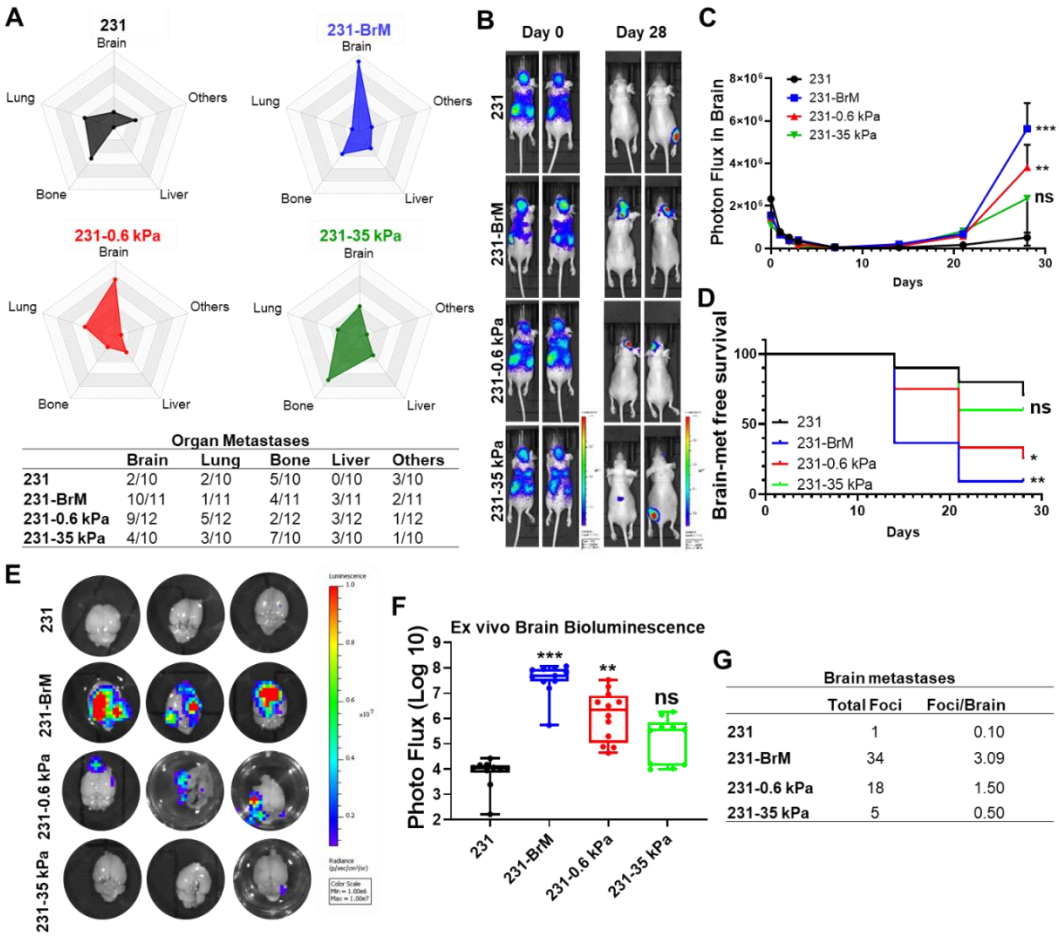

Figure 4.12 Matrix softness conditioning increases the brain metastasis ability of breast cancer cells in vivo. (A) Tumor cells were implanted into nude mice through intracardiac injection and BLI photon flux signals were measured weekly after tumor cell inoculation. Radar charts and table showing Incidence of organ metastasis determined according to BLI *in vivo* imaging. (B) Representative bioluminescent images of mice at day 0 and day 28 in (A) are presented. (C) Quantification of the growth of brain metastasis monitored by BLI in (A). Kaplan-Meier analysis for brain metastasis-free survival compared among these four groups was measured by BLI photon flux signals from (A). On day 28, mice were sacrificed, and the BLI photon flux signals in the brains were measured ex vivo. (E) Representative images and (F) quantification are shown. (G) Quantification of tumor foci within the brains via ex vivo BLI signals. 231, n=10; 231-BrM, n=11; 231-0.6 kPa, n=12; 231-35 kPa, n=10. The data = mean ± SEM. ns, $p > 0.05$; *, $p < 0.05$; **, $p < 0.01$; and ***, $p < 0.001$.

4.2.8 Soft niches-primed breast cancer cells exhibit characteristic biophysical properties

Cell mechanics are important properties involved in regulating cell behaviors and are

usually changed in the processes of transformation and metastasis [260]. In order to further characterize how soft/stiff matrix preconditioning affects breast cancer cells, mechanical properties were measured. Stiffness (measured by AFM) of 231-0.6 kPa cells was higher compared with other cells on soft matrices (Fig. 4.13A and B). The cytoskeleton and its regulators must be involved in alterations to the shape and mechanics of the cell. Thus, Cells were grown on soft/stiff gels to examine the actin cytoskeleton *in situ* using immunostaining (Fig. 4.13 C). In agreement with the stiffness of the cells, the highest F-actin density was observed in 231-0.6 kPa cells on soft matrices, while it was rare on TCPs (Fig. 4.13 D). In addition, in contrast to other groups, 231-0.6 kPa cells on soft gels showed a reduction in cortical actin bundles by comparing the intensity of cortical actin with that of non-cortical actin (Fig. 4.13 E). Phosphorylation of myosin light chains (pMLC) has been identified as the regulator in the actin-myosin II interaction, contributing to cell stiffness and cell contractility [261]. In this study, we measured the level of pMLC in cells on soft matrices and TCPs. 231-0.6 kPa cells had larger levels of pMLC on the soft matrices than their parental 231 cells did, whereas the inverse was true on TCPs (Fig. 4.13 F-G). The contractility of cells is essential for cellular functions, such as spreading, proliferation and motility [262]. Thus, we further examined the contractility of the cells on soft substrates. The data showed that 231-0.6 kPa cells exhibited higher traction force than other cells on soft substrates (Fig. 4.13I and J). Altogether, these results suggested that breast cancer cells gain a greater mechanical cohesion on soft matrices after long-term priming on soft matrices, which was linked to a better adaptation ability to the soft microenvironment in the brain.

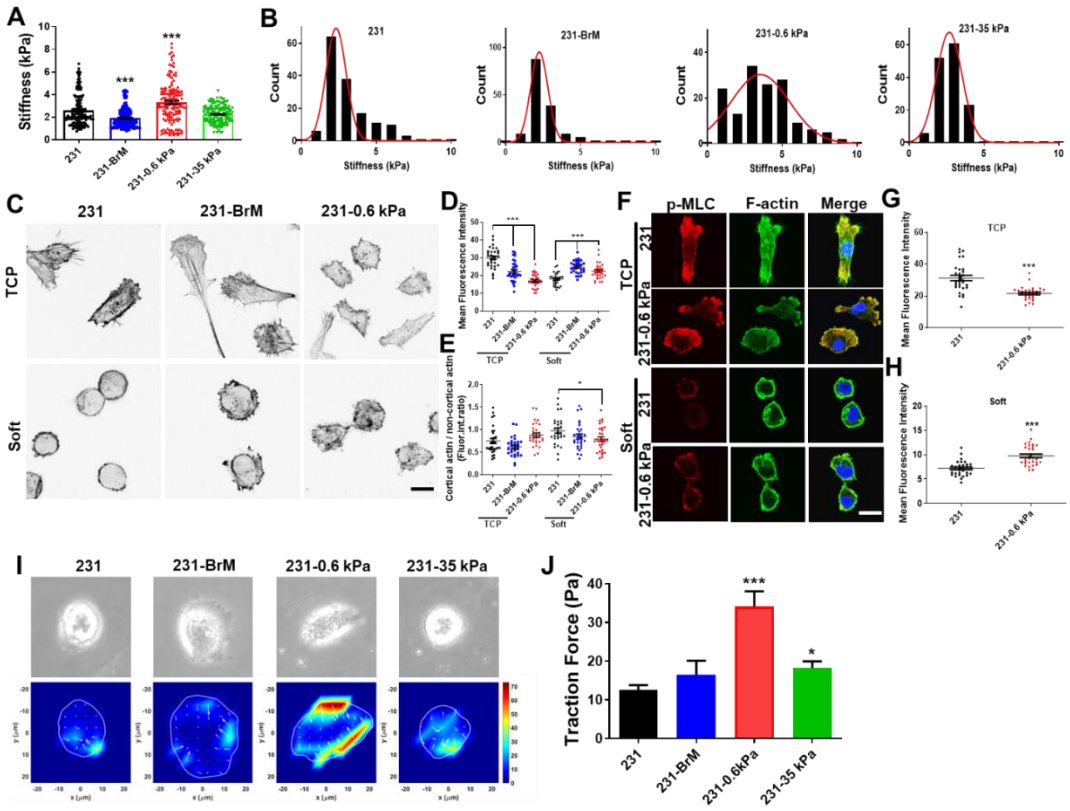

Figure 4.13 Soft matrix-priming cells display unique properties of cell mechanics. (A) Young's modulus of cells was measured by AFM on 0.6 kPa PA gels. (B) The histograms showing the stiffness of tumor cells in (A). (C) The tumor cells cultured on TCPs and 0.6 kPa for 24h were stained with phalloidin and analyzed for actin cytoskeleton. Representative fluorescence images of F-actin in cells are shown. Scale bar, 20 μm. Quantification of F-actin density (D) and the ratio of cortical actin to non-cortical actin (E). (F) Immunofluorescence staining of p-MLC and F-actin of cells seeded on 0.6 kPa PA gels after 24h. Scale bar, 20 μm. (G-H) Quantification of the intensity of p-MLC in (F). (I) The tumor cells were cultured on 0.6 kPa PA gels for 24 h and then cellular traction force was measured by traction force microscopy. Representative bright-field images (upper panel) and traction maps (bottom panel) of cells. Scale bar, 20 μm. (J) Quantification of cellular traction force. N >15 cells. The data = mean ± SEM; *, $p < 0.05$; **, $p < 0.01$; and ***, $p < 0.001$.

4.2.9 Mechanical memory of soft niches-primed breast cancer cells to matrix softness is transiently maintained after transplantation on rigid tissue culture plates

Furthermore, we explored the short- and long-period cellular response of 231-0.6 kPa cells after being transferred to TCPs. Surprisingly, 231-0.6 kPa cells transplanted to TCPs (denoted as 231-0.6T) were rounded and less spread on day 1, which exhibited similar morphology as before transplantation (Fig. 4.14A-D). The morphology of 231-

0.6T from day 3 to day 14 changed significantly to a spread morphology which was similar to that of 231-BrM cells on TCPs. Furthermore, cell stiffness of 231-0.6T cells was measured on day 1 and day 14 after transplantation on TCPs. Likewise, 231-0.6T cells showed high stiffness just like before substrate switching, whereas showed compliant cell mechanics after 14 days of culture on TCPs (Fig. 4.14E-H). The delay of cellular responses to the matrix stiffness switching inspired us that long-term culture on soft matrices might instil mechanical memory in tumor cells. To test our hypothesis, we further evaluated whether the expression levels of brain metastasis-related genes induced by soft priming were permanent or reversible by re-seeding 231-0.6 kPa cells on TCPs for 14 days and confirming brain metastasis-associated gene expression. In comparison with 231 cells, most brain metastasis-related genes were still highly expressed on day 14 following TCP transplantation, although their expression was slowly decreased (Fig. 4.15A). Moreover, 231-0.6T cells (cultured on TCPs for 30 days) re-displayed the gene signature of brain metastasis after 2 passages on the soft matrices (Fig. 4.15B). The proliferation of 231-0.6T cells on the soft matrices was faster than that of 231 cells, despite no difference in BBB transmigration ability being observed (Fig. 4.15C-E). Collectively, these data indicated that matrix softness conditioning established mechanical memory, which allowed tumor cells to retain brain metastasis characteristics during the metastatic process.

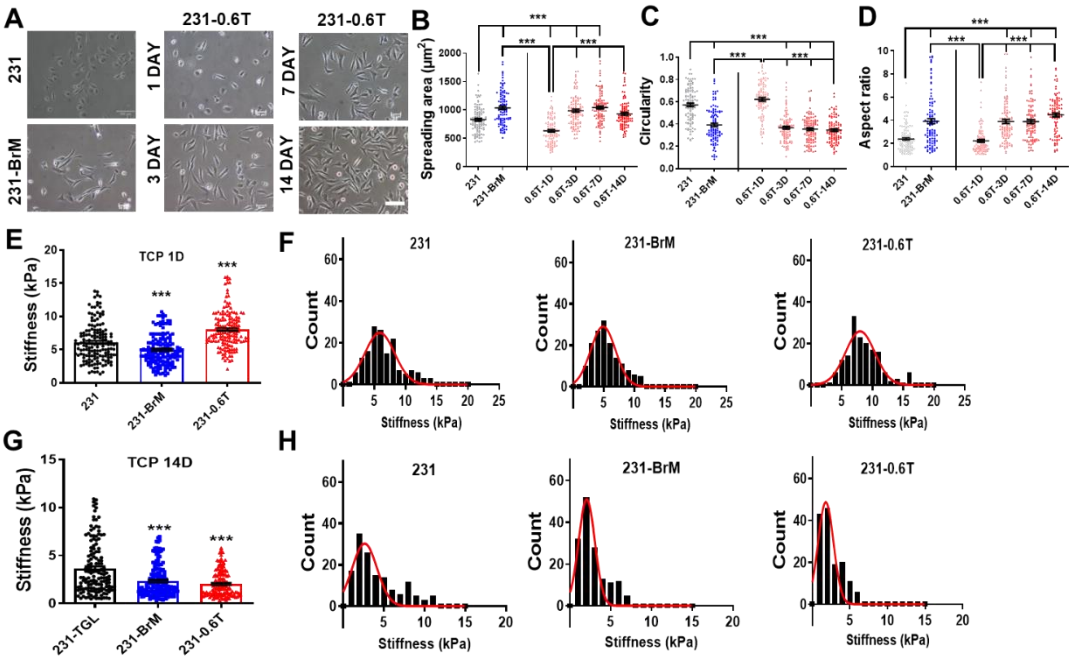

Figure 4.14 Transplantation on TCPs alters the morphology and stiffness of soft matrix-priming cells. (A) 231-0.6 kPa cells were transplanted to TCPs and denoted as 231-0.6T cells. The morphology of cells on TCPs after transplantation was shown by representative images (A) and evaluated by spreading area (B), circularity (C), and aspect ratio (D). Scale bar, 100 μm. (E) Cell stiffness was measured by AFM on day 1 after 231-0.6 kPa cells were transferred to TCPs. (F) The histograms showing the stiffness of tumor cells in (E). (G) Cell stiffness was measured by AFM on day 14 after 231-0.6 kPa cells were transferred to TCPs. (G) The histograms showing the stiffness of tumor cells in (H), N > 100 cells, mean ± SEM; ***, $p < 0.001$.

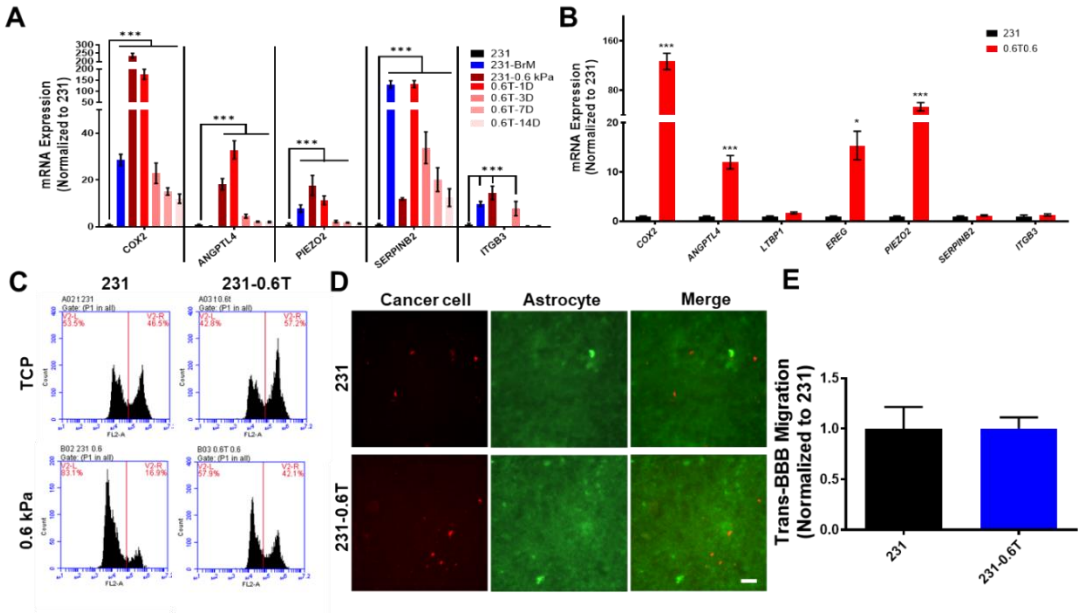

Figure 4.15 Matrix softness conditioning shapes mechanical memory of breast cancer cells. (A) Expression levels of brain metastasis-related genes were measured by qPCR after 231-0.6 kPa cells were transplanted on TCPs on day 1 (0.6T-1D), day 3 (0.6T-3D), day 7 (0.6T-7D), and day 14 (0.6T-14D). (B) 231-0.6T cells were re-seeded on 0.6 kPa PA gels (0.6T0.6) and expression levels of brain metastasis-related genes were measured after 2 passages. (C) 231-0.6T cells were seeded on 0.6 kPa PA gels and TCPs for 24h and then cell proliferation was measured. (D) BBB transmigration ability of 231 cells and 231-0.6T was analyzed using *in vitro* model. Scale bar, 100 μm. (E) Quantification of trans-migrated cells. N=3, isolates; mean ± SEM; *, $p < 0.05$; **, $p < 0.01$; and ***, $p < 0.001$.

4.3 Discussion

Various researches have revealed the crucial details of how intrinsic properties of tumor cells and specific environments of distant organs synergistically determine metastatic organotropism. It is found that 17 genes are associated with brain relapse in breast cancer cells, but not with relapses of the bones, liver, or lymph nodes [65]. CTC lines obtained from cancer patients exhibit metastasis preference, recapitulating metastatic patterns in corresponding patients [73]. Meanwhile, the unique microenvironment of the brain passively selects or actively sculpts tumor cells arriving in the brain [10, 75, 115]. Remarkably, an inspirational study shows tumor cells with bone metastatic capability are preselected by primary tumor stroma, which highlights the potential determinant role of heterogeneous microenvironment in the primary tumor in metastatic

organotropism [4]. In this study, we focused here on the role of the stiffness of the primary niche in organ-specific metastasis. By identifying the matrix softness as a driver of the acquisition of brain metastasis, our present work demonstrated the constructive question of whether mechanical cues in the microenvironment lead to the emergence of metastatic organotropism.

Brain metastatic tumor cells undergo a transition to gain the characteristics of neuron cells, which is termed as neuronal mimicry [250]. A previous study shows that metastatic tumor cells from the brain exhibit GABAergic feature conferring an additional option for the energic source [96]. The neuronal glutamate receptor NMDAR promote the brain metastasis of breast tumor cells [263]. The usual perception is that neuronal mimicry, which is the strategy allowing tumor cells to evade immune surveillance and utilize brain-derived energy sources for outgrowth, is driven by tumor plasticity and neuron niche [250]. However, recent research provides evidence showing that brain-specific gene expression preexists in primary breast tumors of patients with brain metastasis, implying tumor cells may gain neuronal-like features in the primary tumor to prepare for further brain metastasis [264]. Our results showed that long-term priming on the soft matrices was sufficient to induce an increase in neuronal-associated pathways. Moreover, soft niches-primed cells exhibited the transcriptomic signatures of known neuronal cell types. Future studies are needed to further investigate the role of matrix softness in neuronal mimicry and underlying regulatory mechanisms. Meanwhile, we noticed that a similar concept is reported for stiff substrate promoting bone metastasis through transiting tumor cells to the osteomimicry phenotype with increased osteolytic capacity [243, 244, 265]. Again, these studies highlight the enormous functions of mechanics in primary or host microenvironments in regulating organotropism.

In summary, the work in this chapter established that chronic culture on soft matrices drove the acquisition of brain metastatic capability. Our present findings emphasized the vital role of the stiffness of the local niche in determining the metastatic

organotropism of breast cancer.

Chapter 5: The role of HDAC3 in matrix softness-induced breast cancer brain metastasis

5.1 Introduction

In the process of changing metastatic tumor cell behaviors, it is not clear if the microenvironment plays a "selection" or "conversion" role. Many studies have shown that the primary tumor contains subclonal cells with multiple random mutations and those subclonal cells, including mutations conferring metastatic properties, prefer to target distant specific organs and form metastases [4, 266]. In contrast, there is growing evidence showing that tumor cells disseminating to distant organs can affect the phenotype and adapt to the microenvironment of the targeted organ through epigenetic changes [246, 267]. Mechanical stimulation, including matrix stiffness, can regulate epigenetic modifications through mechanotransduction, which affects the chromatin state and thus alters gene expression patterns and cell behaviors [8, 9]. Matrix stiffness regulates the direction of stem cell differentiation by modulating histone H3K9 methylation and Lamin-A [209]. Low matrix stiffness can induce chromatin remodeling and consequently induce cells into a dormant state [268]. Soft matrix reduces histone acetylation levels and induces chromatin condensation, thereby regulating the mechanical memory of MSCs for matrix stiffness [223]. The high stiffness of the three-dimensional extracellular matrix enhances chromatin accessibility through histone deacetylases (HDACs), which mediates malignancy-related gene elevation and promotes tumorigenesis [269]. A few studies have shown that mechanistic microenvironment-induced epigenetic changes play an important role in the metastasis of malignant tumors: local softness of the tumor induces H3K4 trimethylation and H3K9 acetylation to promote CD133 expression, while inducing H3K9 and H3K27 trimethylation to suppress THBS2 expression, which in turn increases the stemness and malignant invasiveness of tumor cells [270]. Three-dimensional soft fibrin gel induces the demethylation of histone H3K9 and improves the tumorigenic and metastatic ability of tumor cells [271]. Although few studies have reported the role of mechanical microenvironment-induced epigenetic modifications in brain metastasis: low tissue stiffness in the brain affects cell survival and proliferation by regulating DNA methyltransferases [10]. Notably, it is worth noting that studies have shown that the high

expression level of histone deacetylase HDAC3 in brain metastases is significantly negatively correlated with the prognosis of patients [272]. In a mouse model, the histone deacetylase HDAC inhibitor Vorinostat (SAHA) has a significant effect on brain metastases from breast cancer[273]. Moreover, HDACs can be regulated by mechanical signals to further affect cellular behaviors [195, 234]. In conclusion, mechanical stimulation can regulate the gene expression pattern and cell behaviors through histone modification and its mediated chromatin remodeling. However, the role and molecular mechanism of matrix softness-induced epigenetic changes in tumor brain metastasis remain to be clarified. In this chapter, we
focused on exploring underlying molecular mechanisms of matrix softness-induced acquisition of brain metastatic ability.

5.2 Results

5.2.1 Matrix softness promotes breast cancer brain metastasis by clonal selection and evolution

The primary tumor contains a variety of subclonal cells with different random mutations and different subclones have different growth rates, metastasis capabilities, and drug sensitivity [274]. Subclones with organotropic traits can be preselected from primary tumors with a genetically heterogeneous composition under a certain biochemical microenvironment [4]. In addition, tumor cells will undergo a series of epigenetic changes in order to adapt to the microenvironment of distant metastatic organs, which refers to phenotypic plasticity [264]. Therefore, the effect of soft matrix on tumor cell brain metastasis may be achieved through the following mechanisms: a. Clonal selection of the subpopulation cells with brain metastasis preference and competitive advantages under selection pressure imposed by soft matrix; b. Epigenetic modification in response to sustained culture on soft matrices, which confers mechanoadaptation ability and brain metastatic properties to tumor cells. To investigate

which mechanism involves in matrix softness enhanced brain metastasis ability, we used single-cell cloning to obtain genetically homogeneous single cell-derived progenies (SCPs) with brain metastasis gene signatures in a low level (SCP low-1 and SCP low-2) (Fig. 5.1A). Both SCP low-1 and SCP low-2 cells showed increased brain metastasis gene expression after long-term culture on the soft matrices (Fig. 5.1B). Moreover, the proliferation rate on the soft matrices and BBB transmigration ability were enhanced significantly in soft-primed SCP low1 cells, suggesting clonal selection-independent epigenomic changes played an important role in the acquisition of brain metastasis ability on the soft matrices (Fig. 5.1C, 5.2F and G).

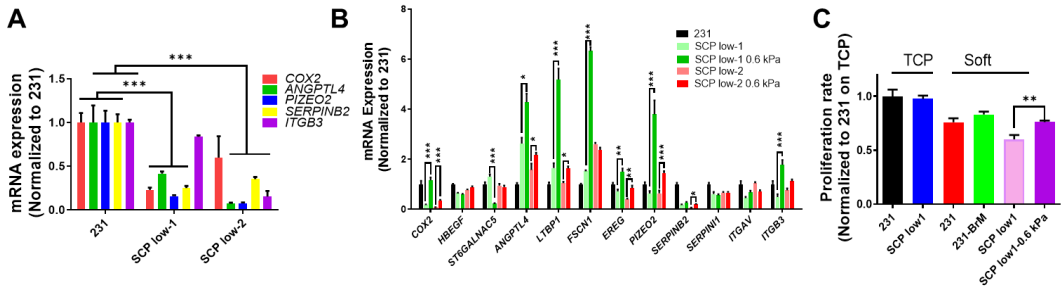

Figure 5.1 Matrix softness induces brain metastatic gene signature and increases proliferation on soft matrices. (A) The expression levels of brain metastasis-related genes were measured in 231, SCP low-1 and SCP low-2 cells. (B) SCP low-1 and SCP low-2 cells were seeded on 0.6 kPa cells. Total RNA was collected at P10 after soft priming, the expression levels of brain metastasis-related genes were measured by qPCR. (C) Cells were seeded on TCPs and 0.6 kPa PA gels, respectively. After 24 h incubation, cell proliferation was measured by EdU proliferation assay. Quantification of proliferation rate is presented. N=3, isolates; mean ± SEM; *, $p < 0.05$; **, $p < 0.01$; and ***, $p < 0.001$.

To demonstrate the role of clonal selection in soft matrix-induced brain metastasis, we further isolated and expanded SCP with a high brain gene signature (SCP high) (Fig. 5.2A). Our results showed that SCP high cells exhibited a higher proliferation rate than SCP low cells (SCP low-1) on soft substrates but not on TCPs (Fig. 5.2B and C). To exclude the potential paracrine effect, SCP high cells were labeled with a green live-cell dye, then cocultured with SCP low cells on soft substrates or TCPs. The results of the proliferation assay also showed the proliferation rate of SCP high cells on the soft

matrices but not TCPs was faster than that of SCP low cells, suggesting there were some subpopulations in breast cancer cells with proliferative advantage on the soft matrices which might contribute to the enhancement of brain metastasis (Fig. 5.2D and E). Moreover, SCP high cells exhibited a high BBB transmigration ability compared to SCP low cells (Fig. 5.2F and G). Together, these results indicated that the epigenetic changes and clonal selection are both involved in the gain of brain metastasis ability on soft matrices.

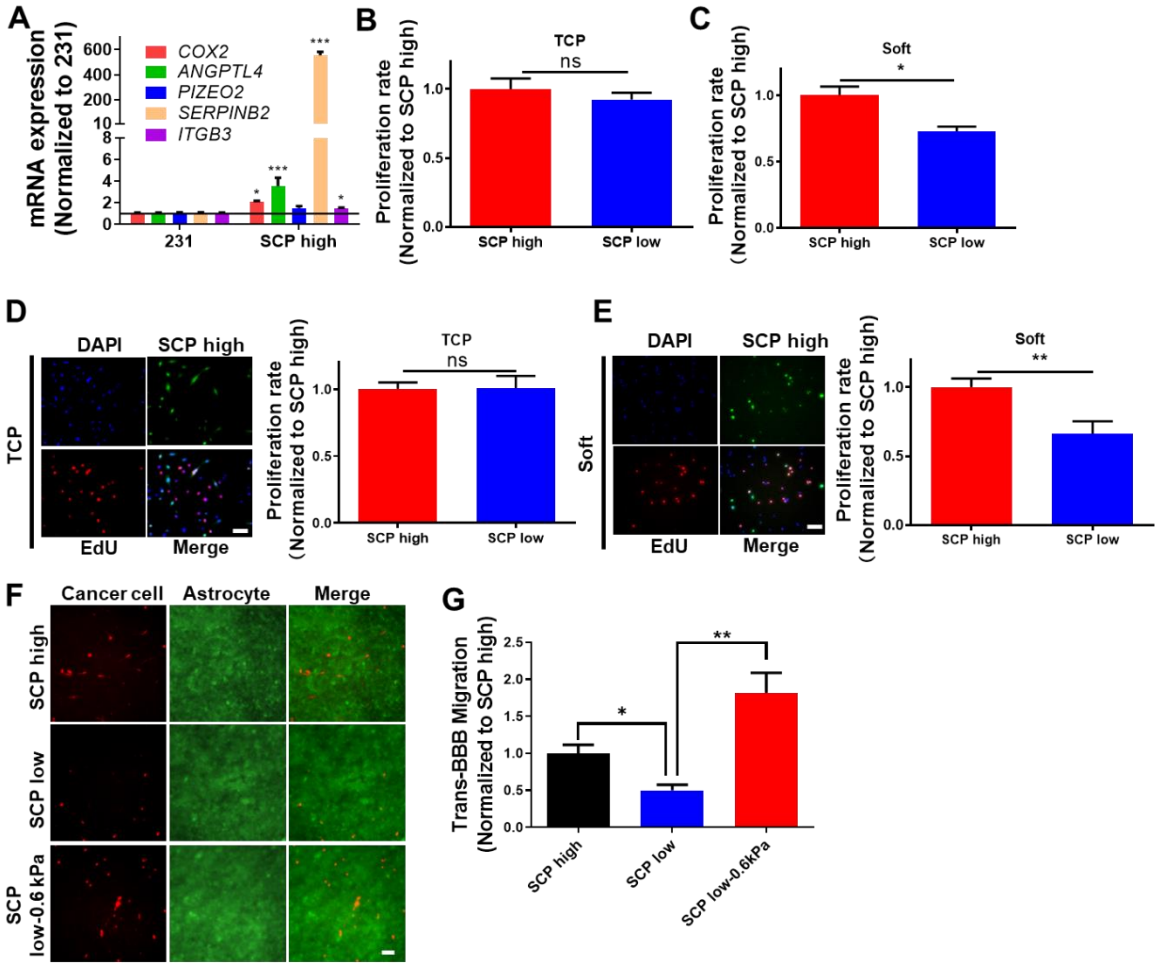

Figure 5.2 SCP with brain metastatic gene signature shows the advantages in mechanoadaptation to soft matrix and BBB transmigration. (A) The expression levels of brain metastasis-related genes were measured in 231 and SCP high cells. (B-C) Cells were seeded on (B) TCPs and (A) 0.6 kPa PA gels for 24h and then cell proliferation was measured by EdU proliferation assay. (D-E) SCP high cells were labeled with green cell tracker, and then mixed with SCP low cells at a density ratio of 1:1. Cells were seed on (D) TCPs and (E) 0.6 kPa PA gels, and then cell proliferation

was measured by EdU proliferation assay. The representative images and quantification of proliferation rate were presented. Scale bar, 100 μm. (F) BBB transmigration ability of SCP high, SCP low and SCP low-0.6 kPa cells was analyzed using *in vitro* model. Scale bar, 100 μm. (G) Quantification of trans-migrated cells. N=3, isolates; mean ± SEM; ns, $p > 0.05$; *, $p < 0.05$; **, $p < 0.01$; and ***, $p < 0.001$.

5.2.2 HDAC activity is required for matrix softness-induced brain metastasis

Chromatin remodeling, which is driven by epigenetic modifications such as acetylation and methylation of histones, modulates gene expression patterns and biological progress in response to the mechanical stimulations [225, 228, 234]. According to GO function annotation of our RNA-seq data, we found that a series of DEGs were involved in covalent chromatin modification, histone modification, regulation of chromatin organization and histone deacetylation in soft primed cells compared to stiff primed cells or cells on TCPs (Fig 5.3A and E). GSEA of DEGs also showed chromatin modification-related pathways were highly enriched in soft primed cells including histone deacetylase complex, protein deacetylation, histone H3 deacetylation and chromatin remodeling (Fig 5.3B and F). To explore the regulation of DEGs involved in chromatin deacetylation, generic protein-protein interactions (PPI) network and gene regulatory network (GRN) were constructed. The results showed that HDACs, especially Class I HDACs (HDAC1, 2, 3 and 8) which primarily catalyze the deacetylation of histone proteins, acted as key regulators in the regulatory networks (Fig 5.3C, D, G and H). These results highlighted the potential regulatory roles of chromatin deacetylation and chromatin remodeling in the brain metastasis ability of soft matrix-preconditioned cells.

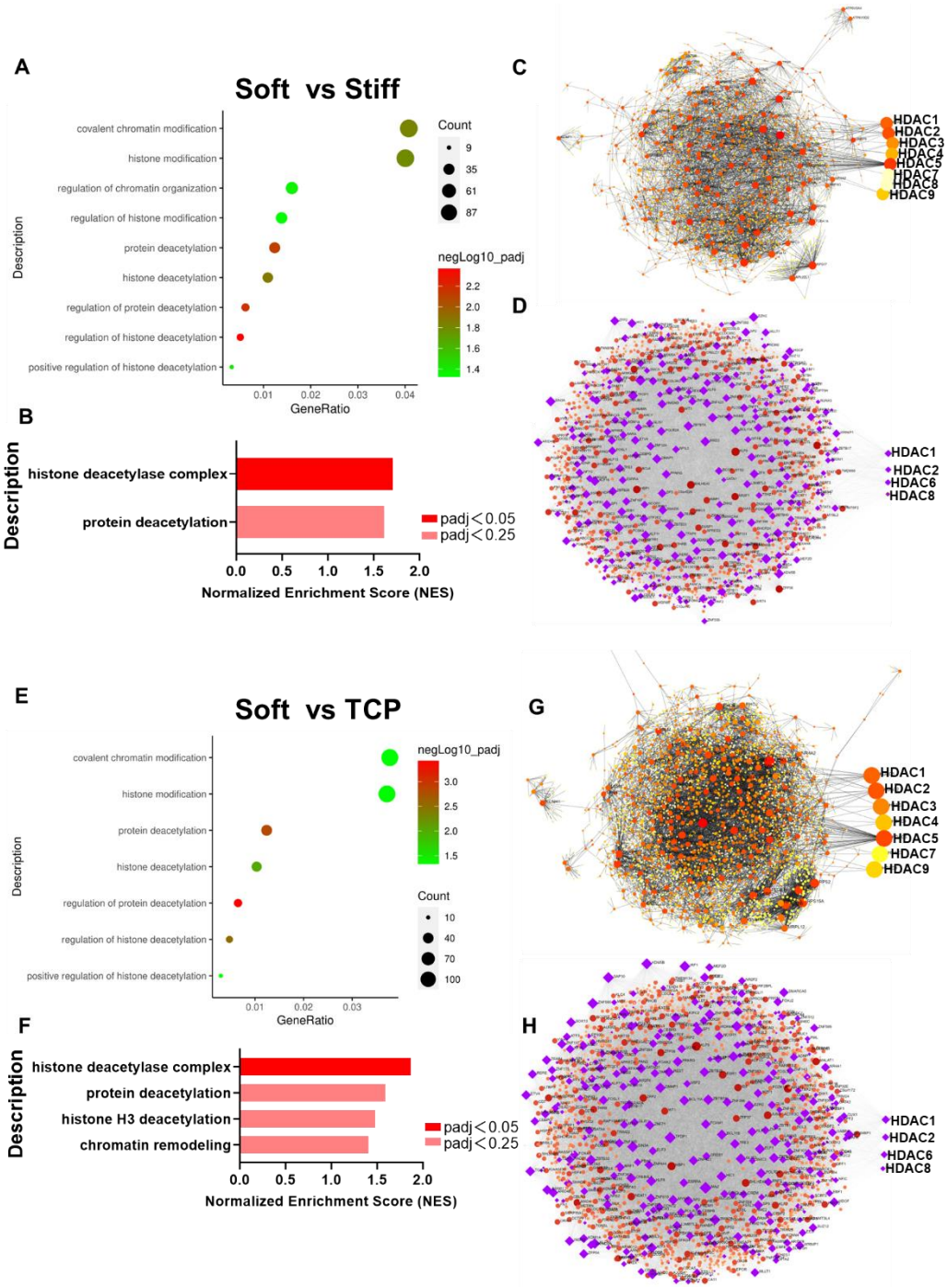

Figure 5.3 Functional enrichments and integrated regulatory network reveal histone deacetylation induced by matrix softness. Cleveland plot for GO over-representation analysis (ORA) of up-regulated genes in 231-0.6 kPa cells versus (A) 231-35 kPa cells or (E) 231 cells on TCPs. Significantly enriched chromatin remodeling-associated pathways are shown in the diagrams (Padj < 0.05). GSEA of DEGs in 231-0.6 kPa cells versus (B) 231-35 kPa cells or (F) 231 cells on TCPs. Significantly enriched chromatin remodeling-associated terms from GO are shown (normalized enrichment score (NES > 1), Padj < 0.25). Generic protein-protein Interactions (PPI) network of DEGs in 231-0.6 kPa cells versus (C) 231-35 kPa cells or (G) 231 cells on TCPs. Different colors of nodes reflect the interaction degree and the

grey edge represents the interaction. The network was generated using PPIs obtained from the STRING database (version 10) and visualized using NetworkAnalyst. The enlarged nodes of HDACs were presented. Gene Regulatory Network (GRN) of DEGs in 231-0.6 kPa cells versus (D) 231-35 kPa cells or (H) 231 cells on TCPs. Round nodes represent genes and purple square nodes represent transcriptional factors (TFs). Grey edge indicates TF regulation. The network was generated using TFs and gene target data obtained from the ENCODE ChIP-seq data and visualized using NetworkAnalyst. The enlarged nodes of HDACs were presented.

To explore the effect of matrix softness on chromatin remodeling, the chromatin condensation parameter (CCP) as a measure of chromatin condensation level was adopted to evaluate the edge density and chromatin compaction in the nucleus using image processing. Based on representative nuclei image analysis of heterochromatin and its edges, more heterochromatin and higher edge density were observed within the nuclei of 231-0.6 kPa cells compared to the nuclei of 231 cells (Fig 5.4A). The calculation of CCP values for both conditions reveals pronounced differences, where the chromatin condensation level of 231-0.6 kPa cells was significantly higher than that of 231 cells (Fig 5.4B). Furthermore, we sought to investigate the adaptive dynamics of chromatin remodeling after 231 cells were transplanted on the soft and stiff matrices. Consistent with the previous study [223], significantly higher chromatin condensation was observed after 1-day post re-seeding on the soft matrices (Fig 5.4C). Interestingly, chromatin condensation levels remained gradually increased even after day 15 on soft matrices and then slightly decreased on day 30 after culture on soft matrices. Although there was a fluctuation of CCP after the cells were cultured on the soft matrices, chromatin maintained a significantly high level of CCP above baseline condensation observed on TCPs. Despite similar fluctuation was also observed, there were no significant changes in CCP after day 1 and day 30 post reseeding on stiff matrices. This result indicated that the matrix softness induces continuous chromatin remodeling and eventually causes chromatin condensation. Chromatin condensation is governed by histone acetyltransferases (HATs) and histone deacetylases (HDACs). Moreover, mechano-sensitivity of HDACs has been reported [195, 214, 223]. In light of bioinformatic analysis, we next probe the activity of HDACs. The activity of HDACs was highly up-

regulated in 231-BrM cells compared to other cells, which indicated that the priming of matrix softness increases HDACs activity and promotes chromatin condensation (Fig 5.4D).

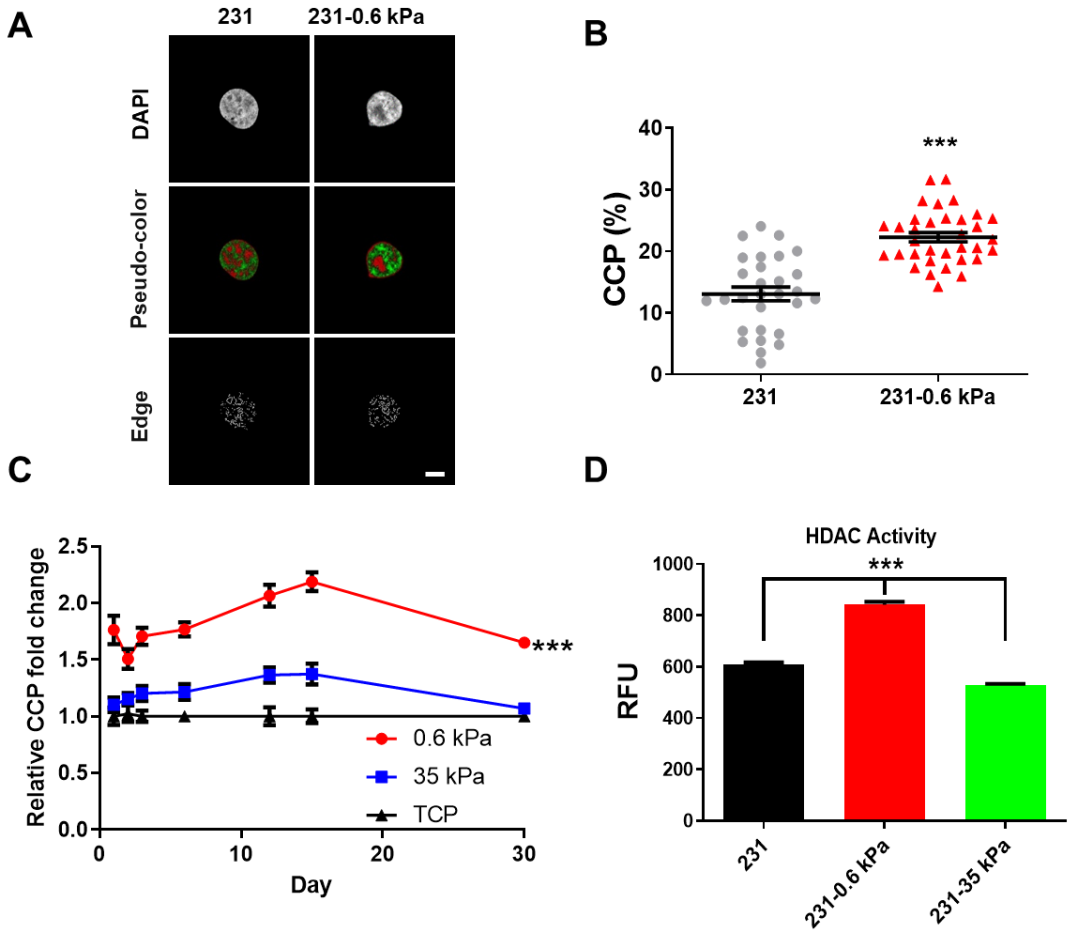

Figure 5.4 Matrix softness promotes chromatin condensation and increases HDAC activity. (A-B) Chromatin condensation parameter (CCP) of 231 on TCPs and 231-0.6 kPa cells on soft matrices were measured. The representative images of nuclei subjected to CCP analysis are presented (upper: DAPI stained nuclei, medium: green color standing for heterochromatin regions, bottom: corresponding edge detection.). Scale bar, 5 μm. (C) 231 Cells were seeded on 0.6kPa, 35 kPa PA gels and TCPs respectively. CCP was measured on days 1, 2, 3, 6, 12, 15 and 30. (D) The activity of HDACs was measured in cells cultured on 0.6kPa for 24 h. N=3, isolates; mean ± SEM; ***, $p < 0.001$.

To investigate the role of chromatin condensation in matrix softness-induced brain metastasis ability, we utilized Vorinostat (SAHA), an HDAC inhibitor, to treat 231-0.6 kPa cells. Firstly, the CCP value was measured to verify the inhibitory effect of SAHA

on chromatin condensation. The result showed that SAHA treatment effectively decreased the degree of chromatin condensation (Fig 5.5A). Then we sought to test whether SAHA can inhibit brain metastasis ability induced by matrix softness. 231-0.6 kPa cells on soft matrices were pretreated with SAHA for 3 days and then the expression of brain metastasis-related genes, proliferation rate on TCPs or soft matrices, and BBB transmigration ability were determined. Notably, the SAHA treatment markedly decreased the expression levels of brain metastasis genes (Fig 5.5B). The proliferation rate of 231-0.6 kPa cells was restrained by SAHA both on TCPs and on soft matrices (Fig 5.5C). Furthermore, SAHA treatment antagonized the BBB transmigration of 231-0.6 kPa cells (Fig 5.5G and H). To exclude the potential false positive caused by the side effect of SAHA, we verified these results by the other known HDAC inhibitor, Trichostatin A (TSA). Consistently, chromatin condensation was decreased and brain metastasis gene signature of 231-0.6 kPa cells was significantly abolished by TSA treatment (Fig 5.5D and E). Without affecting the proliferation on TCPs, TSA also decreased the proliferation rate on soft matrices (Fig 5.5F). In addition, suppression effect of TSA on BBB transmigration was observed (Fig 5.5G and H). We further extended these results to 4T1 cell line. The BBB transmigration ability and proliferation ability of 4T1-0.6 kPa cells on soft matrices were inhibited by TSA treatment (Fig 5.5I and J). All of these findings indicate that disruption of chromatin condensation via HDAC inhibitor attenuates the brain metastasis ability of matrix softness-priming cells.

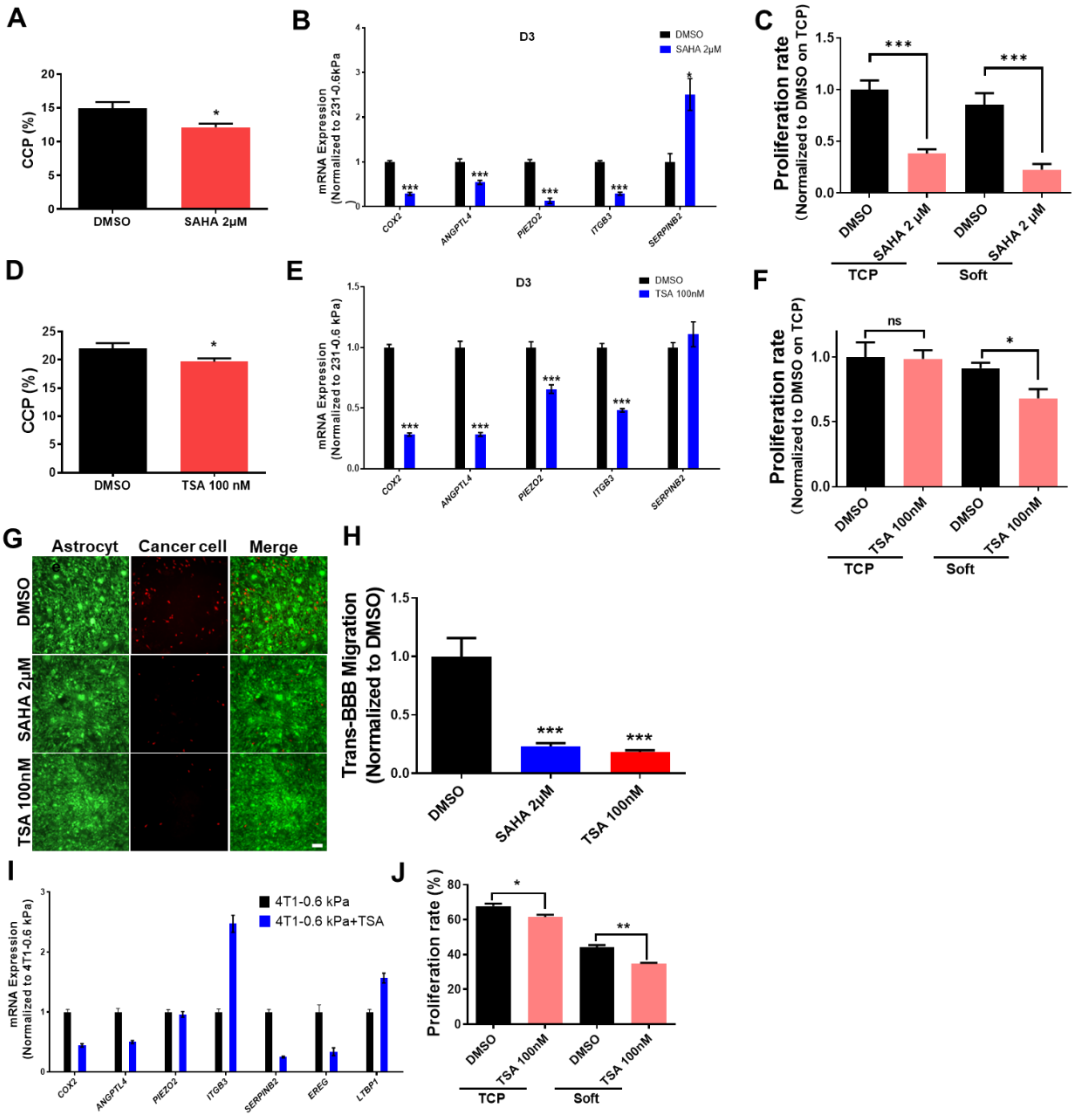

Figure 5.5 The inhibition of HDACs activity disturbs the gene signature associated with brain metastasis, the proliferation on soft matrices and BBB transmigration ability of 231-0.6 kPa cells. (A) 231 cells cultured on TCPs were treated with or without 2 μM SAHA for 24 h. CCP of cells was measured. (B) 231-0.6 kPa cells were treated with or without 2 μM SAHA for 3 days. The expression levels of brain metastasis-related genes were measured by qPCR. (C) After treatment with or without 2 μM SAHA for 3 days, the proliferation of 231-0.6 kPa cells seeded on TCPs or 0.6 kPa gels for 24h was measured by EdU assay. (D) 231-0.6 kPa were treated with or without 100 nM TSA for 24 h. CCP of cells were measured. (E) 231-0.6 kPa cells were treated with or without 100 nM TSA for 3 days. The expression levels of brain metastasis-related genes were measured by qPCR. (F) After treatment with or without 100 nM TSA for 3 days, the proliferation of 231-0.6 kPa cells seeded on TCPs or 0.6 kPa gels for 24h was measured by EdU assay. (G) 231-0.6 kPa cells were pretreated with 2 μM SAHA or 100 nM TSA for 3 days. The BBB *in vitro* model was applied to measure the BBB transmigration ability of cells. The representative images (G) and quantification (H) are shown. Scale bar, 100 μm. (I) 4T1-0.6 kPa cells were treated with

or without 100 nM TSA for 3 days. The expression levels of brain metastasis-related genes were measured by qPCR. (J) After treatment with or without 100 nM TSA for 3 days, the proliferation of 4T1-0.6 kPa cells seeded on 0.6 kPa gels or TCPs for 24h was measured by EdU assay. N=3, isolates; mean ± SEM; ns, $p > 0.05$; *, $p < 0.05$; **, $p < 0.01$; and ***, $p < 0.001$.

We further investigated whether chromatin condensation is sufficient to drive the increase of brain metastasis ability. The inhibitor of HAT, Anacardic acid (ANA), was used to treat 231 cells on TCPs. As shown in the results, ANA treatment failed to induce brain metastasis gene signature and decreased proliferation on TCPs and soft matrices (Fig 5.6A and B). Meanwhile, ANA treatment potently increased the BBB transmigration of tumor cells, which indicated the important role of heterochromatin in promoting tumor cells to penetrate BBB (Fig 5.6C and D). This may be caused by the promotion effect for confined migration ability by the high level of heterochromatin[275]. These results demonstrated that the pharmacologically induced chromatin condensation was not enough to drive the phenotypes of brain metastasis.

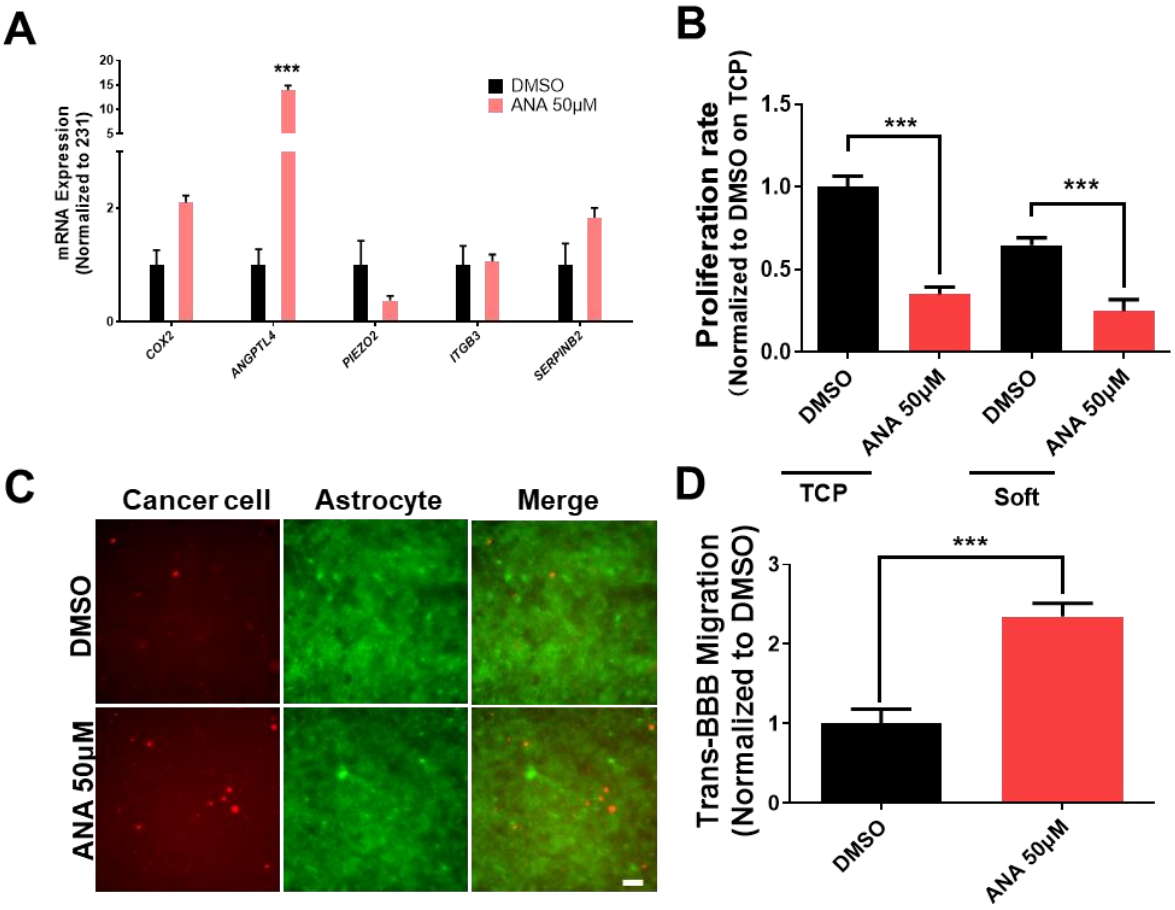

Figure 5.6 The inhibition of HATs enhances BBB transmigration ability but fails to induce the brain metastatic gene signature and high proliferation on soft matrices. (A) 231 cells were treated with 50 μM ANA for 3 days, and then the expression levels of brain metastasis-related genes were measured by qPCR. (B) Cells pretreated with 50 μM ANA for 3 days were seeded on 0.6 kPa PA gels for 24 h, and then the proliferation rate was measured. (D) BBB transmigration ability of cells was analyzed using *in vitro* model. (E) Quantification of trans-migrated cells is shown. Scale bar, 100 μm. N=3, isolates; mean ± SEM; *, $p < 0.05$; **, $p < 0.01$; and ***, $p < 0.001$.

Although the previous findings demonstrated the inhibition of HDACs attenuated the brain metastatic activity of 231-0.6 kPa cells, we wondered if the acquisition of brain metastatic features after the conditioning of matrix softness required HDAC activity. Thus, 231 cells were transplanted on the soft matrices for 10 passages and TSA was supplied to inhibit HDAC activity for this duration. Intriguingly, chronic TSA treatment completely prevented the emergence of the matrix softness-induced brain metastatic gene signature (Fig 5.7A). Cells suffering from chronic HDAC inhibition showed the decrease in proliferation on soft matrices compared to 231 cells and 231-0.6 kPa cells

(Fig 5.7B). Moreover, chronic TSA treatment also markedly antagonized BBB transmigration ability (Fig 5.7C and D). Together, these results demonstrated the dependence of acquisition of brain metastatic ability induced by matrix softness on HDAC activity, as well as the ability of HDAC inhibitors to effectively antagonize these effects.

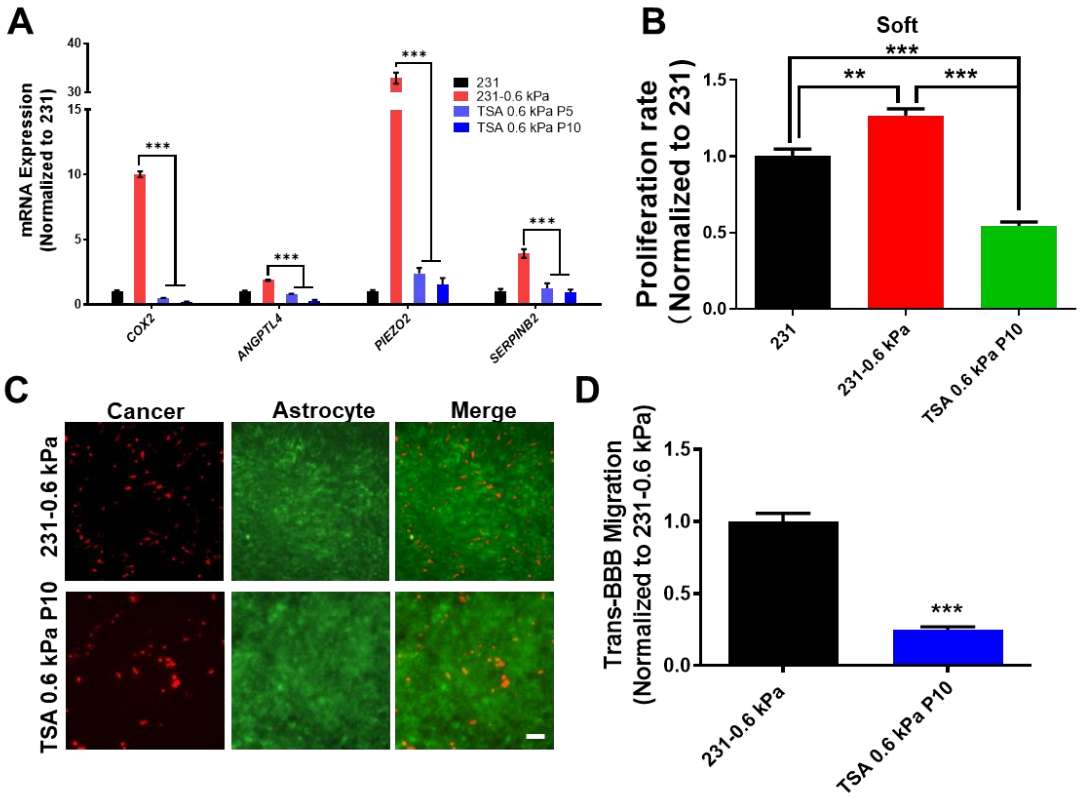

Figure 5.7 HDAC activity is required for matrix softness-induced acquisition of brain metastatic gene expressions, adaptation to soft matrix and BBB penetration ability. (A) 231 cells were cultured on 0.6 kPa PA gels and treated with 100 nM TSA for 10 passages. Total RNA samples were collected at P5 and P10 after priming, and the expression levels of brain metastasis-related genes were measured by qPCR. The pretreated cells were donated with TSA 0.6kPa P5 and with TSA 0.6kPa P10 cells respectively. (B) Cells were seeded on 0.6 kPa PA gels for 24 h, and then the proliferation rate was measured. (C) BBB transmigration ability of cells was analyzed using *in vitro* model. (D) Quantification of trans-migrated cells is shown. Scale bar, 100 μm. N=3, isolates; mean ± SEM; *, $p < 0.05$; **, $p < 0.01$; and ***, $p < 0.001$.

5.2.3 HDAC3 mediates matrix softness-induced brain metastasis

Class I HADCs, including HDAC1, 2, 3 and 8, play the dominant role in promoting chromatin condensation [276]. Motivated by the prior results showing suppression of HDAC activity prevented effectively the brain metastatic phenotype from emergence on soft matrices, these four known class I HDACs were knocked down by using siRNA to investigate the vital epigenetic modulator in response to matrix softness. We observed that HDAC3 knockdown considerably decreased the expressions of the genes related to brain metastasis in 231-0.6 kPa cells on soft matrices, while siHDAC1, 2 and 8 had relatively little effect (Fig 5.8A-D). Although all HDAC1, 2 and 3 knockdowns deregulated the proliferation rate of 231-0.6 kPa cells on the soft matrices, the effect of HDAC3 on proliferation was much more significant (Fig 5.8E). Intriguingly, siHDAC3 upregulates the proliferation of 231-0.6 kPa cells on TCPs, despite an inhibitory effect on the proliferation of 231 cells on soft substrates (Fig 5.8F and G). Of note, siHDAC3 but not other siHDACs effectively disrupted the BBB transmigration ability (Fig 5.8H and I). These results demonstrated that HDAC3 knockdown substantially suppresses brain metastatic phenotype of soft niches-primed cells.

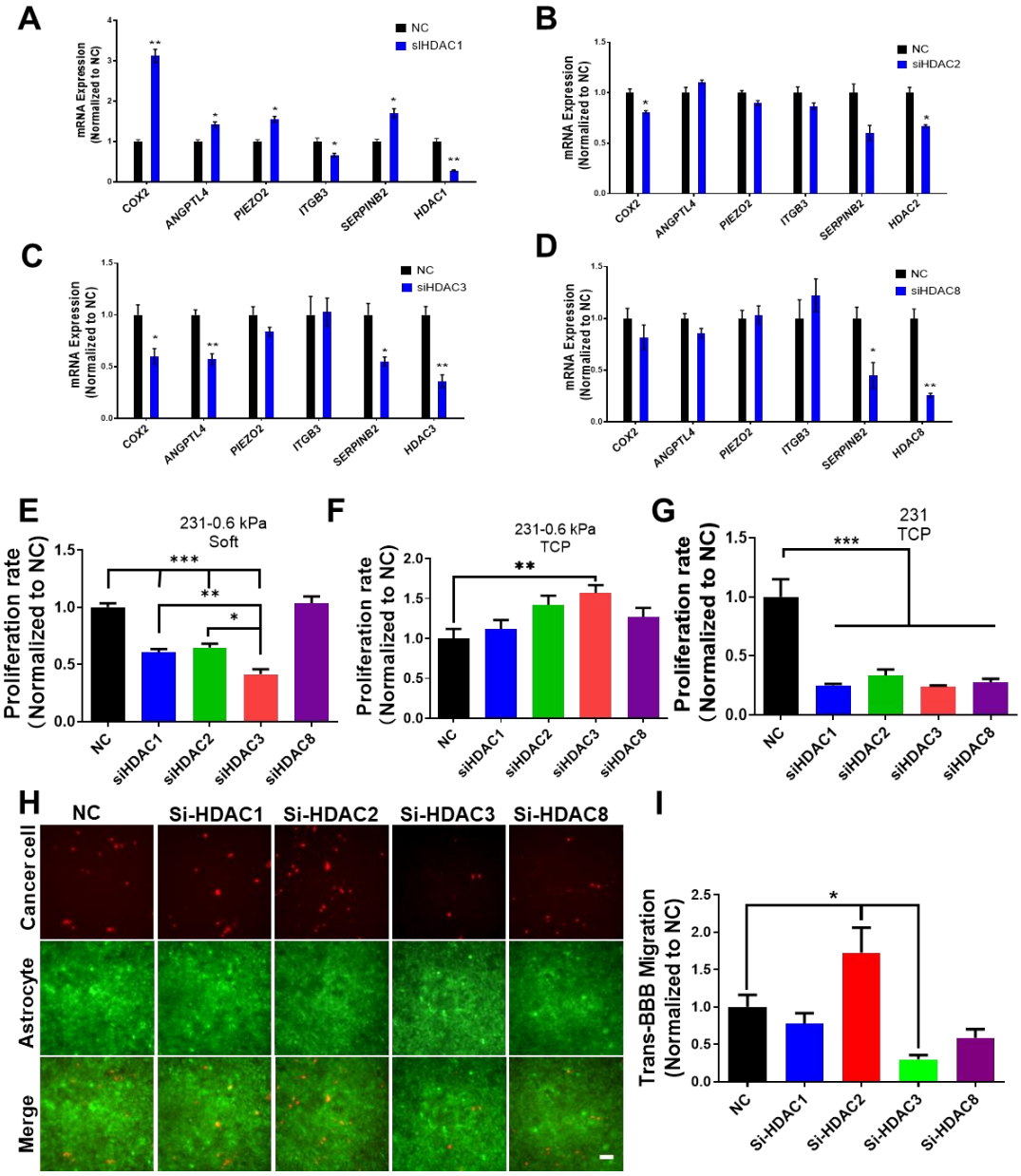

Figure 5.8 HDAC3 knockdown in soft matrix-priming cells decreases brain metastasis-related gene expressions, proliferation on soft matrices and BBB transmigration. (A-D) HDAC1, 2, 3, and 8 were knocked down in 231-0.6 kPa Cells on 0.6kPa substrates respectively. After 72h, the total RNA was collected and the brain metastasis-related gene expressions were measured by qPCR. (E-F) HDAC1, 2, 3 and 8 were knocked down in 231-0.6 kPa Cells on 0.6kPa substrates respectively. After 72h, cells were seeded on TCPs and 0.6 kPa PA gels for 24h. The proliferation rate was measured by EdU assay. (G) HDAC1, 2, 3 and 8 were knocked down in 231 cells on TCPs respectively. After 72h, cells were seeded on TCPs for 24h. The proliferation rate was measured by EdU assay. (H) After HDAC1, 2, 3, and 8 were knocked down in 231-0.6 kPa cells on 0.6kPa substrates for 3 days respectively. The BBB transmigration ability of cells was analyzed using *in vitro* model. (E) Quantification of transmigrated cells is shown. Scale bar, 100 μm. N=3, isolates; mean ± SEM; *, $p < 0.05$; **, $p < 0.01$; and ***, $p < 0.001$.

To delve deeper into the mechanism, we further investigated whether the soft priming resulted in an altered expression level and deacetylation activity of HDAC3. We analyzed the protein expression level of HDAC3. As expected, the result of western blotting showed HDAC3 was highly upregulated in 231-0.6 compared to 231 cells on the soft matrices, and this result was further confirmed using immunostaining (Fig 5.9A-D). Moreover, we verified the activity of HDAC3, which correlated with its protein expression, by HDAC3 immunoprecipitation and activity assay. A significant increase in HDAC3 activity was observed in 231-0.6 kPa cells compared to 231 cells on the soft matrices (Fig 5.9E). We wondered about the role of the increase of HDAC3 activity in the brain metastatic phenotype of 231-0.6 kPa cells. RGFP966, a selective HDAC3 inhibitor, was used to pretreat 231-0.6 kPa cells. Suppression of HDAC3 activity decreased the proliferation rate of 231-0.6 kPa regardless of substrate stiffness (Fig 5.10A and B). However, we noticed that the opposite effects between HDAC3 inhibition with RGFP966 and HDAC3 knockdown with siRNA on the proliferation of cells on TCPs, which may be caused by the side effect of RGFP966. Moreover, RGFP966 pretreatment inhibited the BBB transmigration ability of 231-0.6 kPa cells (Fig 5.10 C and D). Next, we sought to explore whether HDAC3 overexpression is sufficient to increase brain metastasis ability. Interestingly, transient transfection of HDAC3 overexpression (HDAC3 OV) plasmid did not induce the brain metastatic gene signature (Fig 5.11A). To avoid the short duration of transient transfection is not enough to induce brain metastasis ability, we established a stable cell line with HDAC3 overexpression. The validity of the HDAC3 OV stable cell line was confirmed by qPCR and immunofluorescence (Fig 5.11B and C). Indeed, the brain metastatic gene signature was not observed in HDAC3 OV stable cell line (Fig 5.11D). Overexpression of HDAC3 did not change proliferation rate of cells not matter on soft matrices or TCPs (Fig 5.11E and F). Furthermore, overexpression of HDAC3 had no effect on BBB transmigration ability (Fig 5.11G and H). Together, these results demonstrated that HDAC3 activity was necessary but not sufficient for the gain of brain metastatic phenotype post-soft priming.

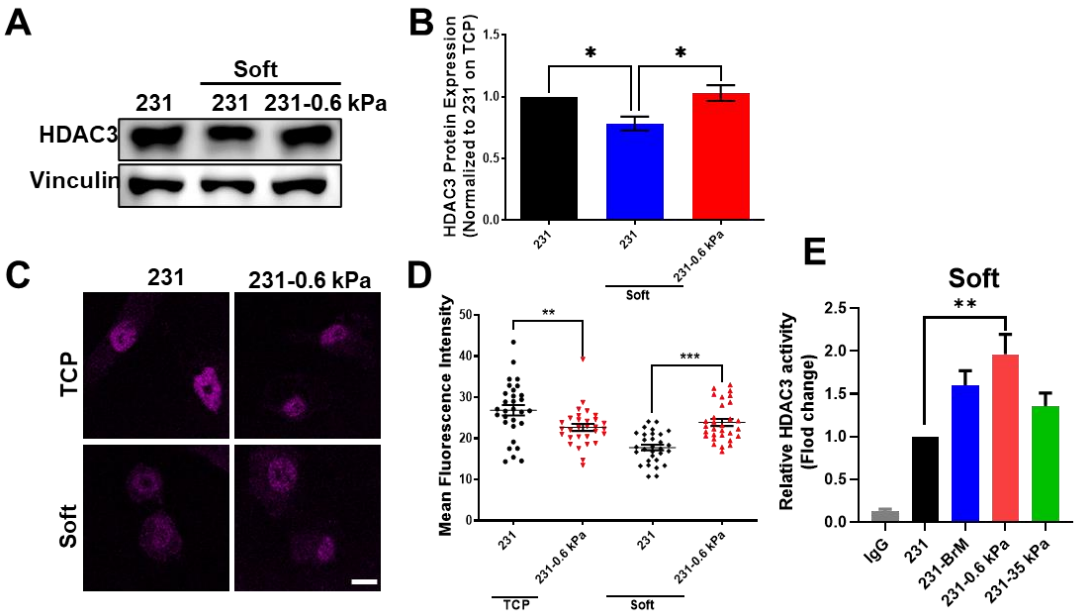

Figure 5.9 Matrix softness priming increases the expression and activity of HDAC3. (A) Cells were seeded on 0.6 kPa PA gels or TCPs for 24 h. The expression levels of HDAC3 protein were analyzed by Western blotting. (B) Quantification of HDAC3 expression normalized to Vinculin from (D). (C) The expression levels of HDAC3 were examined by immunofluorescence. The representative images are shown. Scale bar, 20 μm. (D) Quantification of mean fluorescence intensity in (C). (E) Cells were seeded on soft matrices for 24 h, and then the activity of HDAC3 was measured. N=3, isolates; mean ± SEM; *, $p < 0.05$; **, $p < 0.01$; and ***, $p < 0.001$.

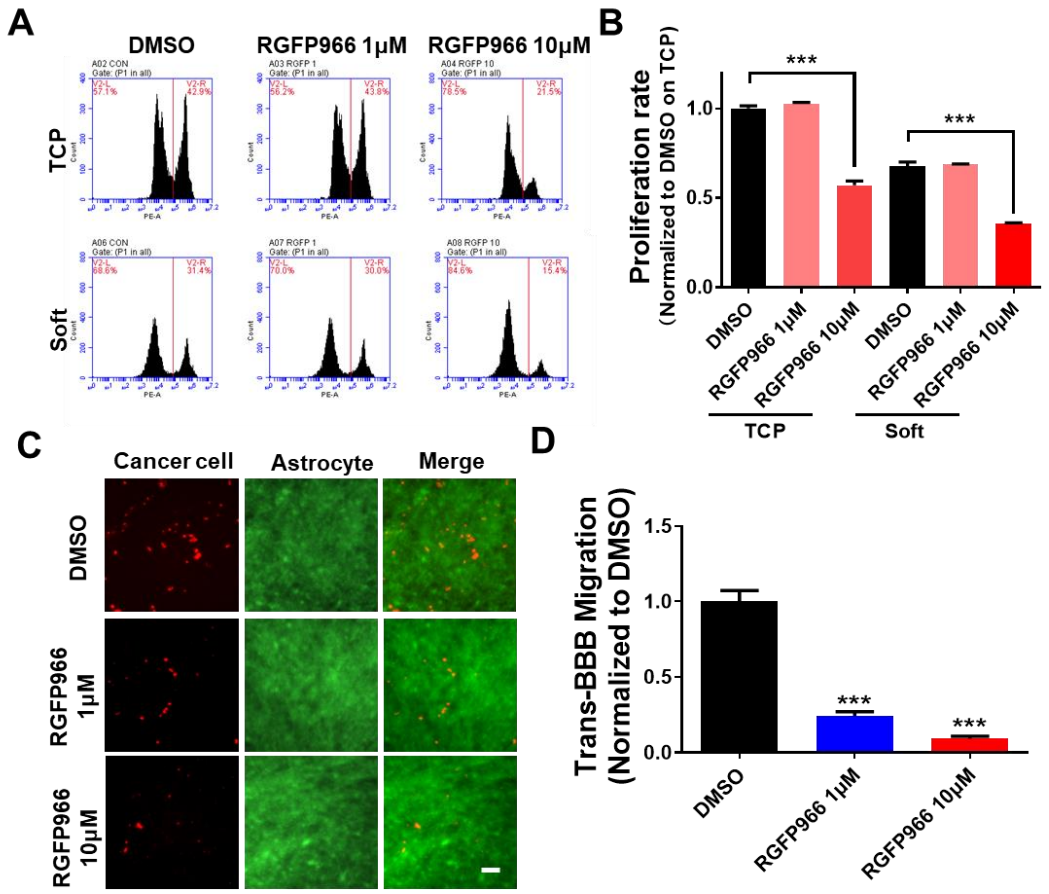

Figure 5.10 Pharmacological disruption of HDAC3 activity inhibits matrix softness-induced enhancements in proliferation on soft matrices and BBB transmigration. (A) 231-0.6 kPa cells were treated with RGFP966 for 3 days, and then cells were seeded on 0.6 kPa PA gels or TCPs for 24 h. (B) The proliferation rate was measured. (D) BBB transmigration ability of cells pretreated with RGFP966 was analyzed using *in vitro* model. (E) Quantification of trans-migrated cells is shown. Scale bar, 100 μm. N=3, isolates; mean ± SEM; *, $p < 0.05$; **, $p < 0.01$; and ***, $p < 0.001$.

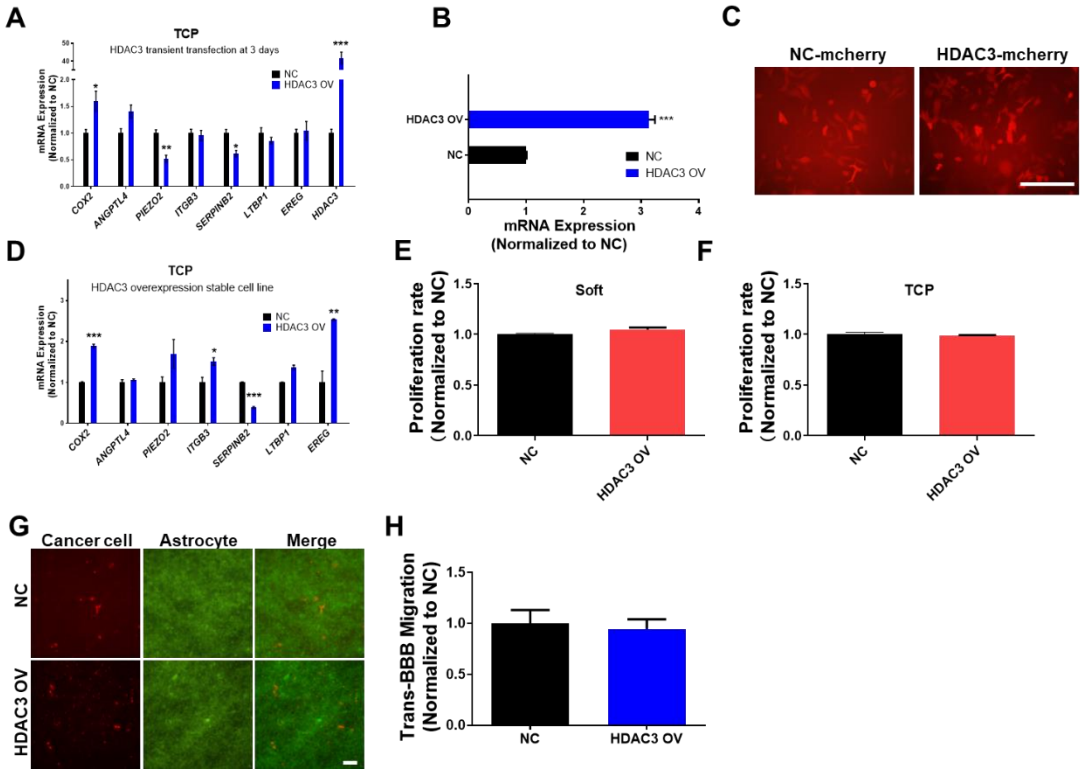

Figure 5.11 HDAC3 overexpression is not sufficient to induce brain metastatic gene signature and increase proliferation on soft matrices and BBB transmigration. (A) 231 cells were transiently transfected with HDAC3 for 3 days and then the expression levels of brain metastasis-related genes were measured using qPCR. (B) 231 cell line with HDAC3-mcherry stable overexpression was established. The RNA expression levels of HDAC3 were examined using qPCR. (C) The expression of NC-mcherry and HDAC3-mcherry was examined by fluorescence microscope. Scale bar, 100 μm. (D) The expression levels of brain metastasis-related genes were measured in HDAC3 stable overexpression cells using qPCR. The proliferation rate of HDAC3 stable overexpression cells on (E) 0.6 kPa PA gels and (F) TCPs was measured by EdU assay. (G) BBB transmigration ability of HDAC3 stable overexpression cells was analyzed using *in vitro* model. Scale bar, 100 μm. (H) Quantification of trans-migrated cells is shown. N=3, isolates; mean ± SEM; *, $p < 0.05$; **, $p < 0.01$; and ***, $p < 0.001$.

5.2.4 Inhibition of HDAC3 effectively antagonizes brain metastasis *in vivo*

It is worth noting that RGFP966, serving as a highly selective HDAC3 inhibitor, can penetrate BBB [277]. Thus, to further examined whether HDAC3 inhibition led to the decrease of brain metastasis incidence and the suppression of tumor outgrowth in the brain, we followed brain metastasis progression of 231-0.6 kPa cells in response to RGFP966 intervention. 231-0.6 kPa cells were inoculated into nude mice through

intracardiac injection and tracked with bioluminescence imaging every week. After implantation of tumor cells, RGFP966 or vehicle was given every 2 days (Fig 5.12A). We evaluated brain metastasis-free survival and found that RGFP966 treatment significantly increased the brain metastasis-free survival time in both concentrations (Fig 5.12B). Furthermore, high-dose RGFP966 treatment effectively suppressed the outgrowth of brain metastasis (Fig 5.12C and D). Of note, RGFP966 treatment also decreased the bioluminescence signal in the rest of the body besides the brain, highlighting the broad inhibitory effect on tumors (Fig 5.12E). To further confirm the effect of RGFP966 on brain metastasis, we also performed the brain slice assay. The results showed that RGFP966 significantly decreased the burden of brain tumor and the number of macroscopic lesions (Fig 5.12F-H). Together, these results strongly indicated the inhibition of HDAC3 impaired the brain metastasis progression of 231-0.6 kPa cells.

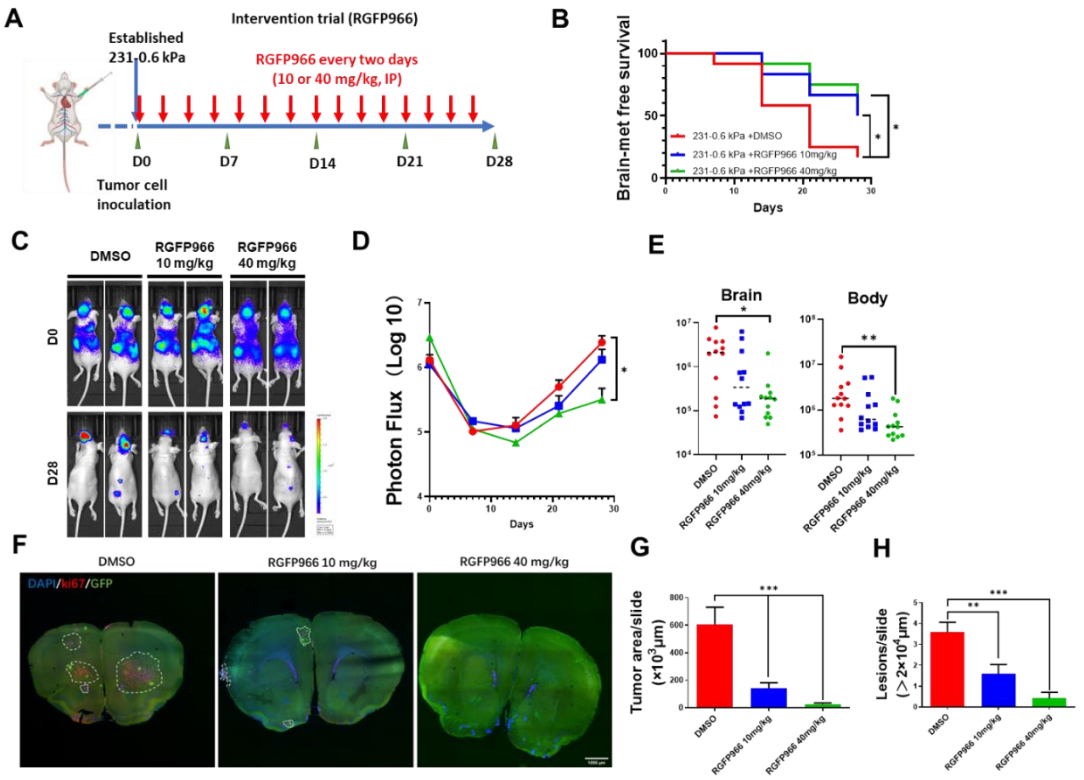

Figure 5.12 HDAC3 inhibitor decreases matrix softness-induced brain metastasis in vivo. (A) Scheme of experimental design of intervention trial. Following inoculation of 231-0.6 kPa cells *via* intracardiac injection, HDAC3 inhibitor RGFP966 was injected through the intraperitoneal injection every two days. BLI photon flux signals were measured on days 1, 2, 3, 7, 14, 21, and 28. (B) Kaplan-Meier analysis for brain metastasis-free survival compared among groups was measured by BLI photon flux

signals from (A). (C) Representative images of whole-body BLI photon flux signals on days 0 and 28. (D) Quantification of the growth of brain metastasis monitored by BLI in (A). (E) Quantification of BLI photon flux signals in the brain and body of mice on day 28. (F) Immunofluorescence images of brain slice tissue from (A) detected with ki67 antibody. (G)Quantification of tumor area (G) and lesion numbers (H) in (F). N=3, isolates; mean ± SEM; *, $p < 0.05$; **, $p < 0.01$; and ***, $p < 0.001$.

5.2.5 Strengthening/weakening mechanotransduction suppresses/promotes breast cancer brain metastasis

The actin cytoskeleton acts as a vital mechanotransducer and has been reported to regulate chromatin remodeling and accessibility in response to the various mechanical stimuli [11, 225]. In light of the weak actin cytoskeleton in the cells on the soft matrices, we investigate whether destabilization of the cytoskeleton was responsible for brain metastatic phenotype induced by matrix softness. Thus, to disrupt the cytoskeleton and tension transmission, cells on TCPs were chronically treated with actin polymerization inhibitor cytochalasin D (CytoD) or ROCK inhibitor Y-27632 (Fig 5.13 A). Interestingly, chronic CytoD treatment significantly enhanced the activity of HDAC3 (Fig 5.13B). Moreover, long-term treatment of CytoD but not Y-27632 induced the gene signature related to brain metastasis, whereas short-term treatment of these inhibitors did not exert a similar effect (Fig 5.13 C and D). The proliferation ability on TCPs or soft matrices was increased by both CytoD and Y-27632 chronic treatment (Fig 5.13 E and F). Furthermore, cells treated with CytoD exhibited a high BBB transmigration ability compared to DMSO and Y-27632-treated cells. Together, these results indicated that extended disruption of the actin cytoskeleton was sufficient to induce the acquisition of brain metastasis ability (Fig 5.13 G and H). Aside from that, these results duplicated the phenomenon post cell re-seeded on the soft matrices, which implied brain metastatic phenotype is the consequence of long-term shaping following cellular responses to matrix compliance.

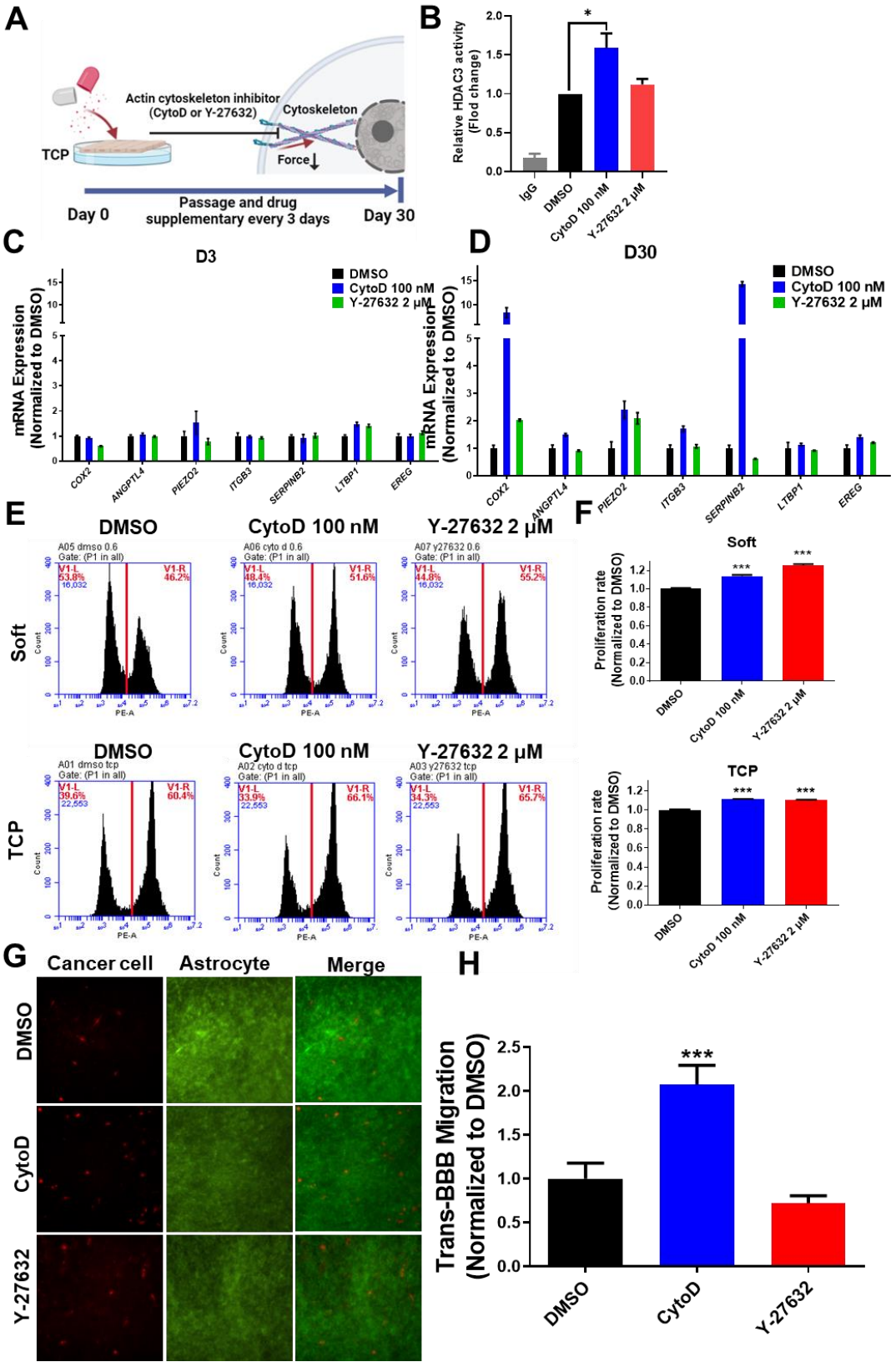

Figure 5.13 Disruption of F-actin polymerization in long term induces brain metastatic gene signature and increases proliferation on soft matrices and BBB transmigration of breast cancer cells. (A) Scheme of experimental design. 231cells were cultured on TCPs and treated with DMSO, 100 nM CytoD or 2 μM Y-27632 for

10 passages. (B) HDAC3 activity was measured after cells were treated with inhibitors for 30 days. Total RNA samples were collected on day 3 (C) and day 30 (D) after inhibitor treatment, and the expression levels of brain metastasis-related genes were measured by qPCR. (E-F) The pretreated cells were seeded on 0.6 kPa PA gels or TCPs for 24 h, and then the proliferation rate was measured. (G) After pretreatment, BBB transmigration ability of cells was analyzed using *in vitro* model. (H) Quantification of trans-migrated cells is shown. Scale bar, 100 μm. N=3, isolates; mean ± SEM; *, $p < 0.05$; **, $p < 0.01$; and ***, $p < 0.001$.

We then verified whether stabilization of actin cytoskeleton could also prevent the acquisition of brain metastasis ability. Actin polymerization activator jasplakinolide (Jas) and Rho activator narciclasine (Narci) were used to treat 231 cells transferred to the soft matrices for 30 days (Fig 5.14A). The result showed that chronic Jas treatment notably antagonized HDAC3 activity (Fig 5.14B). The brain metastatic gene signature induced by matrix softness was partially rescued by chronic Jas treatment but not Narci treatment (Fig 5.14C). Both inhibitors suppressed proliferation ability on soft matrices (Fig 5.14D and E). Moreover, obvious inhibitory effects on BBB transmigration ability were obtained after chronic treatment with Jas or Narci (Fig 5.14F and G). Next, we wondered if the transient activation of actin cytoskeleton on TCPs had similar effect on brain metastasis ability. Of note, the treatment with Jas or Narci did not result in deregulation of brain metastasis genes expression (Fig 5.15A). Opposite to suppression effects on soft matrices, treatment with Narci promoted the proliferation ability of cells on TCPs, whereas treatment with Jas had no effect (Fig 5.15B and C). Based on these results, the effects of actin cytoskeleton activators on cells differ depending on the stiffness of the substrate. Together, these data demonstrated that actin polymerization or the promotion of contractility inhibited the establishment of brain metastatic phenotypes caused by the matrix softness.

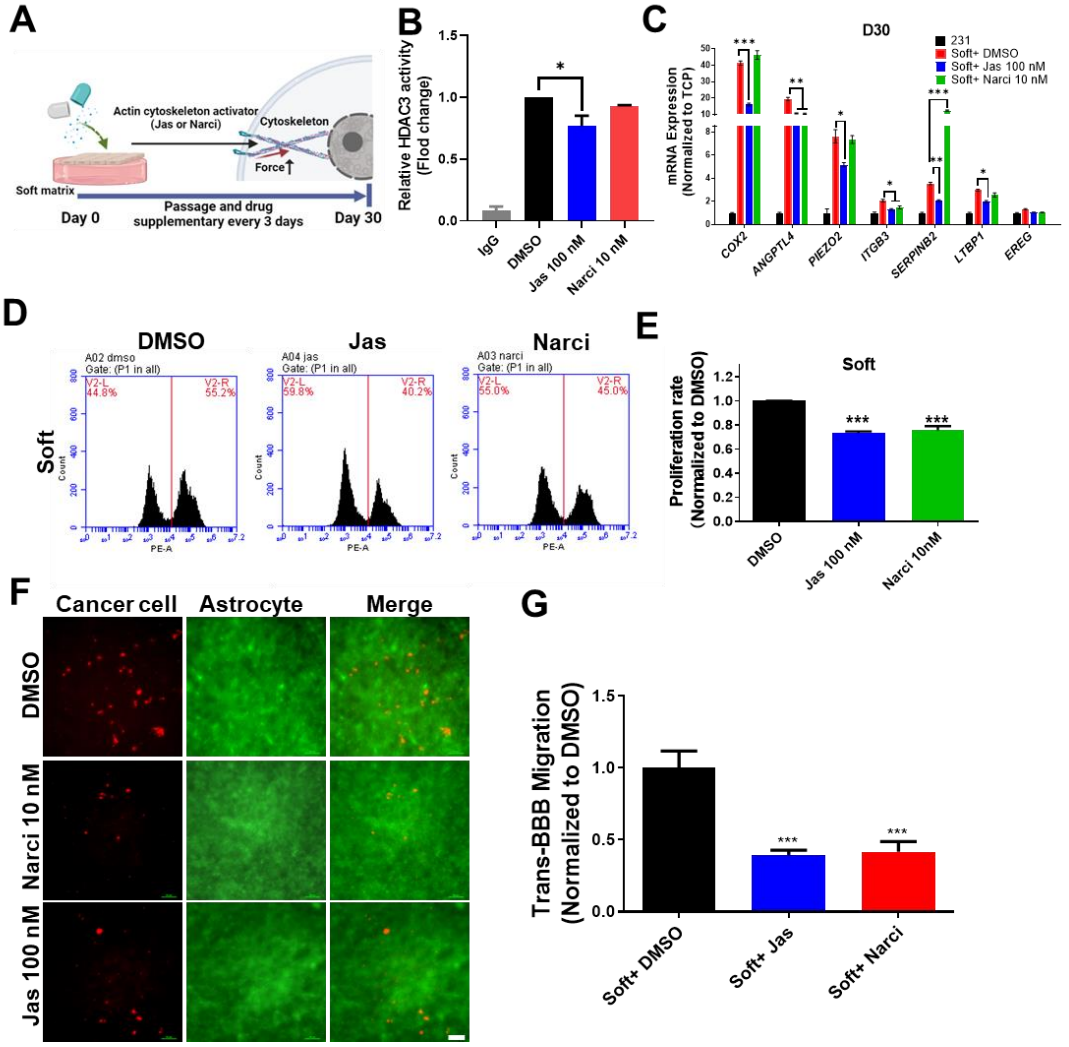

Figure 5.14 Promotion of F-actin polymerization prevents the acquisition of brain metastatic phenotype induced by matrix softness. (A) Scheme of experimental design. 231 cells were cultured on 0.6 kPa PA gels and treated with DMSO, 100 nM Jas or 10 nm Narci for 10 passages. (B) HDAC3 activity was measured after 10 passages. (C) Total RNA samples were collected on day 30 after inhibitor treatment, and the expression levels of brain metastasis-related genes were measured by qPCR. (D-E) The pretreated cells were seeded on 0.6 kPa PA gels for 24 h, and then the proliferation rate was measured. (F) After pretreatment, BBB transmigration ability of cells was analyzed using *in vitro* model. (G) Quantification of trans-migrated cells is shown. Scale bar, 100 μm. N=3, isolates; mean ± SEM; *, $p < 0.05$; **, $p < 0.01$; and ***, $p < 0.001$.

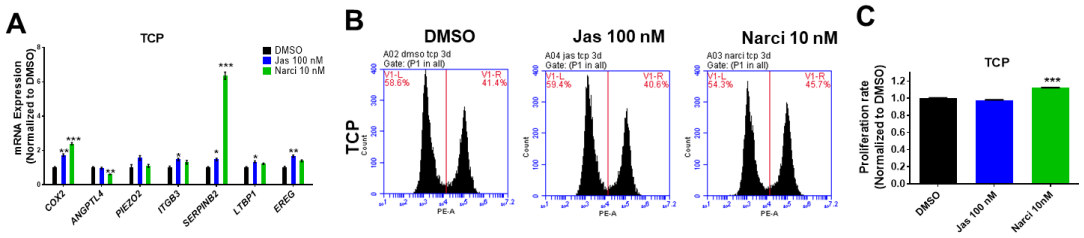

Figure 5.15 The interference effect of F-actin polymerization on gene signature related to brain metastasis and proliferation on soft matrices is matrix stiffness-dependent. (A) 231 cells were treated with DMSO, 100 nM Jas or 10 nm Narci for 3 days. Total RNA samples were collected and the expression levels of brain metastasis-related genes were measured by qPCR. (B-C) The pretreated cells were seeded on TCPs for 24 h, and the proliferation rate was measured. N=3, isolates; mean ± SEM; *, $p < 0.05$; **, $p < 0.01$; and ***, $p < 0.001$.

5.3 Discussion

Metastatic seeds for distant organic metastasis are believed to preexist in the primary site containing heterogeneous tumor cells. It has been demonstrated that subpopulations derived from the same parental cell line exhibit distinct organotropism [266]. The Mesenchymal Stroma in primary tumor contributes to the selection of bone metastatic clones [4]. Of note, selection pressure imposed by matrix stiffness leads to the arising of cell populations with novel phenotypes [278]. In this study, we gained a comprehensive view of matrix softness-mediated brain metastasis by clone selection as well as epigenetic changes. SCP with brain metastatic gene signature showed the proliferative advantage on soft matrices, indicating matrix softness may impose selection pressure for enriching brain metastatic seeds in the primary tumor. However, plasticity in epigenetics cannot be ignored. Carcinoma cells are facilitated to further metastasize to other organs via the EZH2-mediated epigenomic changes. Moreover, HDACs can respond to mechanical signals to regulate cellular functions [267]. Although with homogeneous genetic background, SCP with poor gene signature for brain metastasis still gained phenotype associated with brain metastasis after matrix softness priming, which demonstrated epigenetic change by matrix softness was an effective way to enhance brain metastasis.

Besides clonal selection, we demonstrated that alterations in chromatin state were driven by matrix softness, which was needed by phenotypic changes to brain metastasis. Compliance matrix enhanced HDAC activity and chromatin condensation in regulating brain metastasis ability in breast cancer cells, which highlighted an indispensable role of HDAC-mediated chromatin condensation in mechanotransduction and response to the change of matrix mechanics. A growing number of studies have focused on global chromatin remodeling and its main regulator-epigenetic modification in mechanoresponse. Cells under stretching undergo chromatin-mediated mechanosensing to further modulate cellular behaviors [194, 225]. Switching from matrix stiffness has been shown to regulate cell differentiation, fibroblast activation and malignant transformation through the class I HDACs-mediated chromatin remodeling [11, 195, 223, 269]. It is worth noticing that chromatin condensation is regarded as a keeper to instil the mechanical memory to maintain certain gene expression patterns and cellular functions, which provides a possible explanation for transcriptional memory of brain metastasis gene signature imposed by matrix softness in our study [11, 279].

HDAC3, a vital member of class I HDACs, has been reported as a mechanoresponsive element in mechanotransduction [216]. Rigid substrate enhances tumorigenic properties in breast epithelium *via* Sp1–HDAC3/8 axis-mediated alteration in chromatin accessibility[269]. The total level and distribution of HDAC3 are both increased on the soft matrices to regulate chromatin architecture [223]. The decrease of actomyosin contractility leads to translocation of HDAC3 from cytoplasm to nucleus [234]. However, although protein expression of HDAC3 was upregulated after soft priming, translocation of HDAC3 was not observed and mainly distribution of HDAC3 was within nuclear in our study, which was possibly caused by the different cell types. We also showed that HDAC3 activity was increased by matrix softness, which relayed on the stabilization of actin cytoskeleton but not Rho/ROCK mediated actomyosin contractility. Interestingly, HDAC3 has been reported to suppress osteoclasts to inhibit

bone remodeling which is important for the outgrowth of tumor cells in bone [280]. Runx2, which is a skeletal transcription factor and plays an essential role in osteolysis during bone development, exhibits aberrant expression in tumor cells that metastasize aggressively to bones [244, 281]. Many studies show HDAC3 can directly interact with Runx2 and antagonize the transcriptional activity, which is similar to the phenomenon that HDACs inhibitor reduces the localization of Runx2 in nuclear [195, 282, 283]. In our study, HDAC3 activity was significantly increased after soft priming. Moreover, matrix softness-induced HDAC3 activity was required by brain metastatic phenotype. Previous studies study has shown that HDAC3 is highly expressed in brain metastases, and its expression level is related to the prognosis of patients [272]. The HDAC inhibitor Vorinostat (SAHA) has a significant therapeutic effect on brain metastases of breast cancer [273]. Together, these shreds of evidence and our data spotlighted HDAC3 playing diametrically opposed roles in brain and bone metastasis, which is similar to the Janus-faced role of DKK1 in lung and bone metastasis [69].

In summary, the present results in this chapter established a paradigm for the mechanism underlying how matrix softness in the primary niche induced the acquisition of brain metastatic characteristics. Not only clonal selection but also epigenetic modification was involved in the matrix softness-induced brain metastasis ability. Matrix softness induced chromatin condensation and upregulated HDAC activity *via* actin cytoskeleton, which was required for the gain of brain metastasis ability.

Chapter 6: The role of cell stiffness in organotropism

6.1 Introduction

A considerable increase in the capacity of cancer cells from a particular organ to spread to specific locations in body was observed [1]. It has been extensively researched how intrinsic biochemical variables affect the metastatic preference of cancer cells. In further research, inherent characteristics of cancer cells were discovered, including gene patterns for organ tropism and molecular routes for regulating extravasation and colonization under the unique microenvironment of targeted organs [1, 65, 70, 71, 80, 284]. In breast cancer cells, Dickkopf-1 secreted by the tumor has diametrically opposed effects on bone and lung metastatic processes; it promotes bone metastasis while inhibiting lung metastatic process via canonical and non-canonical Wnt signaling respectively [69]. Tumor cells are reported to exhibit low cell stiffness that is highly associated with their malignancy [15, 16]. Unfortunately, it is unclear if organotropism depends on certain mechanical characteristics of cancer cells.

Specific alterations in cellular mechanical characteristics, such as stiffness and viscosity, also accompany malignant transformation caused by genetic abnormalities in cells. For instance, the normal breast epithelial cells following transformation become noticeably softer [17, 18]. Related investigations have shown that the stiffness of tumor cells is very diverse and greatly relates to their malignancy [19]. The intrinsic softness of cells serves as a distinct hallmark of tumor cells with highly tumorigenic and metastatic abilities [20]. As a result of low stiffness, tumor cells are more likely to extravasate through the endothelial barrier in the metastasis [21]. Additionally, soften cells can enhance self-renewal potential of cancer stem cells [22, 23]. Cellular mechanical properties have not been linked to metastasis preference, despite the role of stiffness in malignancy behaviors have been explored widely over the past two decades.

The significance of mechanical properties of breast cancer cell in organotropism was investigated in this chapter. We observed that the stiffness of breast cancer cells with different metastatic tropisms corresponds to the tissue stiffness of target organs. By

regulating the stiffness of cancer cells through pharmacological or genetic methods, expression levels of organotropism-related genes and mechanoresponse of cells were altered in soft substrates mimicking mechanical microenvironment of brain tissues. Altogether, our findings indicated breast cancer subpopulations with different organotropism had unique biophysical properties, while cell stiffness could be a potential biomarker for organic metastasis diagnosis and treatment.

6.2 Results

6.2.1 The metastatic organotropism of breast cancer cell derivatives correlates with their cellular mechanics

Several cellular behaviors are coupled to biophysical properties of cells [285]. There is, however, a hazy relation between metastatic tropism and the mechanics of tumor cells. By using AFM, we assessed the cellular stiffness of the breast cancer cell line 231 cells and its derivatives that prefer to metastasis to the bone (231-BoM cells), lung (231-LM cells), and brain (231-BrM cells) to answer this question [65, 70, 71]. As shown in the findings (Fig. 6.1A and B), 231-BrM cells had less cellular stiffness than other cells whereas 231-LM and 231-BoM cells showed higher stiffness than 231 cells. Additionally, across these groups, 231-BoM cells displayed the highest level of cell stiffness. Our experimental results demonstrated the cellular stiffness of 231-BrM, 231-LM, and 231-BoM cells gradually increases and shows a similar trend with the stiffness of the organs that they like to spread to. The actin filament network, a fundamental component of the cytoskeleton, is essential for determining how stiff the cell is [286]. Subsequently, F-actin levels in breast cancer cells with various metastatic organotropisms were assessed. The minimum level of F-actin was found in 231-BrM cells, whereas the maximum level was found in 231-BoM cells, supporting the results of cell stiffness (Fig. 6.1C and D). Additionally, there was a strong upward trend for F-actin levels from the 231-BrM, 231-LM, to 231-BoM cells. All of these

findings show that various breast cancer cell derivatives with distinct metastasis patterns have diverse biophysical characteristics and that the cellular mechanics of breast cancer cells may be a reflection of their organotropism.

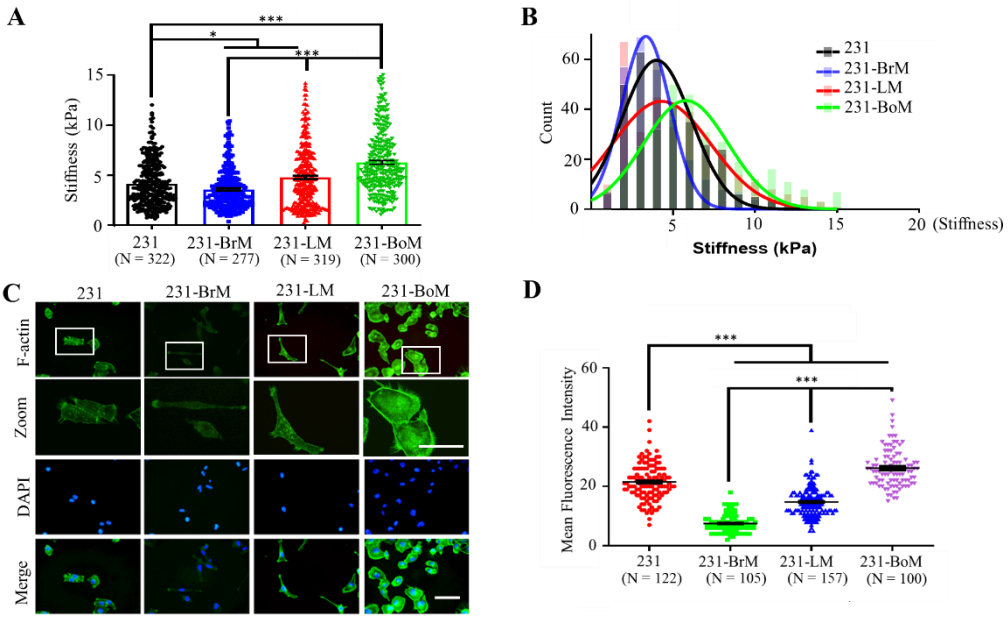

Figure 6.1 MDA-MB-231 subpopulations with different organotropisms exhibit distinct cell mechanics. (A) Young's modulus of tumor cells on TCPs was assessed using AFM. n > 100 cells for each condition. (B) The histogram showing the distribution of Young's modulus and fitting a Gaussian line. (C) Immunostaining images of F-actin (green) and nuclei (blue). Zoomed images of outlined regions are presented in the second pane. Scale bar: 100 μm. (D) Average of fluorescence intensity of F-actin in (D). Number of cells is given for each group. N=3, isolates; mean ± SEM; *, $p < 0.05$; **, $p < 0.01$; and ***, $p < 0.001$.

6.2.2 Gene signature related to organotropism is modulated by cell cytoskeleton

Results have shown that the cellular stiffness of cells and organotropism are correlated. It is still unknown, nevertheless, how the mechanical characteristics of cancer cells affect organotropism. Thus, we hypothesized that the organ-specific metastasis of breast cancer cells can be modulated by the cytoskeleton network. The consequence of the changes in cell cytoskeleton on the gene expression profiling associated with metastatic preference to brain or bone was examined to test this hypothesis. On one hand, 231-BoM cells were treated with the F-actin polymerization antagonist CytoD,

the ROCK antagonist Y-27632, or the myosin II antagonist blebbistatin to destabilize the actin cytoskeleton. On the other hand, 231-BrM cells were treated with Rho activator Narci and the F-actin assembly activator Jas to reinforce the actin cytoskeleton. The expression levels of the previously reported gene signatures related to brain and bonemetastasis were investigated. Except for a few exceptional genes, the results reveal that interrupting the actin network of 231-BoM cells with CytoD or Y-27632 had little effect on the expression of genes relevant to bone metastasis. Contrarily, the majority of brain metastasis-associated genes were noticeably increased by these inhibitors in 231-BoM cells (Fig 6.2A and B). Nevertheless, neither bone metastasis genes nor brain metastasis genes were affected by blebbistatin. The expressions of genes associated with bone and brain metastases were not visibly altered when 231-BrM cells were given treatment with Jas. In contrast, Narci supplementation considerably improved five out of nine genes associated with bone metastasis and did not impact the expression of genes associated with brain metastasis, with the exception of the unexpected elevation of SERPINB2 and COX2 (Fig. 6.2C and D). These results demonstrate that pharmacological perturbation /stabilization on the actin cytoskeleton of breast cancer cell derivatives with metastatic patterns to bone/brain alters gene signatures related to organotropism.

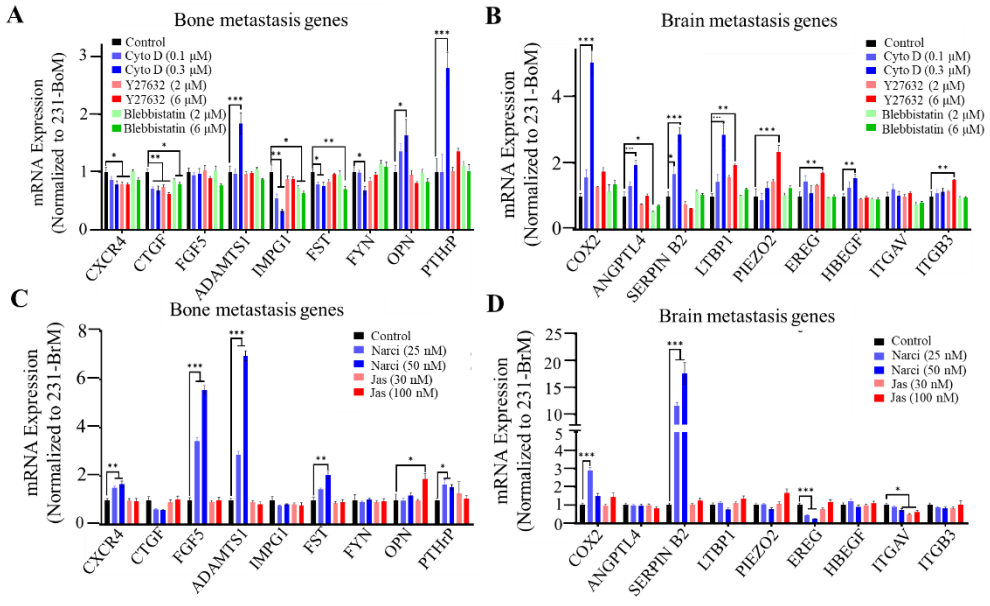

Figure 6.2 Inhibition/stabilization of cell cytoskeleton increases the expressions of

brain/bone metastasis-related genes. (A, B) 231-BoM cells were treated with the indicated concentration of CytoD, Y-27632, and Blebbistatin for 1 day. After then, the expression levels of genes associated with (A) bone metastasis and (B) brain metastasis were evaluated by qPCR. (C, D) 231-BrM cells were treated with the indicated concentration of Narci and Jas for 1 day. After then, the expression levels of genes associated with (C) bone metastasis and (D) brain metastasis were evaluated by qPCR. N=3, isolates; mean ± SEM; *, $p < 0.05$; **, $p < 0.01$; and ***, $p < 0.001$.

6.2.3 Derivatives of breast cancer with distinct organotropism exhibit different mechanoresponses to substrate rigidity depending on the cytoskeleton

Our findings demonstrate that the transcription levels of genes associated with brain/ bone metastasis are influenced by the actin cytoskeleton. Our findings demonstrate that the transcription levels of genes associated with brain/ bone metastasis are influenced by the actin cytoskeleton. Noticeably, 231-BrM, 231-LM, and 231-BoM cells preferentially disseminate to the brain, lung and bone, all of these organs with different tissue stiffness [230, 287]. Thereafter, we investigated how the cellular cytoskeleton affected the mechanoresponses of brain/ bone-metastatic tumor cells to substrate stiffness. To achieve this, CytoD was used to depolymerize the actin cytoskeleton of 231-BoM cells whereas Narci was used to stabilize the actin filament of 231-BrM cells. Then, to simulate the response to the rigidity of brain tissue, these treated tumor cells were grown on TCPs or PA gels with a stiffness of 0.6 kPa. The migration and proliferation abilities of cells are positively and significantly associated with cell spreading and shape which serve as useful indicators to show compatibility between microenvironment and metastatic tumors [255, 256]. After treatment with Narci, 231-BrM cells showed a higher circularity and a lower aspect ratio compared to cells without treatment, even though there is no difference in spreading area. Contrary to this, disruption of the cytoskeleton of 231-BoM cells with CytoD improved spreading and aspect ratio regardless of substrate but had little effect on circularity (Fig. 6.3A and B). When metastatic tumor cells reach distant sites, proliferation is necessary for the formation of marometastases. Our results show that promoting the actin cytoskeleton of 231-BrM cells with 25 nM Narci inhibited the proliferation on the soft matrices but

not TCPs. 50 nM Narci treatment boosted the proliferation rate on TCPs, but this effect was eliminated on soft matrices (Fig. 6.3C and D). The growth of 231-BoM cells on TCPs was unaffected when the cytoskeleton was inhibited with CytoD. On the other hand, proliferation rate of 231-BoM cells on soft substrates was boosted after CytoD treatment (Fig. 6E and F). Together, these results indicate that the actin cytoskeleton may be a unique modulator of the mechanical adaptation ability of breast cancer cells with different metastatic tropisms on the soft matrices.

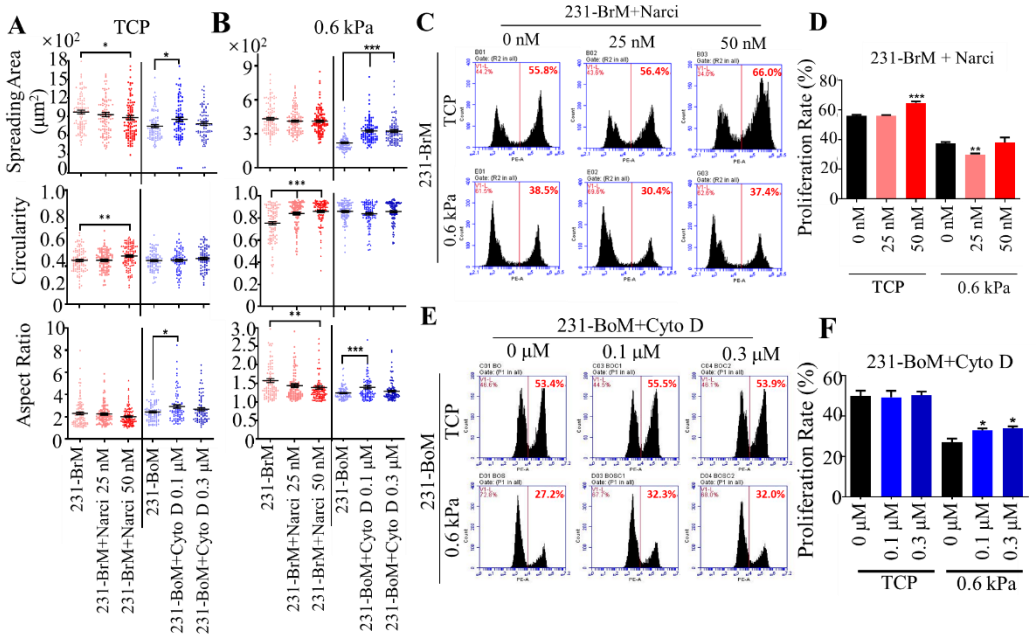

Figure 6.3 Stabilizing/disturbing the actin cytoskeleton of breast cancer cells with bone/brain tropism affects cell morphology and proliferation ability on soft matrices. (A, B) 231-BrM cells were pretreated with Narci at the concentration of 25 nM and 50 nM, and 231-BoM cells were pretreated with CytoD at the concentration of 0.1 μM or 0.3 μM. Cell spreading area, circularity, and aspect ratio were evaluated on (A) TCPs and (B) 0.6 kPa substrates after 1 day of incubation. The data are collected from 100 cells/group. (C, D) 231-BrM cells were pretreated with 25 or 50 nM Narci and seeded on TCPs and 0.6 kPa matrices for 1 day, respectively. Then, the proliferation rate of cells was evaluated by EdU assay. (E, F) 231-BoM cells were pretreated with 0.1 or 0.3 μM CytoD and seeded on TCPs and 0.6 kPa matrices for 1 day, respectively. Then, the proliferation rate of cells was evaluated by EdU assay. N=3, isolates; mean ± SEM; *, $p < 0.05$; **, $p < 0.01$; and ***, $p < 0.001$.

6.2.4 Knocking down mDia 1 induces the transition to brain metastatic phenotype of 231-BoM cells

One of the downstream targets of RhoA signaling, mDia1, plays a crucial role in actin polymerization, which influences cell stiffness [288, 289]. The role of actin cytoskeleton and biophysical property in organotropism was further investigated by transfecting 231-BoM cells with siRNA targeting mDia1 (Fig. 6.4A). Bone metastasis-associated genes were not consistently affected when mDia1 was knocked down in 231-BoM cells (Fig. 6.4B). Conversely, upregulation of seven out of nine genes associated with brain metastasis was observed in 231-BoM cells when mDia1 was knocked down (Fig. 6.4C). Moreover, the proliferation rate of 231-BoM cells on soft matrices but not on TCPs was increased when mDia1 was knocked down with low doses siRNA (1 nM). According to these data, mDia1 knockdown increases the expression of brain metastasis-related genes in 231-BoM cells and promotes proliferation on soft matrices, which suggests they have an increased capability to form brain metastases.

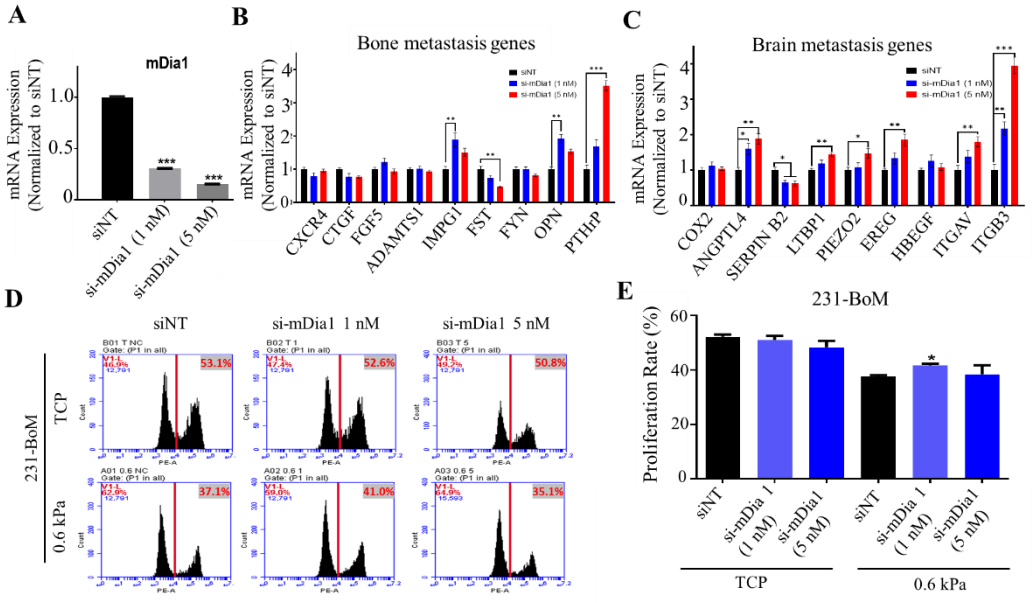

Figure 6.4 mDia1 knockdown in 231-BoM cells influences the expression levels of the genes related to metastatic preference and increases cell proliferation on soft matrices. (A) The knockdown efficiency of mDia1. The expression levels of genes associated with (B) bone metastasis and (C) brain metastasis were evaluated by qPCR

after mDia1 knockdown. (D, E) 231-BoM cells transfected with si-mDia1 were cultured on TCPs and 0.6 kPa matrices and cell proliferation were measured by EdU assay. N=3, isolates; mean ± SEM; *, $p < 0.05$; **, $p < 0.01$; and ***, $p < 0.001$.

6.3 Discussion

Metastatic organotropism is present in many malignancies. The "seed and soil" theory, put out by Steven Paget [3], which defines "seed" as tumor cells with the capacity to metastasis and "soil" as the organs with the supporting milieu, was the first to provide an explanation for metastatic tropism. It is thus possible for the metastases to form in distant sites when the "seed" and "soil" match well. The ineffectiveness of the metastatic process is determined by both tumor cells and the microenvironment in distant organs [78, 290]. The critical features in cancer cells, including genetic profiling, stemness, dormancy, and tumor-secreted molecules, are vital in regulating metastatic organotropism [52]. Mechanical factors, such as the biophysical properties of tumor cells, play significant roles in metastatic progress in addition to these biochemical factors [291]. It is well acknowledged that the invasive capability of malignant cells in cases of pancreatic, ovarian, and breast cancer is correlated with their mechanical characteristics [15, 292, 293]. Metastatic tumor cells with strong invasion and metastasis abilities show more compliant than counterparts with weak invasion ability, and the softness of cells may assist tumor cells to pass through confined spaces during the metastatic process. Our prior findings demonstrate that the decrease of cytoskeleton and cell mechanics increases the CSCs exposed to fluid shear forces and increases the chemoresistance of CSCs [232, 294]. It is yet unknown how metastatic tropism is impacted by the actin cytoskeleton and stiffness of tumor cells. The recent work reveals a link between the biophysical feature and metastatic preference in tumor cells. The rigidity of the preferred organs is matched by the cell stiffness of the breast carcinoma derivatives with diverse organotropism. Moreover, brain metastasis-associated gene features are increased and mechanoadaptation abilities, including spreading and

proliferation on the soft matrices, are enhanced by disturbing the actin cytoskeleton network of derivatives. Vice versa, stabilization of actin cytoskeleton induces the bone metastasis gene signature and inhibits the mechanoadaptation abilities required by brain metastasis in brain metastatic tumor cells. These results point to a potential role for cell cytoskeleton in organic metastasis, suggesting that it may not only be correlated with but also play a vital regulatory role in organotropism. Cells with optional cell stiffness and cellular cytoskeleton network that are compatible with the rigidity of the target organ may be better able to adapt to the soil of the host organ. However, our findings demonstrate that not all organotropism-related gene expression levels change in an expected way after inhibitor treatments and genetic regulation. Such as ADAMTS1, OPN, and PTHrP expressions in the CytoD treatment group. These unforeseen results following the cytoskeleton modification may be attributable to side effects of pharmacological treatment and gene manipulation which also induce various changes in other intracellular signaling and actin network rearrangement.

It is important to keep in mind that different extracellular cues can affect the cytoskeleton network and mechanical features of cells [295]. The cell stiffness of tumor cells can be modulated by EVs released by fibroblasts [296]. The cells can actively control their actin network and modify their mechanical state by responding to mechanical inputs from their surroundings [295]. Numerous investigations have demonstrated that by cytoskeletal rearrangement, cells adjust their stiffness to fit the elasticity of their matrix [297, 298]. Consistent with this observation, the heterogeneous stiffness of niches in the primary tumor may account for the different levels of stiffness of cancer cells within a given tumor tissue [19]. Malignant cells from metastatic tumors in the brain and bone with distinctive tissue stiffness were collected to generate the MDA-MB-231 derivatives with different tropisms. Thus, it begs the issue of whether these distinctive mechanical properties are a result of their adaptation to the particular mechanical milieu of the target organ or a result of their inherent properties independent of external stimuli. Moreover, the mechanical features of these derivates may alter as a

consequence of the prolonged growth on TCPs with artificial stiffness following cell harvest. In the future, these crucial concerns need to be carefully studied.

Biophysical characteristics are widely accepted to be governed by the cytoskeleton network and actomyosin-dependent contractility. Cell stiffness is decreased by destabilizing the cytoskeleton or by suppressing myosin activity, whereas cellular stiffness is increased by strengthening the cytoskeleton or by stimulating myosin activity [176, 299, 300, 301]. In our investigation, a number of pharmacological compounds that modulate the cytoskeleton stabilization and cellular contraction force are employed to evaluate the function of the cytoskeleton in metastatic preference. By obstructing the rapid extension barbed ends of actin filaments, CytoD can prevent actin polymerization. Actin filaments are bound by Jas, which prevents them from disassembling. By activating the small GTPase RhoA, Narci causes the increasing activity of myosin II and then enhances the contractility. Y-27632 inhibits the ROCK, upstream of myosin II, and blebbistatin selectively suppresses myosin II activity to decrease contraction force. Thus, these medications affect the cytoskeleton and mechanics of cells in various ways. We observed that CytoD greatly impacts gene expression, but blebbistatin and Y-27632 have just a little impact on the pattern of gene expression in 231-BoM cells. This result might be attributed to the various molecular targets of these pharmacologic therapies, as well as the modest dosage of the medications utilized in our research. Furthermore, earlier research has demonstrated that the cytoskeleton affects the development of human pluripotent stem cells into pancreatic cells. But the researchers also noted that not all cytoskeleton-targeting medications could promote endocrine differentiation [302]. This disparity is probably caused by the various mechanistic principles of these compounds [303]. Thus, this impact cannot be ruled out in the present research and might make a substantial contribution to the diverse effects of various pharmacologic interventions on gene expression.

It is essential for the outgrowth of cancer cells in the target organs that they respond to

mechanical signals, and this responsiveness is dependent on both cellular structure and physical properties. Additionally, in order to sense and adapt to the mechanical stimuli in the environment optimally, the cell cytoskeleton and mechanics should fit the stiffness of the microenvironment, indicating that it is possible for soft/stiff tumor cells to subsist and thrive in a soft/stiff habitat [304]. The research showing breast cancer subpopulations with different metastatic preferences can greatly increase cell proliferation and motility when cultured on substrates with comparable stiffness is evidence in favor of this hypothesis [245]. Our study looked into the function of the cell mechanics in the adaptation of tumor cells with various metastatic tropisms to the compliant substrates. Although the transcriptional features and mechanoadaptation to matrix stiffness can partially reflect organotropism, direct evidence will need to be presented in the future to show how cell mechanics affect organotropism, particularly in tests of organotropism using intracardiac injection models.

Chapter 7: Conclusion and Future Perspectives

7.1 Conclusion

There is a poor prognosis for brain metastases resulting from breast cancer and neurological impairment is commonly associated with these metastases. However, very little is known about the mechanisms that drive brain metastases. For the development of novel treatment approaches, deeper comprehension of the underlying causal reasons for brain metastases is necessary. A number of studies have looked at the role those inherent genetic characteristics of tumor cells play in brain metastasis, as well as the interaction that tumor cells have with the biochemical milieu of the brain. There is a lack of understanding of how biomechanics, especially local niche stiffness and cell mechanics, regulate tumor cell metastasizing to the brain. This study aims to explore the brain metastasis of breast cancer cells from a biophysical viewpoint. To answer the raised scientifical question, we investigate the role of the niche softness of primary tumor in brain metastasis, clarify the underlying mechanisms of microenvironmental softness inducing brain metastasis preference, and establish the correlation between cell stiffness and metastatic tropism.

As the relationship between matrix stiffness and metastatic organ preference is still unclear, we focused on investigating whether matrix softness influences brain metastatic capability of breast cancer at first. Our data showed chronic culture on soft matrices induced brain metastasis gene signature, which is not the consequence of genetic drift and is independent of ligand- and cell type. In addition, RNA-seq data verified this finding and showed matrix softness induced the transcriptomic characteristics of neuronal mimicry which may confer tumor cells with the ability to metastasize to the brain. Furthermore, we systematically examined the metastasis capabilities of soft niches-primed cells in each essential step of brain metastasis processes, including survival in the circulation system, intravascular arrest in the brain, BBB extravasation and outgrowth in the brain. Compared to their parental cells without soft priming, soft niches-primed cells showed enhanced survival under shear flow in the circulation system, enhanced adhesion in the brain endothelial layer, and increased

BBB transmigration. Besides, soft priming promoted both mechanoadaptation and defense-evasion abilities, which facilitate the colonization of tumor cells in the brain. Following that, we verified the metastasis abilities of tumor cells in crucial brain metastasis stages using *in vivo* models. Enhanced BBB transmigration and brain colonization abilities were observed in soft niches-primed cells. Moreover, soft priming breast cancer cells preferred to metastasize to the brain. Soft matrix-priming cells displayed unique biophysics properties and mechanical memory, which might facilitate the progress of brain metastasis. Moreover, our *in vitro* data further confirmed our postulation that soft priming breast cancer cells preferred to metastasize to the brain. It was also found that soft matrix-priming cells had unique biophysics properties and mechanical memory, which might favor brain metastasis.

To investigate the mechanism involved in matrix softness-induced brain metastasis preference, we used single-cell cloning to generate genetically homogeneous SCPs. We found that epigenetic changes and clonal selection both can drive the acquisition of brain metastasis ability after long-term culture on the soft matrices. Chromatin remodeling regulates gene expression patterns and cellular behaviors in response to the mechanical signals from microenvironment, which is governed by epigenetic modifications. Mechanistic studies have shown that the changes in gene expression pattern and brain metastasis abilities caused by soft priming required chromatin condensation and remodeling. The chromatin decondensation via inhibition of HDAC activity impaired the soft priming-induced acquisition of brain metastasis phenotype. Chromatin condensation is primarily mediated by Class I HADCs, including HDAC1, 2, 3 and 8. A high level of HDAC3 activity, which was required, but not sufficient, for the acquisition of a brain metastatic phenotype post-soft priming, was observed in soft niches-primed cells. Furthermore, we revealed the regulation mechanism of HDAC3 activity is determined by the actin filamin polymerization-mediated mechanotransduction in response to the matrix softness. In detail, disruption/ activation of the actin cytoskeleton was sufficient to increase/ decrease the activity of HDAC3

and induce/prevent the acquisition of brain metastasis ability. Moreover, we evaluated whether HDAC3 can be served as an effective clinical therapeutical target against the brain metastasis of breast cancer. It was shown *in vivo* that pharmacological inhibition of HDAC3 effectively antagonized brain metastases formation.

The mechanical characteristics of tumor cells are far less well-known than the intrinsic biochemical features that have been extensively studied in metastatic organotropism. Here, we revealed a correlation between metastatic tropism and cell mechanics. The stiffness of tumor cells with distinct organotropism reflects the matrix stiffness of target organs. The gene signature reflecting the specific-organ metastasis and mechanoresponses to soft substrates mimicking the stiffness of brain tissue are greatly influenced by the cell cytoskeleton state. These findings emphasize the critical functions of the cell mechanics in metastatic tropism, which may not only indicate but also determine the preferred organ for metastasis.

Taken together, our studies explore the metastatic organotropism of breast cancer cells from the perspective of biomechanics, investigate the role of the softness of the primary niche in brain metastasis and the relationship between cell mechanics and organotropism. This is the first study, as far as we know, to demonstrate that the matrix softness of local tumor niches drives the acquisition of brain metastasis preference in breast cancer. Moreover, we also reveal its underlying mechanisms and indicate HDAC3 may serve as a key molecular in clinal interevent. In addition, we establish the correlation between cell stiffness and organotropism, which clarifies the potential role of cell stiffness acting as the marker to reflect metastatic preference.

7.2 Limitations and future perspectives

Human breast cancer cell line MDA-MB-231 was chosen as the primary experimental object in our study. Even though the murine mammary carcinoma cell line 4T1 was also

used to verify our conclusions *in vitro*, we plan to develop patient-derived xenografts (PDX) cell line and use the spontaneous animal model to make our study to be more pathologically relevant and comprehensive.

In this study, we used 0.6 kPa PA gels to mimic the mechanical microenvironment exiting in the primary tumor and proved that the niches softness induced the acquisition of brain metastasis phenotype. However, it is still unclear whether tumor cells with brain metastatic preference preexist within soft niches in the primary tumor. To answer this question, we are working on this by manipulating tissue stiffness in the spontaneous model. Tumor cells will be encapsulated into the soft/stiff alginate hydrogels and then transplanted into the fat pad of female mice. After primary tumor formation, tumor cells will be isolated and the organotropism of collected tumor cells will be examined in mice model through intracardiac injection. Furthermore, primary tumors generated from the spontaneous models or fresh primary tissue from patients can be used to detect the tissue stiffness surrounding the brain metastatic tumor cells using AFM combined with immunofluorescence staining. However, there is no well-accepted biomarker for brain metastatic tumor cells. Alternatively, single-cell RNA sequencing with spatial transcriptomics provides us with a powerful tool to investigate heterogeneous cancerous tissues. Using this innovative approach, we may establish a clear correlation between organotropism and local niche stiffness.

In the study of the mechanisms underlying the matrix softness-induced brain metastatic phenotype, we found actin cytoskeleton plays a vital role. However, we do not know how the actin cytoskeleton involves in this process and regulates the HDAC3 activity until now. As actin cytoskeleton-LINC complex is an essential pathway for force transmission to nuclear. we can hypothesize that the LINC complex is downstream of the actin cytoskeleton in response to the matrix softness, which in turn, regulates HDAC3 activity, gene expression pattern and brain metastasis abilities. To prove this hypothesis, we plan to use the plasmid expressing Tet-on inducible KASH with a

dominant negative mutation to impair the function of the LINC complex, and then investigate the role of the LINC complex in the matrix softness-induced brain metastasis.

References

1. Lu X, Kang Y. Organotropism of breast cancer metastasis. *J Mammary Gland Biol Neoplasia* 2007, **12**(2-3)**:** 153-162.

2. Liu Q, Zhang H, Jiang X, Qian C, Liu Z, Luo D. Factors involved in cancer metastasis: a better understanding to "seed and soil" hypothesis. *Mol Cancer* 2017, **16**(1)**:** 176.

3. Paget S. The distribution of secondary growths in cancer of the breast. 1889. *Cancer Metastasis Rev* 1989, **8**(2)**:** 98-101.

4. Zhang XH, Jin X, Malladi S, Zou Y, Wen YH, Brogi E*, et al.* Selection of bone metastasis seeds by mesenchymal signals in the primary tumor stroma. *Cell* 2013, **154**(5)**:** 1060-1073.

5. Bray F, Ferlay J, Soerjomataram I, Siegel RL, Torre LA, Jemal A. Global cancer statistics 2018: GLOBOCAN estimates of incidence and mortality worldwide for 36 cancers in 185 countries. *CA Cancer J Clin* 2018, **68**(6)**:** 394-424.

6. Witzel I, Oliveira-Ferrer L, Pantel K, Muller V, Wikman H. Breast cancer brain metastases: biology and new clinical perspectives. *Breast Cancer Res* 2016, **18**(1)**:** 8.

7. Friedl P, Alexander S. Cancer invasion and the microenvironment: plasticity and reciprocity. *Cell* 2011, **147**(5)**:** 992-1009.

8. Chen LJ, Wei SY, Chiu JJ. Mechanical regulation of epigenetics in vascular biology and pathobiology. *J Cell Mol Med* 2013, **17**(4)**:** 437-448.

9. Miroshnikova YA, Nava MM, Wickstrom SA. Emerging roles of mechanical forces in chromatin regulation. *J Cell Sci* 2017, **130**(14)**:** 2243-2250.

10. Hirata E, Ishibashi K, Kohsaka S, Shinjo K, Kojima S, Kondo Y*, et al.* The Brain Microenvironment Induces DNMT1 Suppression and Indolence of Metastatic Cancer Cells. *iScience* 2020, **23**(9)**:** 101480.

11. Walker CJ, Crocini C, Ramirez D, Killaars AR, Grim JC, Aguado BA*, et al.* Nuclear mechanosensing drives chromatin remodelling in persistently activated fibroblasts. *Nat Biomed Eng* 2021, **5**(12)**:** 1485-1499.

12. Pickup MW, Mouw JK, Weaver VM. The extracellular matrix modulates the hallmarks of cancer. *EMBO Rep* 2014, **15**(12)**:** 1243-1253.

13. Wirtz D, Konstantopoulos K, Searson PC. The physics of cancer: the role of physical interactions and mechanical forces in metastasis. *Nat Rev Cancer* 2011, **11**(7)**:** 512-522.

14. Pathak A, Kumar S. Independent regulation of tumor cell migration by matrix stiffness and confinement. *Proc Natl Acad Sci U S A* 2012, **109**(26)**:** 10334-10339.

15. Swaminathan V, Mythreye K, O'Brien ET, Berchuck A, Blobe GC, Superfine R. Mechanical stiffness grades metastatic potential in patient tumor cells and in cancer cell lines. *Cancer Res* 2011, **71**(15)**:** 5075-5080.

16. Luo Q, Kuang D, Zhang B, Song G. Cell stiffness determined by atomic force microscopy and its correlation with cell motility. *Biochim Biophys Acta* 2016, **1860**(9)**:** 1953-1960.

17. Suresh S. Biomechanics and biophysics of cancer cells. *Acta Biomater* 2007, **3**(4)**:** 413-438.

18. Guck J, Schinkinger S, Lincoln B, Wottawah F, Ebert S, Romeyke M*, et al.* Optical deformability as an inherent cell marker for testing malignant transformation and metastatic competence. *Biophys J* 2005, **88**(5)**:** 3689-3698.

19. Plodinec M, Loparic M, Monnier CA, Obermann EC, Zanetti-Dallenbach R, Oertle P*, et al.* The nanomechanical signature of breast cancer. *Nat Nanotechnol* 2012, **7**(11)**:** 757-765.

20. Lv J, Liu Y, Cheng F, Li J, Zhou Y, Zhang T*, et al.* Cell softness regulates tumorigenicity and stemness of cancer cells. *EMBO J* 2021, **40**(2)**:** e106123.

21. Chen J, Zhou W, Jia Q, Chen J, Zhang S, Yao W*, et al.* Efficient extravasation of tumor-repopulating cells depends on cell deformability. *Sci Rep* 2016, **6:** 19304.

22. Ohata H, Ishiguro T, Aihara Y, Sato A, Sakai H, Sekine S*, et al.* Induction of the stem-like cell regulator CD44 by Rho kinase inhibition contributes to the maintenance of colon cancer-initiating cells. *Cancer Res* 2012, **72**(19)**:** 5101-5110.

23. Castro DJ, Maurer J, Hebbard L, Oshima RG. ROCK1 inhibition promotes the self-renewal of a novel mouse mammary cancer stem cell. *Stem Cells* 2013, **31**(1)**:** 12-22.

24. Sung H, Ferlay J, Siegel RL, Laversanne M, Soerjomataram I, Jemal A*, et al.* Global Cancer Statistics 2020: GLOBOCAN Estimates of Incidence and Mortality Worldwide for 36 Cancers in 185 Countries. *CA Cancer J Clin* 2021, **71**(3)**:** 209-249.

25. Zheng RS, Sun KX, Zhang SW, Zeng HM, Zou XN, Chen R*, et al.* [Report of cancer epidemiology in China, 2015]. *Zhonghua Zhong Liu Za Zhi* 2019, **41**(1)**:** 19-28.

26. Hsiao YH, Chou MC, Fowler C, Mason JT, Man YG. Breast cancer heterogeneity: mechanisms, proofs, and implications. *J Cancer* 2010, **1:** 6-13.

27. Viale G. The current state of breast cancer classification. *Ann Oncol* 2012, **23 Suppl 10:**

x207-210.

28. Kennecke H, Yerushalmi R, Woods R, Cheang MC, Voduc D, Speers CH*, et al.* Metastatic behavior of breast cancer subtypes. *J Clin Oncol* 2010, **28**(20)**:** 3271-3277.

29. Amin MB, Greene FL, Edge SB, Compton CC, Gershenwald JE, Brookland RK*, et al.* The Eighth Edition AJCC Cancer Staging Manual: Continuing to build a bridge from a population-based to a more "personalized" approach to cancer staging. *CA Cancer J Clin* 2017, **67**(2)**:** 93-99.

30. Valastyan S, Weinberg RA. Tumor metastasis: molecular insights and evolving paradigms. *Cell* 2011, **147**(2)**:** 275-292.

31. Waks AG, Winer EP. Breast Cancer Treatment: A Review. *JAMA* 2019, **321**(3)**:** 288-300.

32. Carmeliet P, Jain RK. Principles and mechanisms of vessel normalization for cancer and other angiogenic diseases. *Nat Rev Drug Discov* 2011, **10**(6)**:** 417-427.

33. Fidler IJ. The pathogenesis of cancer metastasis: the 'seed and soil' hypothesis revisited. *Nat Rev Cancer* 2003, **3**(6)**:** 453-458.

34. Bissell MJ, Hines WC. Why don't we get more cancer? A proposed role of the microenvironment in restraining cancer progression. *Nat Med* 2011, **17**(3)**:** 320-329.

35. Reuten R, Zendehroud S, Nicolau M, Fleischhauer L, Laitala A, Kiderlen S*, et al.* Basement membrane stiffness determines metastases formation. *Nat Mater* 2021, **20**(6)**:** 892-903.

36. Giampieri S, Manning C, Hooper S, Jones L, Hill CS, Sahai E. Localized and reversible TGFbeta signalling switches breast cancer cells from cohesive to single cell motility. *Nat Cell Biol* 2009, **11**(11)**:** 1287-1296.

37. Gupta GP, Massague J. Cancer metastasis: building a framework. *Cell* 2006, **127**(4)**:** 679-695.

38. Guo W, Giancotti FG. Integrin signalling during tumour progression. *Nat Rev Mol Cell Biol* 2004, **5**(10)**:** 816-826.

39. Brown DM, Ruoslahti E. Metadherin, a cell surface protein in breast tumors that mediates lung metastasis. *Cancer Cell* 2004, **5**(4)**:** 365-374.

40. Joyce JA, Pollard JW. Microenvironmental regulation of metastasis. *Nat Rev Cancer* 2009, **9**(4)**:** 239-252.

41. Chambers AF, Groom AC, MacDonald IC. Dissemination and growth of cancer cells in

metastatic sites. *Nat Rev Cancer* 2002, **2**(8)**:** 563-572.

42. Barkan D, El Touny LH, Michalowski AM, Smith JA, Chu I, Davis AS*, et al.* Metastatic growth from dormant cells induced by a col-I-enriched fibrotic environment. *Cancer Res* 2010, **70**(14)**:** 5706-5716.

43. McAllister SS, Gifford AM, Greiner AL, Kelleher SP, Saelzler MP, Ince TA*, et al.* Systemic endocrine instigation of indolent tumor growth requires osteopontin. *Cell* 2008, **133**(6)**:** 994-1005.

44. Hiratsuka S, Duda DG, Huang Y, Goel S, Sugiyama T, Nagasawa T*, et al.* C-X-C receptor type 4 promotes metastasis by activating p38 mitogen-activated protein kinase in myeloid differentiation antigen (Gr-1)-positive cells. *Proc Natl Acad Sci U S A* 2011, **108**(1)**:** 302-307.

45. Nagrath S, Sequist LV, Maheswaran S, Bell DW, Irimia D, Ulkus L*, et al.* Isolation of rare circulating tumour cells in cancer patients by microchip technology. *Nature* 2007, **450**(7173)**:** 1235-1239.

46. Luzzi KJ, MacDonald IC, Schmidt EE, Kerkvliet N, Morris VL, Chambers AF*, et al.* Multistep nature of metastatic inefficiency: dormancy of solitary cells after successful extravasation and limited survival of early micrometastases. *Am J Pathol* 1998, **153**(3)**:** 865-873.

47. Massague J, Obenauf AC. Metastatic colonization by circulating tumour cells. *Nature* 2016, **529**(7586)**:** 298-306.

48. Edlund M, Sung SY, Chung LW. Modulation of prostate cancer growth in bone microenvironments. *J Cell Biochem* 2004, **91**(4)**:** 686-705.

49. Triozzi PL, Eng C, Singh AD. Targeted therapy for uveal melanoma. *Cancer Treat Rev* 2008, **34**(3)**:** 247-258.

50. Urosevic J, Garcia-Albeniz X, Planet E, Real S, Cespedes MV, Guiu M*, et al.* Colon cancer cells colonize the lung from established liver metastases through p38 MAPK signalling and PTHLH. *Nat Cell Biol* 2014, **16**(7)**:** 685-694.

51. Obenauf AC, Massague J. Surviving at a Distance: Organ-Specific Metastasis. *Trends Cancer* 2015, **1**(1)**:** 76-91.

52. Chen W, Hoffmann AD, Liu H, Liu X. Organotropism: new insights into molecular mechanisms of breast cancer metastasis. *NPJ Precis Oncol* 2018, **2**(1)**:** 4.

53. Savci-Heijink CD, Halfwerk H, Koster J, van de Vijver MJ. A novel gene expression signature for bone metastasis in breast carcinomas. *Breast Cancer Res Treat* 2016, **156**(2)**:** 249-259.

54. Kimbung S, Johansson I, Danielsson A, Veerla S, Egyhazi Brage S, Frostvik Stolt M*, et al.* Transcriptional Profiling of Breast Cancer Metastases Identifies Liver Metastasis-Selective Genes Associated with Adverse Outcome in Luminal A Primary Breast Cancer. *Clin Cancer Res* 2016, **22**(1)**:** 146-157.

55. Smid M, Wang Y, Zhang Y, Sieuwerts AM, Yu J, Klijn JG*, et al.* Subtypes of breast cancer show preferential site of relapse. *Cancer Res* 2008, **68**(9)**:** 3108-3114.

56. Akhtar M, Haider A, Rashid S, Al-Nabet A. Paget's "Seed and Soil" Theory of Cancer Metastasis: An Idea Whose Time has Come. *Adv Anat Pathol* 2019, **26**(1)**:** 69-74.

57. Neoplastic Diseases: A Treatise on Tumours. By James Ewing, A.M., M.D., Sc.D., Professor of Pathology at Cornell University Medical College, N.Y.; Pathologist to the Memorial Hospital. Third edition. Royal 8vo. Pp. 1127, with 546 illustrations. 1928. Philadelphia and London: W. B. Saunders Co. Ltd. 63s. net. *British Journal of Surgery* 2005, **16**(61)**:** 174-175.

58. Budczies J, von Winterfeld M, Klauschen F, Bockmayr M, Lennerz JK, Denkert C*, et al.* The landscape of metastatic progression patterns across major human cancers. *Oncotarget* 2015, **6**(1)**:** 570-583.

59. Ribatti D, Mangialardi G, Vacca A. Stephen Paget and the 'seed and soil' theory of metastatic dissemination. *Clin Exp Med* 2006, **6**(4)**:** 145-149.

60. Hart IR, Fidler IJ. Role of organ selectivity in the determination of metastatic patterns of B16 melanoma. *Cancer Res* 1980, **40**(7)**:** 2281-2287.

61. Wang J, Loberg R, Taichman RS. The pivotal role of CXCL12 (SDF-1)/CXCR4 axis in bone metastasis. *Cancer Metastasis Rev* 2006, **25**(4)**:** 573-587.

62. Simonetti O, Goteri G, Lucarini G, Filosa A, Pieramici T, Rubini C*, et al.* Potential role of CCL27 and CCR10 expression in melanoma progression and immune escape. *Eur J Cancer* 2006, **42**(8)**:** 1181-1187.

63. Tichet M, Prod'Homme V, Fenouille N, Ambrosetti D, Mallavialle A, Cerezo M*, et al.* Tumour-derived SPARC drives vascular permeability and extravasation through endothelial VCAM1 signalling to promote metastasis. *Nat Commun* 2015, **6:** 6993.

64. Weidle UH, Birzele F, Kollmorgen G, Ruger R. Dissection of the Process of Brain Metastasis Reveals Targets and Mechanisms for Molecular-based Intervention. *Cancer Genomics Proteomics* 2016, **13**(4)**:** 245-258.

65. Bos PD, Zhang XH, Nadal C, Shu W, Gomis RR, Nguyen DX*, et al.* Genes that mediate breast cancer metastasis to the brain. *Nature* 2009, **459**(7249)**:** 1005-1009.

66. Fidler IJ. Metastasis: quantitative analysis of distribution and fate of tumor emboli labeled with 125 I-5-iodo-2'-deoxyuridine. *J Natl Cancer Inst* 1970, **45**(4)**:** 773-782.

67. Lee SK, Park KK, Kim HJ, Park J, Son SH, Kim KR*, et al.* Human antigen R-regulated CCL20 contributes to osteolytic breast cancer bone metastasis. *Sci Rep* 2017, **7**(1)**:** 9610.

68. Delliaux C, Tian TV, Bouchet M, Fradet A, Vanpouille N, Flourens A*, et al.* TMPRSS2:ERG gene fusion expression regulates bone markers and enhances the osteoblastic phenotype of prostate cancer bone metastases. *Cancer Lett* 2018, **438:** 32-43.

69. Zhuang X, Zhang H, Li X, Li X, Cong M, Peng F*, et al.* Differential effects on lung and bone metastasis of breast cancer by Wnt signalling inhibitor DKK1. *Nat Cell Biol* 2017, **19**(10)**:** 1274-1285.

70. Kang Y, Siegel PM, Shu W, Drobnjak M, Kakonen SM, Cordon-Cardo C*, et al.* A multigenic program mediating breast cancer metastasis to bone. *Cancer Cell* 2003, **3**(6)**:** 537-549.

71. Minn AJ, Gupta GP, Siegel PM, Bos PD, Shu W, Giri DD*, et al.* Genes that mediate breast cancer metastasis to lung. *Nature* 2005, **436**(7050)**:** 518-524.

72. Gupta GP, Minn AJ, Kang Y, Siegel PM, Serganova I, Cordon-Cardo C*, et al.* Identifying site-specific metastasis genes and functions. *Cold Spring Harb Symp Quant Biol* 2005, **70:** 149-158.

73. Klotz R, Thomas A, Teng T, Han SM, Iriondo O, Li L*, et al.* Circulating Tumor Cells Exhibit Metastatic Tropism and Reveal Brain Metastasis Drivers. *Cancer Discov* 2020, **10**(1)**:** 86-103.

74. Ghajar CM, Peinado H, Mori H, Matei IR, Evason KJ, Brazier H*, et al.* The perivascular niche regulates breast tumour dormancy. *Nat Cell Biol* 2013, **15**(7)**:** 807-817.

75. Valiente M, Obenauf AC, Jin X, Chen Q, Zhang XH, Lee DJ*, et al.* Serpins promote cancer cell survival and vascular co-option in brain metastasis. *Cell* 2014, **156**(5)**:** 1002-1016.

76. Shi Z, Mirza M, Wang B, Kennedy MA, Weber GF. Osteopontin-a alters glucose homeostasis in anchorage-independent breast cancer cells. *Cancer Lett* 2014, **344**(1)**:** 47-53.

77. Ebert D, Haller RG, Walton ME. Energy contribution of octanoate to intact rat brain metabolism measured by 13C nuclear magnetic resonance spectroscopy. *J Neurosci* 2003, **23**(13)**:** 5928-5935.

78. Gao Y, Bado I, Wang H, Zhang W, Rosen JM, Zhang XH. Metastasis Organotropism:

Redefining the Congenial Soil. *Dev Cell* 2019, **49**(3)**:** 375-391.

79. Peinado H, Zhang H, Matei IR, Costa-Silva B, Hoshino A, Rodrigues G*, et al.* Pre-metastatic niches: organ-specific homes for metastases. *Nat Rev Cancer* 2017, **17**(5)**:** 302-317.

80. Cox TR, Rumney RMH, Schoof EM, Perryman L, Hoye AM, Agrawal A*, et al.* The hypoxic cancer secretome induces pre-metastatic bone lesions through lysyl oxidase. *Nature* 2015, **522**(7554)**:** 106-110.

81. Costa-Silva B, Aiello NM, Ocean AJ, Singh S, Zhang H, Thakur BK*, et al.* Pancreatic cancer exosomes initiate pre-metastatic niche formation in the liver. *Nat Cell Biol* 2015, **17**(6)**:** 816-826.

82. Peinado H, Aleckovic M, Lavotshkin S, Matei I, Costa-Silva B, Moreno-Bueno G*, et al.* Melanoma exosomes educate bone marrow progenitor cells toward a pro-metastatic phenotype through MET. *Nat Med* 2012, **18**(6)**:** 883-891.

83. Hoshino A, Costa-Silva B, Shen TL, Rodrigues G, Hashimoto A, Tesic Mark M*, et al.* Tumour exosome integrins determine organotropic metastasis. *Nature* 2015, **527**(7578)**:** 329-335.

84. Anborgh PH, Mutrie JC, Tuck AB, Chambers AF. Role of the metastasis-promoting protein osteopontin in the tumour microenvironment. *J Cell Mol Med* 2010, **14**(8)**:** 2037-2044.

85. Kelly T, Suva LJ, Huang Y, Macleod V, Miao HQ, Walker RC*, et al.* Expression of heparanase by primary breast tumors promotes bone resorption in the absence of detectable bone metastases. *Cancer Res* 2005, **65**(13)**:** 5778-5784.

86. Sanders JL, Chattopadhyay N, Kifor O, Yamaguchi T, Butters RR, Brown EM. Extracellular calcium-sensing receptor expression and its potential role in regulating parathyroid hormone-related peptide secretion in human breast cancer cell lines. *Endocrinology* 2000, **141**(12)**:** 4357-4364.

87. Greaves M, Maley CC. Clonal evolution in cancer. *Nature* 2012, **481**(7381)**:** 306-313.

88. Naxerova K, Jain RK. Using tumour phylogenetics to identify the roots of metastasis in humans. *Nat Rev Clin Oncol* 2015, **12**(5)**:** 258-272.

89. Klein CA. Selection and adaptation during metastatic cancer progression. *Nature* 2013, **501**(7467)**:** 365-372.

90. Gundem G, Van Loo P, Kremeyer B, Alexandrov LB, Tubio JMC, Papaemmanuil E*, et al.* The evolutionary history of lethal metastatic prostate cancer. *Nature* 2015, **520**(7547)**:** 353-357.

91. Rucci N, Teti A. Osteomimicry: how tumor cells try to deceive the bone. *Front Biosci (Schol Ed)* 2010, **2**(3)**:** 907-915.

92. Huang WC, Xie Z, Konaka H, Sodek J, Zhau HE, Chung LW. Human osteocalcin and bone sialoprotein mediating osteomimicry of prostate cancer cells: role of cAMP-dependent protein kinase A signaling pathway. *Cancer Res* 2005, **65**(6)**:** 2303-2313.

93. Knerr K, Ackermann K, Neidhart T, Pyerin W. Bone metastasis: Osteoblasts affect growth and adhesion regulons in prostate tumor cells and provoke osteomimicry. *Int J Cancer* 2004, **111**(1)**:** 152-159.

94. Bendinelli P, Maroni P, Matteucci E, Luzzati A, Perrucchini G, Desiderio MA. Microenvironmental stimuli affect Endothelin-1 signaling responsible for invasiveness and osteomimicry of bone metastasis from breast cancer. *Biochim Biophys Acta* 2014, **1843**(4)**:** 815-826.

95. LeBleu VS, O'Connell JT, Gonzalez Herrera KN, Wikman H, Pantel K, Haigis MC*, et al.* PGC-1alpha mediates mitochondrial biogenesis and oxidative phosphorylation in cancer cells to promote metastasis. *Nat Cell Biol* 2014, **16**(10)**:** 992-1003, 1001-1015.

96. Neman J, Termini J, Wilczynski S, Vaidehi N, Choy C, Kowolik CM*, et al.* Human breast cancer metastases to the brain display GABAergic properties in the neural niche. *Proc Natl Acad Sci U S A* 2014, **111**(3)**:** 984-989.

97. Zhang XH, Wang Q, Gerald W, Hudis CA, Norton L, Smid M*, et al.* Latent bone metastasis in breast cancer tied to Src-dependent survival signals. *Cancer Cell* 2009, **16**(1)**:** 67-78.

98. Nguyen B, Fong C, Luthra A, Smith SA, DiNatale RG, Nandakumar S*, et al.* Genomic characterization of metastatic patterns from prospective clinical sequencing of 25,000 patients. *Cell* 2022, **185**(3)**:** 563-575 e511.

99. Brastianos PK, Carter SL, Santagata S, Cahill DP, Taylor-Weiner A, Jones RT*, et al.* Genomic Characterization of Brain Metastases Reveals Branched Evolution and Potential Therapeutic Targets. *Cancer Discov* 2015, **5**(11)**:** 1164-1177.

100. Hess KR, Varadhachary GR, Taylor SH, Wei W, Raber MN, Lenzi R*, et al.* Metastatic patterns in adenocarcinoma. *Cancer* 2006, **106**(7)**:** 1624-1633.

101. Bachmann C, Schmidt S, Staebler A, Fehm T, Fend F, Schittenhelm J*, et al.* CNS metastases in breast cancer patients: prognostic implications of tumor subtype. *Med Oncol* 2015, **32**(1)**:** 400.

102. Kotecha R, Gondi V, Ahluwalia MS, Brastianos PK, Mehta MP. Recent advances in managing brain metastasis. *F1000Res* 2018, **7**.

103. Scott BJ, Kesari S. Leptomeningeal metastases in breast cancer. *Am J Cancer Res* 2013, **3**(2)**:** 117-126.

104. Weil RJ, Palmieri DC, Bronder JL, Stark AM, Steeg PS. Breast cancer metastasis to the central nervous system. *Am J Pathol* 2005, **167**(4)**:** 913-920.

105. Peters A, Schweiger U, Pellerin L, Hubold C, Oltmanns KM, Conrad M*, et al.* The selfish brain: competition for energy resources. *Neurosci Biobehav Rev* 2004, **28**(2)**:** 143-180.

106. Winkler F. The brain metastatic niche. *J Mol Med (Berl)* 2015, **93**(11)**:** 1213-1220.

107. Salhia B, Kiefer J, Ross JT, Metapally R, Martinez RA, Johnson KN*, et al.* Integrated genomic and epigenomic analysis of breast cancer brain metastasis. *PLoS One* 2014, **9**(1)**:** e85448.

108. McGranahan N, Swanton C. Clonal Heterogeneity and Tumor Evolution: Past, Present, and the Future. *Cell* 2017, **168**(4)**:** 613-628.

109. Fischer GM, Jalali A, Kircher DA, Lee WC, McQuade JL, Haydu LE*, et al.* Molecular Profiling Reveals Unique Immune and Metabolic Features of Melanoma Brain Metastases. *Cancer Discov* 2019, **9**(5)**:** 628-645.

110. Ouzounova M, Lee E, Piranlioglu R, El Andaloussi A, Kolhe R, Demirci MF*, et al.* Monocytic and granulocytic myeloid derived suppressor cells differentially regulate spatiotemporal tumour plasticity during metastatic cascade. *Nat Commun* 2017, **8:** 14979.

111. Basnet H, Tian L, Ganesh K, Huang YH, Macalinao DG, Brogi E*, et al.* Flura-seq identifies organ-specific metabolic adaptations during early metastatic colonization. *Elife* 2019, **8**.

112. Vinay DS, Ryan EP, Pawelec G, Talib WH, Stagg J, Elkord E*, et al.* Immune evasion in cancer: Mechanistic basis and therapeutic strategies. *Semin Cancer Biol* 2015, **35 Suppl:** S185-S198.

113. Yuzhalin AE, Yu D. Brain Metastasis Organotropism. *Cold Spring Harb Perspect Med* 2020, **10**(5).

114. Schwartz H, Blacher E, Amer M, Livneh N, Abramovitz L, Klein A*, et al.* Incipient Melanoma Brain Metastases Instigate Astrogliosis and Neuroinflammation. *Cancer Res* 2016, **76**(15)**:** 4359-4371.

115. Zhang L, Zhang S, Yao J, Lowery FJ, Zhang Q, Huang WC*, et al.* Microenvironment-induced PTEN loss by exosomal microRNA primes brain metastasis outgrowth. *Nature* 2015, **527**(7576)**:** 100-104.

116. Carbonell WS, Ansorge O, Sibson N, Muschel R. The vascular basement membrane as "soil" in brain metastasis. *PLoS One* 2009, **4**(6)**:** e5857.

117. Dityatev A, Schachner M, Sonderegger P. The dual role of the extracellular matrix in synaptic plasticity and homeostasis. *Nat Rev Neurosci* 2010, **11**(11)**:** 735-746.

118. Kwok JC, Dick G, Wang D, Fawcett JW. Extracellular matrix and perineuronal nets in CNS repair. *Dev Neurobiol* 2011, **71**(11)**:** 1073-1089.

119. Yuzhalin AE, Gordon-Weeks AN, Tognoli ML, Jones K, Markelc B, Konietzny R*, et al.* Colorectal cancer liver metastatic growth depends on PAD4-driven citrullination of the extracellular matrix. *Nat Commun* 2018, **9**(1)**:** 4783.

120. Zhang H, Pan YZ, Cheung M, Cao M, Yu C, Chen L*, et al.* LAMB3 mediates apoptotic, proliferative, invasive, and metastatic behaviors in pancreatic cancer by regulating the PI3K/Akt signaling pathway. *Cell Death Dis* 2019, **10**(3)**:** 230.

121. Barnes JM, Przybyla L, Weaver VM. Tissue mechanics regulate brain development, homeostasis and disease. *J Cell Sci* 2017, **130**(1)**:** 71-82.

122. Steeg PS, Camphausen KA, Smith QR. Brain metastases as preventive and therapeutic targets. *Nat Rev Cancer* 2011, **11**(5)**:** 352-363.

123. Barros CS, Franco SJ, Muller U. Extracellular matrix: functions in the nervous system. *Cold Spring Harb Perspect Biol* 2011, **3**(1)**:** a005108.

124. Correction: Extracellular Matrix Receptor Expression in Subtypes of Lung Adenocarcinoma Potentiates Outgrowth of Micrometastases. *Cancer Res* 2018, **78**(3)**:** 840.

125. Helmlinger G, Netti PA, Lichtenbeld HC, Melder RJ, Jain RK. Solid stress inhibits the growth of multicellular tumor spheroids. *Nat Biotechnol* 1997, **15**(8)**:** 778-783.

126. Griffon-Etienne G, Boucher Y, Brekken C, Suit HD, Jain RK. Taxane-induced apoptosis decompresses blood vessels and lowers interstitial fluid pressure in solid tumors: clinical implications. *Cancer Res* 1999, **59**(15)**:** 3776-3782.

127. Jain RK. Antiangiogenesis strategies revisited: from starving tumors to alleviating hypoxia. *Cancer Cell* 2014, **26**(5)**:** 605-622.

128. Munn LL, Jain RK. Vascular regulation of antitumor immunity. *Science* 2019, **365**(6453)**:** 544-545.

129. Padera TP, Stoll BR, Tooredman JB, Capen D, di Tomaso E, Jain RK. Pathology: cancer cells compress intratumour vessels. *Nature* 2004, **427**(6976)**:** 695.

130. Stylianopoulos T, Martin JD, Chauhan VP, Jain SR, Diop-Frimpong B, Bardeesy N*, et al.* Causes, consequences, and remedies for growth-induced solid stress in murine and human tumors. *Proc Natl Acad Sci U S A* 2012, **109**(38)**:** 15101-15108.

131. Tse JM, Cheng G, Tyrrell JA, Wilcox-Adelman SA, Boucher Y, Jain RK*, et al.* Mechanical compression drives cancer cells toward invasive phenotype. *Proc Natl Acad Sci U S A* 2012, **109**(3)**:** 911-916.

132. Fernandez-Sanchez ME, Barbier S, Whitehead J, Bealle G, Michel A, Latorre-Ossa H*, et al.* Mechanical induction of the tumorigenic beta-catenin pathway by tumour growth pressure. *Nature* 2015, **523**(7558)**:** 92-95.

133. Swartz MA, Lund AW. Lymphatic and interstitial flow in the tumour microenvironment: linking mechanobiology with immunity. *Nat Rev Cancer* 2012, **12**(3)**:** 210-219.

134. Polacheck WJ, Charest JL, Kamm RD. Interstitial flow influences direction of tumor cell migration through competing mechanisms. *Proc Natl Acad Sci U S A* 2011, **108**(27)**:** 11115-11120.

135. Qazi H, Palomino R, Shi ZD, Munn LL, Tarbell JM. Cancer cell glycocalyx mediates mechanotransduction and flow-regulated invasion. *Integr Biol (Camb)* 2013, **5**(11)**:** 1334-1343.

136. Qazi H, Shi ZD, Tarbell JM. Fluid shear stress regulates the invasive potential of glioma cells via modulation of migratory activity and matrix metalloproteinase expression. *PLoS One* 2011, **6**(5)**:** e20348.

137. Mitchell MJ, Denais C, Chan MF, Wang Z, Lammerding J, King MR. Lamin A/C deficiency reduces circulating tumor cell resistance to fluid shear stress. *Am J Physiol Cell Physiol* 2015, **309**(11)**:** C736-746.

138. Fan R, Emery T, Zhang Y, Xia Y, Sun J, Wan J. Circulatory shear flow alters the viability and proliferation of circulating colon cancer cells. *Sci Rep* 2016, **6:** 27073.

139. Avvisato CL, Yang X, Shah S, Hoxter B, Li W, Gaynor R*, et al.* Mechanical force modulates global gene expression and beta-catenin signaling in colon cancer cells. *J Cell Sci* 2007, **120**(Pt 15)**:** 2672-2682.

140. Regmi S, Fu A, Luo KQ. High Shear Stresses under Exercise Condition Destroy Circulating Tumor Cells in a Microfluidic System. *Sci Rep* 2017, **7:** 39975.

141. Xiong N, Li S, Tang K, Bai H, Peng Y, Yang H*, et al.* Involvement of caveolin-1 in low shear stress-induced breast cancer cell motility and adhesion: Roles of FAK/Src and ROCK/p-

MLC pathways. *Biochim Biophys Acta Mol Cell Res* 2017, **1864**(1)**:** 12-22.

142. Cochlin DL, Ganatra RH, Griffiths DF. Elastography in the detection of prostatic cancer. *Clin Radiol* 2002, **57**(11)**:** 1014-1020.

143. Boyd NF, Li Q, Melnichouk O, Huszti E, Martin LJ, Gunasekara A*, et al.* Evidence that breast tissue stiffness is associated with risk of breast cancer. *PLoS One* 2014, **9**(7)**:** e100937.

144. Maskarinec G, Pagano IS, Little MA, Conroy SM, Park SY, Kolonel LN. Mammographic density as a predictor of breast cancer survival: the Multiethnic Cohort. *Breast Cancer Res* 2013, **15**(1)**:** R7.

145. Carrara S, Di Leo M, Grizzi F, Correale L, Rahal D, Anderloni A*, et al.* EUS elastography (strain ratio) and fractal-based quantitative analysis for the diagnosis of solid pancreatic lesions. *Gastrointest Endosc* 2018, **87**(6)**:** 1464-1473.

146. Shahryari M, Tzschatzsch H, Guo J, Marticorena Garcia SR, Boning G, Fehrenbach U*, et al.* Tomoelastography Distinguishes Noninvasively between Benign and Malignant Liver Lesions. *Cancer Res* 2019, **79**(22)**:** 5704-5710.

147. Rouviere O, Melodelima C, Hoang Dinh A, Bratan F, Pagnoux G, Sanzalone T*, et al.* Stiffness of benign and malignant prostate tissue measured by shear-wave elastography: a preliminary study. *Eur Radiol* 2017, **27**(5)**:** 1858-1866.

148. Sahai E, Astsaturov I, Cukierman E, DeNardo DG, Egeblad M, Evans RM*, et al.* A framework for advancing our understanding of cancer-associated fibroblasts. *Nat Rev Cancer* 2020, **20**(3)**:** 174-186.

149. Ohlund D, Elyada E, Tuveson D. Fibroblast heterogeneity in the cancer wound. *J Exp Med* 2014, **211**(8)**:** 1503-1523.

150. Pang MF, Siedlik MJ, Han S, Stallings-Mann M, Radisky DC, Nelson CM. Tissue Stiffness and Hypoxia Modulate the Integrin-Linked Kinase ILK to Control Breast Cancer Stem-like Cells. *Cancer Res* 2016, **76**(18)**:** 5277-5287.

151. Ulrich TA, de Juan Pardo EM, Kumar S. The mechanical rigidity of the extracellular matrix regulates the structure, motility, and proliferation of glioma cells. *Cancer Res* 2009, **69**(10)**:** 4167-4174.

152. Bordeleau F, Mason BN, Lollis EM, Mazzola M, Zanotelli MR, Somasegar S*, et al.* Matrix stiffening promotes a tumor vasculature phenotype. *Proc Natl Acad Sci U S A* 2017, **114**(3)**:** 492-497.

153. Tung JC, Barnes JM, Desai SR, Sistrunk C, Conklin MW, Schedin P*, et al.* Tumor mechanics

and metabolic dysfunction. *Free Radic Biol Med* 2015, **79:** 269-280.

154. Lang NR, Skodzek K, Hurst S, Mainka A, Steinwachs J, Schneider J*, et al.* Biphasic response of cell invasion to matrix stiffness in three-dimensional biopolymer networks. *Acta Biomater* 2015, **13:** 61-67.

155. Levental KR, Yu H, Kass L, Lakins JN, Egeblad M, Erler JT*, et al.* Matrix crosslinking forces tumor progression by enhancing integrin signaling. *Cell* 2009, **139**(5)**:** 891-906.

156. Paszek MJ, Zahir N, Johnson KR, Lakins JN, Rozenberg GI, Gefen A*, et al.* Tensional homeostasis and the malignant phenotype. *Cancer Cell* 2005, **8**(3)**:** 241-254.

157. Miller BW, Morton JP, Pinese M, Saturno G, Jamieson NB, McGhee E*, et al.* Targeting the LOX/hypoxia axis reverses many of the features that make pancreatic cancer deadly: inhibition of LOX abrogates metastasis and enhances drug efficacy. *EMBO Mol Med* 2015, **7**(8)**:** 1063-1076.

158. Alvarez R, Musteanu M, Garcia-Garcia E, Lopez-Casas PP, Megias D, Guerra C*, et al.* Stromal disrupting effects of nab-paclitaxel in pancreatic cancer. *Br J Cancer* 2013, **109**(4)**:** 926-933.

159. Miroshnikova YA, Mouw JK, Barnes JM, Pickup MW, Lakins JN, Kim Y*, et al.* Tissue mechanics promote IDH1-dependent HIF1alpha-tenascin C feedback to regulate glioblastoma aggression. *Nat Cell Biol* 2016, **18**(12)**:** 1336-1345.

160. Chaudhuri O, Koshy ST, Branco da Cunha C, Shin JW, Verbeke CS, Allison KH*, et al.* Extracellular matrix stiffness and composition jointly regulate the induction of malignant phenotypes in mammary epithelium. *Nat Mater* 2014, **13**(10)**:** 970-978.

161. Chowdhury F, Huang B, Wang N. Forces in stem cells and cancer stem cells. *Cells Dev* 2022, **170:** 203776.

162. Liu J, Tan Y, Zhang H, Zhang Y, Xu P, Chen J*, et al.* Soft fibrin gels promote selection and growth of tumorigenic cells. *Nat Mater* 2012, **11**(8)**:** 734-741.

163. Tang X, Kuhlenschmidt TB, Li Q, Ali S, Lezmi S, Chen H*, et al.* A mechanically-induced colon cancer cell population shows increased metastatic potential. *Mol Cancer* 2014, **13:** 131.

164. Liu Y, Lv J, Liang X, Yin X, Zhang L, Chen D*, et al.* Fibrin Stiffness Mediates Dormancy of Tumor-Repopulating Cells via a Cdc42-Driven Tet2 Epigenetic Program. *Cancer Res* 2018, **78**(14)**:** 3926-3937.

165. Barney LE, Hall CL, Schwartz AD, Parks AN, Sparages C, Galarza S*, et al.* Tumor cell-

organized fibronectin maintenance of a dormant breast cancer population. *Sci Adv* 2020, **6**(11)**:** eaaz4157.

166. Di Martino JS, Nobre AR, Mondal C, Taha I, Farias EF, Fertig EJ*, et al.* A tumor-derived type III collagen-rich ECM niche regulates tumor cell dormancy. *Nat Cancer* 2022, **3**(1)**:** 90-107.

167. Chen J, Wang N. Tissue cell differentiation and multicellular evolution via cytoskeletal stiffening in mechanically stressed microenvironments. *Acta Mech Sin* 2019, **35**(2)**:** 270-274.

168. Vashisth M, Cho S, Irianto J, Xia Y, Wang M, Hayes B*, et al.* Scaling concepts in 'omics: Nuclear lamin-B scales with tumor growth and often predicts poor prognosis, unlike fibrosis. *Proc Natl Acad Sci U S A* 2021, **118**(48).

169. Jiang H, Torphy RJ, Steiger K, Hongo H, Ritchie AJ, Kriegsmann M*, et al.* Pancreatic ductal adenocarcinoma progression is restrained by stromal matrix. *J Clin Invest* 2020, **130**(9)**:** 4704-4709.

170. Acerbi I, Cassereau L, Dean I, Shi Q, Au A, Park C*, et al.* Human breast cancer invasion and aggression correlates with ECM stiffening and immune cell infiltration. *Integr Biol (Camb)* 2015, **7**(10)**:** 1120-1134.

171. Fiore VF, Krajnc M, Quiroz FG, Levorse J, Pasolli HA, Shvartsman SY*, et al.* Mechanics of a multilayer epithelium instruct tumour architecture and function. *Nature* 2020, **585**(7825)**:** 433-439.

172. Shellard A, Mayor R. Collective durotaxis along a self-generated stiffness gradient in vivo. *Nature* 2021, **600**(7890)**:** 690-694.

173. Cross SE, Jin YS, Rao J, Gimzewski JK. Nanomechanical analysis of cells from cancer patients. *Nat Nanotechnol* 2007, **2**(12)**:** 780-783.

174. Katira P, Bonnecaze RT, Zaman MH. Modeling the mechanics of cancer: effect of changes in cellular and extra-cellular mechanical properties. *Front Oncol* 2013, **3:** 145.

175. Chen X, Fan Y, Sun J, Zhang Z, Xin Y, Li K*, et al.* Nanoparticle-mediated specific elimination of soft cancer stem cells by targeting low cell stiffness. *Acta Biomater* 2021, **135:** 493-505.

176. Liu Y, Zhang T, Zhang H, Li J, Zhou N, Fiskesund R*, et al.* Cell Softness Prevents Cytolytic T-cell Killing of Tumor-Repopulating Cells. *Cancer Res* 2021, **81**(2)**:** 476-488.

177. Lei K, Kurum A, Kaynak M, Bonati L, Han Y, Cencen V*, et al.* Cancer-cell stiffening via cholesterol depletion enhances adoptive T-cell immunotherapy. *Nat Biomed Eng* 2021, **5**(12)**:** 1411-1425.

178. Sosale NG, Rouhiparkouhi T, Bradshaw AM, Dimova R, Lipowsky R, Discher DE. Cell rigidity and shape override CD47's "self"-signaling in phagocytosis by hyperactivating myosin-II. *Blood* 2015, **125**(3)**:** 542-552.

179. Tello-Lafoz M, Srpan K, Sanchez EE, Hu J, Remsik J, Romin Y*, et al.* Cytotoxic lymphocytes target characteristic biophysical vulnerabilities in cancer. *Immunity* 2021, **54**(5)**:** 1037-1054 e1037.

180. Delattre JY, Krol G, Thaler HT, Posner JB. Distribution of brain metastases. *Arch Neurol* 1988, **45**(7)**:** 741-744.

181. Linninger AA, Tsakiris C, Zhu DC, Xenos M, Roycewicz P, Danziger Z*, et al.* Pulsatile cerebrospinal fluid dynamics in the human brain. *IEEE Trans Biomed Eng* 2005, **52**(4)**:** 557-565.

182. Franze K. The mechanical control of nervous system development. *Development* 2013, **140**(15)**:** 3069-3077.

183. Momin A, Bahrampour S, Min HK, Chen X, Wang X, Sun Y*, et al.* Channeling Force in the Brain: Mechanosensitive Ion Channels Choreograph Mechanics and Malignancies. *Trends Pharmacol Sci* 2021, **42**(5)**:** 367-384.

184. Athamneh AI, Suter DM. Quantifying mechanical force in axonal growth and guidance. *Front Cell Neurosci* 2015, **9:** 359.

185. Leipzig ND, Shoichet MS. The effect of substrate stiffness on adult neural stem cell behavior. *Biomaterials* 2009, **30**(36)**:** 6867-6878.

186. Segel M, Neumann B, Hill MFE, Weber IP, Viscomi C, Zhao C*, et al.* Niche stiffness underlies the ageing of central nervous system progenitor cells. *Nature* 2019, **573**(7772)**:** 130-134.

187. Kim Y, Kumar S. CD44-mediated adhesion to hyaluronic acid contributes to mechanosensing and invasive motility. *Mol Cancer Res* 2014, **12**(10)**:** 1416-1429.

188. Umesh V, Rape AD, Ulrich TA, Kumar S. Microenvironmental stiffness enhances glioma cell proliferation by stimulating epidermal growth factor receptor signaling. *PLoS One* 2014, **9**(7)**:** e101771.

189. Wagh K, Ishikawa M, Garcia DA, Stavreva DA, Upadhyaya A, Hager GL. Mechanical Regulation of Transcription: Recent Advances. *Trends Cell Biol* 2021, **31**(6)**:** 457-472.

190. Przybyla L, Muncie JM, Weaver VM. Mechanical Control of Epithelial-to-Mesenchymal Transitions in Development and Cancer. *Annu Rev Cell Dev Biol* 2016, **32:** 527-554.

191. Matthews BD, Overby DR, Mannix R, Ingber DE. Cellular adaptation to mechanical stress: role of integrins, Rho, cytoskeletal tension and mechanosensitive ion channels. *J Cell Sci* 2006, **119**(Pt 3)**:** 508-518.

192. Kirby TJ, Lammerding J. Emerging views of the nucleus as a cellular mechanosensor. *Nat Cell Biol* 2018, **20**(4)**:** 373-381.

193. Iyer KV, Pulford S, Mogilner A, Shivashankar GV. Mechanical activation of cells induces chromatin remodeling preceding MKL nuclear transport. *Biophys J* 2012, **103**(7)**:** 1416-1428.

194. Tajik A, Zhang Y, Wei F, Sun J, Jia Q, Zhou W*, et al.* Transcription upregulation via force-induced direct stretching of chromatin. *Nat Mater* 2016, **15**(12)**:** 1287-1296.

195. Killaars AR, Walker CJ, Anseth KS. Nuclear mechanosensing controls MSC osteogenic potential through HDAC epigenetic remodeling. *Proc Natl Acad Sci U S A* 2020, **117**(35)**:** 21258-21266.

196. Dupont S, Morsut L, Aragona M, Enzo E, Giulitti S, Cordenonsi M*, et al.* Role of YAP/TAZ in mechanotransduction. *Nature* 2011, **474**(7350)**:** 179-183.

197. Caille N, Thoumine O, Tardy Y, Meister JJ. Contribution of the nucleus to the mechanical properties of endothelial cells. *J Biomech* 2002, **35**(2)**:** 177-187.

198. Lammerding J. Mechanics of the nucleus. *Compr Physiol* 2011, **1**(2)**:** 783-807.

199. Dreger M, Bengtsson L, Schoneberg T, Otto H, Hucho F. Nuclear envelope proteomics: novel integral membrane proteins of the inner nuclear membrane. *Proc Natl Acad Sci U S A* 2001, **98**(21)**:** 11943-11948.

200. Jovanovic-Talisman T, Zilman A. Protein Transport by the Nuclear Pore Complex: Simple Biophysics of a Complex Biomachine. *Biophys J* 2017, **113**(1)**:** 6-14.

201. Lombardi ML, Jaalouk DE, Shanahan CM, Burke B, Roux KJ, Lammerding J. The interaction between nesprins and sun proteins at the nuclear envelope is critical for force transmission between the nucleus and cytoskeleton. *J Biol Chem* 2011, **286**(30)**:** 26743-26753.

202. Crisp M, Liu Q, Roux K, Rattner JB, Shanahan C, Burke B*, et al.* Coupling of the nucleus and cytoplasm: role of the LINC complex. *J Cell Biol* 2006, **172**(1)**:** 41-53.

203. Tapley EC, Starr DA. Connecting the nucleus to the cytoskeleton by SUN-KASH bridges across the nuclear envelope. *Curr Opin Cell Biol* 2013, **25**(1)**:** 57-62.

204. Horn HF. LINC complex proteins in development and disease. *Curr Top Dev Biol* 2014, **109:** 287-321.

205. Rothballer A, Kutay U. The diverse functional LINCs of the nuclear envelope to the cytoskeleton and chromatin. *Chromosoma* 2013, **122**(5)**:** 415-429.

206. Banerjee I, Zhang J, Moore-Morris T, Pfeiffer E, Buchholz KS, Liu A*, et al.* Targeted ablation of nesprin 1 and nesprin 2 from murine myocardium results in cardiomyopathy, altered nuclear morphology and inhibition of the biomechanical gene response. *PLoS Genet* 2014, **10**(2)**:** e1004114.

207. Isermann P, Lammerding J. Nuclear mechanics and mechanotransduction in health and disease. *Curr Biol* 2013, **23**(24)**:** R1113-1121.

208. Ihalainen TO, Aires L, Herzog FA, Schwartlander R, Moeller J, Vogel V. Differential basal-to-apical accessibility of lamin A/C epitopes in the nuclear lamina regulated by changes in cytoskeletal tension. *Nat Mater* 2015, **14**(12)**:** 1252-1261.

209. Swift J, Ivanovska IL, Buxboim A, Harada T, Dingal PC, Pinter J*, et al.* Nuclear lamin-A scales with tissue stiffness and enhances matrix-directed differentiation. *Science* 2013, **341**(6149)**:** 1240104.

210. Guilluy C, Osborne LD, Van Landeghem L, Sharek L, Superfine R, Garcia-Mata R*, et al.* Isolated nuclei adapt to force and reveal a mechanotransduction pathway in the nucleus. *Nat Cell Biol* 2014, **16**(4)**:** 376-381.

211. Enyedi B, Niethammer P. Nuclear membrane stretch and its role in mechanotransduction. *Nucleus* 2017, **8**(2)**:** 156-161.

212. Elosegui-Artola A, Andreu I, Beedle AEM, Lezamiz A, Uroz M, Kosmalska AJ*, et al.* Force Triggers YAP Nuclear Entry by Regulating Transport across Nuclear Pores. *Cell* 2017, **171**(6)**:** 1397-1410 e1314.

213. Enyedi B, Jelcic M, Niethammer P. The Cell Nucleus Serves as a Mechanotransducer of Tissue Damage-Induced Inflammation. *Cell* 2016, **165**(5)**:** 1160-1170.

214. Li Y, Chu JS, Kurpinski K, Li X, Bautista DM, Yang L*, et al.* Biophysical regulation of histone acetylation in mesenchymal stem cells. *Biophys J* 2011, **100**(8)**:** 1902-1909.

215. Le HQ, Ghatak S, Yeung CY, Tellkamp F, Gunschmann C, Dieterich C*, et al.* Mechanical regulation of transcription controls Polycomb-mediated gene silencing during lineage commitment. *Nat Cell Biol* 2016, **18**(8)**:** 864-875.

216. Jain N, Iyer KV, Kumar A, Shivashankar GV. Cell geometric constraints induce modular

gene-expression patterns via redistribution of HDAC3 regulated by actomyosin contractility. *Proc Natl Acad Sci U S A* 2013, **110**(28)**:** 11349-11354.

217. Heo SJ, Han WM, Szczesny SE, Cosgrove BD, Elliott DM, Lee DA*, et al.* Mechanically Induced Chromatin Condensation Requires Cellular Contractility in Mesenchymal Stem Cells. *Biophys J* 2016, **111**(4)**:** 864-874.

218. Maurer M, Lammerding J. The Driving Force: Nuclear Mechanotransduction in Cellular Function, Fate, and Disease. *Annu Rev Biomed Eng* 2019, **21:** 443-468.

219. Li M, Liu GH, Izpisua Belmonte JC. Navigating the epigenetic landscape of pluripotent stem cells. *Nat Rev Mol Cell Biol* 2012, **13**(8)**:** 524-535.

220. Uhler C, Shivashankar GV. Regulation of genome organization and gene expression by nuclear mechanotransduction. *Nat Rev Mol Cell Biol* 2017, **18**(12)**:** 717-727.

221. Hadden WJ, Young JL, Holle AW, McFetridge ML, Kim DY, Wijesinghe P*, et al.* Stem cell migration and mechanotransduction on linear stiffness gradient hydrogels. *Proc Natl Acad Sci U S A* 2017, **114**(22)**:** 5647-5652.

222. Downing TL, Soto J, Morez C, Houssin T, Fritz A, Yuan F*, et al.* Biophysical regulation of epigenetic state and cell reprogramming. *Nat Mater* 2013, **12**(12)**:** 1154-1162.

223. Killaars AR, Grim JC, Walker CJ, Hushka EA, Brown TE, Anseth KS. Extended Exposure to Stiff Microenvironments Leads to Persistent Chromatin Remodeling in Human Mesenchymal Stem Cells. *Adv Sci (Weinh)* 2019, **6**(3)**:** 1801483.

224. Boros J, Arnoult N, Stroobant V, Collet JF, Decottignies A. Polycomb repressive complex 2 and H3K27me3 cooperate with H3K9 methylation to maintain heterochromatin protein 1alpha at chromatin. *Mol Cell Biol* 2014, **34**(19)**:** 3662-3674.

225. Nava MM, Miroshnikova YA, Biggs LC, Whitefield DB, Metge F, Boucas J*, et al.* Heterochromatin-Driven Nuclear Softening Protects the Genome against Mechanical Stress-Induced Damage. *Cell* 2020, **181**(4)**:** 800-817 e822.

226. Wang Y, Nagarajan M, Uhler C, Shivashankar GV. Orientation and repositioning of chromosomes correlate with cell geometry-dependent gene expression. *Mol Biol Cell* 2017, **28**(14)**:** 1997-2009.

227. Makhija E, Jokhun DS, Shivashankar GV. Nuclear deformability and telomere dynamics are regulated by cell geometric constraints. *Proc Natl Acad Sci U S A* 2016, **113**(1)**:** E32-40.

228. Alisafaei F, Jokhun DS, Shivashankar GV, Shenoy VB. Regulation of nuclear architecture, mechanics, and nucleocytoplasmic shuttling of epigenetic factors by cell geometric

constraints. *Proc Natl Acad Sci U S A* 2019, **116**(27)**:** 13200-13209.

229. Roy B, Venkatachalapathy S, Ratna P, Wang Y, Jokhun DS, Nagarajan M*, et al.* Laterally confined growth of cells induces nuclear reprogramming in the absence of exogenous biochemical factors. *Proc Natl Acad Sci U S A* 2018, **115**(21)**:** E4741-E4750.

230. Tse JR, Engler AJ. Preparation of hydrogel substrates with tunable mechanical properties. *Curr Protoc Cell Biol* 2010, **Chapter 10:** Unit 10 16.

231. Rotsch C, Jacobson K, Radmacher M. Dimensional and mechanical dynamics of active and stable edges in motile fibroblasts investigated by using atomic force microscopy. *Proc Natl Acad Sci U S A* 1999, **96**(3)**:** 921-926.

232. Jin J, Tang K, Xin Y, Zhang T, Tan Y. Hemodynamic shear flow regulates biophysical characteristics and functions of circulating breast tumor cells reminiscent of brain metastasis. *Soft Matter* 2018, **14**(47)**:** 9528-9533.

233. Irianto J, Lee DA, Knight MM. Quantification of chromatin condensation level by image processing. *Med Eng Phys* 2014, **36**(3)**:** 412-417.

234. Damodaran K, Venkatachalapathy S, Alisafaei F, Radhakrishnan AV, Sharma Jokhun D, Shenoy VB*, et al.* Compressive force induces reversible chromatin condensation and cell geometry-dependent transcriptional response. *Mol Biol Cell* 2018, **29**(25)**:** 3039-3051.

235. Nguyen DX, Bos PD, Massague J. Metastasis: from dissemination to organ-specific colonization. *Nat Rev Cancer* 2009, **9**(4)**:** 274-284.

236. Weilbaecher KN, Guise TA, McCauley LK. Cancer to bone: a fatal attraction. *Nat Rev Cancer* 2011, **11**(6)**:** 411-425.

237. Achrol AS, Rennert RC, Anders C, Soffietti R, Ahluwalia MS, Nayak L*, et al.* Brain metastases. *Nat Rev Dis Primers* 2019, **5**(1)**:** 5.

238. Chen MT, Sun HF, Zhao Y, Fu WY, Yang LP, Gao SP*, et al.* Comparison of patterns and prognosis among distant metastatic breast cancer patients by age groups: a SEER population-based analysis. *Sci Rep* 2017, **7**(1)**:** 9254.

239. Klein-Goldberg A, Maman S, Witz IP. The role played by the microenvironment in site-specific metastasis. *Cancer Lett* 2014, **352**(1)**:** 54-58.

240. Panciera T, Citron A, Di Biagio D, Battilana G, Gandin A, Giulitti S*, et al.* Reprogramming normal cells into tumour precursors requires ECM stiffness and oncogene-mediated changes of cell mechanical properties. *Nat Mater* 2020, **19**(7)**:** 797-806.

241. Fenner J, Stacer AC, Winterroth F, Johnson TD, Luker KE, Luker GD. Macroscopic stiffness of breast tumors predicts metastasis. *Sci Rep* 2014, **4:** 5512.

242. McGrail DJ, Kieu QM, Dawson MR. The malignancy of metastatic ovarian cancer cells is increased on soft matrices through a mechanosensitive Rho-ROCK pathway. *J Cell Sci* 2014, **127**(Pt 12)**:** 2621-2626.

243. Page JM, Merkel AR, Ruppender NS, Guo R, Dadwal UC, Cannonier S*, et al.* Matrix rigidity regulates the transition of tumor cells to a bone-destructive phenotype through integrin beta3 and TGF-beta receptor type II. *Biomaterials* 2015, **64:** 33-44.

244. Watson AW, Grant AD, Parker SS, Hill S, Whalen MB, Chakrabarti J*, et al.* Breast tumor stiffness instructs bone metastasis via maintenance of mechanical conditioning. *Cell Rep* 2021, **35**(13)**:** 109293.

245. Kostic A, Lynch CD, Sheetz MP. Differential matrix rigidity response in breast cancer cell lines correlates with the tissue tropism. *PLoS One* 2009, **4**(7)**:** e6361.

246. Kondapaneni RV, Rao SS. Matrix stiffness and cluster size collectively regulate dormancy versus proliferation in brain metastatic breast cancer cell clusters. *Biomater Sci* 2020, **8**(23)**:** 6637-6646.

247. Drain AP, Zahir N, Northey JJ, Zhang H, Huang PJ, Maller O*, et al.* Matrix compliance permits NF-kappaB activation to drive therapy resistance in breast cancer. *J Exp Med* 2021, **218**(5).

248. Li CX, Talele NP, Boo S, Koehler A, Knee-Walden E, Balestrini JL*, et al.* MicroRNA-21 preserves the fibrotic mechanical memory of mesenchymal stem cells. *Nat Mater* 2017, **16**(3)**:** 379-389.

249. Pardo-Pastor C, Rubio-Moscardo F, Vogel-Gonzalez M, Serra SA, Afthinos A, Mrkonjic S*, et al.* Piezo2 channel regulates RhoA and actin cytoskeleton to promote cell mechanobiological responses. *Proc Natl Acad Sci U S A* 2018, **115**(8)**:** 1925-1930.

250. Wingrove E, Liu ZZ, Patel KD, Arnal-Estape A, Cai WL, Melnick MA*, et al.* Transcriptomic Hallmarks of Tumor Plasticity and Stromal Interactions in Brain Metastasis. *Cell Rep* 2019, **27**(4)**:** 1277-1292 e1277.

251. Klemm F, Mockl A, Salamero-Boix A, Alekseeva T, Schaffer A, Schulz M*, et al.* Compensatory CSF2-driven macrophage activation promotes adaptive resistance to CSF1R inhibition in breast-to-brain metastasis. *Nat Cancer* 2021, **2**(10)**:** 1086-1101.

252. Huang Q, Hu X, He W, Zhao Y, Hao S, Wu Q*, et al.* Fluid shear stress and tumor metastasis. *Am J Cancer Res* 2018, **8**(5)**:** 763-777.

253. Wu K, Fukuda K, Xing F, Zhang Y, Sharma S, Liu Y*, et al.* Roles of the cyclooxygenase 2 matrix metalloproteinase 1 pathway in brain metastasis of breast cancer. *J Biol Chem* 2015, **290**(15)**:** 9842-9854.

254. Tanner K. Perspective: The role of mechanobiology in the etiology of brain metastasis. *APL Bioeng* 2018, **2**(3)**:** 031801.

255. Mogilner A, Keren K. The shape of motile cells. *Curr Biol* 2009, **19**(17)**:** R762-771.

256. Chen CS, Mrksich M, Huang S, Whitesides GM, Ingber DE. Geometric control of cell life and death. *Science* 1997, **276**(5317)**:** 1425-1428.

257. Berens EB, Holy JM, Riegel AT, Wellstein A. A Cancer Cell Spheroid Assay to Assess Invasion in a 3D Setting. *J Vis Exp* 2015(105).

258. Toole BP. Hyaluronan: from extracellular glue to pericellular cue. *Nat Rev Cancer* 2004, **4**(7)**:** 528-539.

259. Kienast Y, von Baumgarten L, Fuhrmann M, Klinkert WE, Goldbrunner R, Herms J*, et al.* Real-time imaging reveals the single steps of brain metastasis formation. *Nat Med* 2010, **16**(1)**:** 116-122.

260. Chowdhury F, Huang B, Wang N. Cytoskeletal prestress: The cellular hallmark in mechanobiology and mechanomedicine. *Cytoskeleton (Hoboken)* 2021, **78**(6)**:** 249-276.

261. Kampourakis T, Sun YB, Irving M. Myosin light chain phosphorylation enhances contraction of heart muscle via structural changes in both thick and thin filaments. *Proc Natl Acad Sci U S A* 2016, **113**(21)**:** E3039-3047.

262. Hairapetian L, Cortes E, Zhao J, Wang Y, Huang R, Damoiseaux R*, et al.* Simplified, High-throughput Analysis of Single-cell Contractility using Micropatterned Elastomers. *J Vis Exp* 2022(182).

263. Zeng Q, Michael IP, Zhang P, Saghafinia S, Knott G, Jiao W*, et al.* Synaptic proximity enables NMDAR signalling to promote brain metastasis. *Nature* 2019, **573**(7775)**:** 526-531.

264. Teng S, Li YE, Yang M, Qi R, Huang Y, Wang Q*, et al.* Tissue-specific transcription reprogramming promotes liver metastasis of colorectal cancer. *Cell Res* 2020, **30**(1)**:** 34-49.

265. Ruppender NS, Merkel AR, Martin TJ, Mundy GR, Sterling JA, Guelcher SA. Matrix rigidity induces osteolytic gene expression of metastatic breast cancer cells. *PLoS One* 2010, **5**(11)**:**

e15451.

266. Minn AJ, Kang Y, Serganova I, Gupta GP, Giri DD, Doubrovin M, *et al.* Distinct organ-specific metastatic potential of individual breast cancer cells and primary tumors. *J Clin Invest* 2005, **115**(1)**:** 44-55.

267. Zhang W, Bado IL, Hu J, Wan YW, Wu L, Wang H, *et al.* The bone microenvironment invigorates metastatic seeds for further dissemination. *Cell* 2021, **184**(9)**:** 2471-2486 e2420.

268. Rabineau M, Flick F, Mathieu E, Tu A, Senger B, Voegel JC, *et al.* Cell guidance into quiescent state through chromatin remodeling induced by elastic modulus of substrate. *Biomaterials* 2015, **37:** 144-155.

269. Stowers RS, Shcherbina A, Israeli J, Gruber JJ, Chang J, Nam S, *et al.* Matrix stiffness induces a tumorigenic phenotype in mammary epithelium through changes in chromatin accessibility. *Nat Biomed Eng* 2019, **3**(12)**:** 1009-1019.

270. Ng KY, Shea QT, Wong TL, Luk ST, Tong M, Lo CM, *et al.* Chemotherapy-Enriched THBS2-Deficient Cancer Stem Cells Drive Hepatocarcinogenesis through Matrix Softness Induced Histone H3 Modifications. *Adv Sci (Weinh)* 2021, **8**(5)**:** 2002483.

271. Tan Y, Tajik A, Chen J, Jia Q, Chowdhury F, Wang L, *et al.* Matrix softness regulates plasticity of tumour-repopulating cells via H3K9 demethylation and Sox2 expression. *Nat Commun* 2014, **5:** 4619.

272. Ma L, Qi L, Li S, Yin Q, Liu J, Wang J, *et al.* Aberrant HDAC3 expression correlates with brain metastasis in breast cancer patients. *Thorac Cancer* 2020, **11**(9)**:** 2493-2505.

273. Palmieri D, Lockman PR, Thomas FC, Hua E, Herring J, Hargrave E, *et al.* Vorinostat inhibits brain metastatic colonization in a model of triple-negative breast cancer and induces DNA double-strand breaks. *Clin Cancer Res* 2009, **15**(19)**:** 6148-6157.

274. Vogelstein B, Papadopoulos N, Velculescu VE, Zhou S, Diaz LA, Jr., Kinzler KW. Cancer genome landscapes. *Science* 2013, **339**(6127)**:** 1546-1558.

275. Hsia CR, McAllister J, Hasan O, Judd J, Lee S, Agrawal R, *et al.* Confined migration induces heterochromatin formation and alters chromatin accessibility. *iScience* 2022, **25**(9)**:** 104978.

276. Stengel KR, Hiebert SW. Class I HDACs Affect DNA Replication, Repair, and Chromatin Structure: Implications for Cancer Therapy. *Antioxid Redox Signal* 2015, **23**(1)**:** 51-65.

277. Zhang MJ, Zhao QC, Xia MX, Chen J, Chen YT, Cao X, *et al.* The HDAC3 inhibitor RGFP966

ameliorated ischemic brain damage by downregulating the AIM2 inflammasome. *FASEB J* 2020, **34**(1)**:** 648-662.

278. Purkayastha P, Pendyala K, Saxena AS, Hakimjavadi H, Chamala S, Baer CF*, et al.* Natural selection imposed by mechanical properties of a biomaterial results in novel cellular phenotypes. 2020**:** 2020.2004.2026.061911.

279. Heo SJ, Thorpe SD, Driscoll TP, Duncan RL, Lee DA, Mauck RL. Biophysical Regulation of Chromatin Architecture Instills a Mechanical Memory in Mesenchymal Stem Cells. *Sci Rep* 2015, **5:** 16895.

280. Molstad DHH, Mattson AM, Begun DL, Westendorf JJ, Bradley EW. Hdac3 regulates bone modeling by suppressing osteoclast responsiveness to RANKL. *J Biol Chem* 2020, **295**(51)**:** 17713-17723.

281. Pratap J, Lian JB, Javed A, Barnes GL, van Wijnen AJ, Stein JL*, et al.* Regulatory roles of Runx2 in metastatic tumor and cancer cell interactions with bone. *Cancer Metastasis Rev* 2006, **25**(4)**:** 589-600.

282. Schroeder TM, Kahler RA, Li X, Westendorf JJ. Histone deacetylase 3 interacts with runx2 to repress the osteocalcin promoter and regulate osteoblast differentiation. *J Biol Chem* 2004, **279**(40)**:** 41998-42007.

283. Lamour V, Detry C, Sanchez C, Henrotin Y, Castronovo V, Bellahcene A. Runx2- and histone deacetylase 3-mediated repression is relieved in differentiating human osteoblast cells to allow high bone sialoprotein expression. *J Biol Chem* 2007, **282**(50)**:** 36240-36249.

284. Chang Q, Bournazou E, Sansone P, Berishaj M, Gao SP, Daly L*, et al.* The IL-6/JAK/Stat3 feed-forward loop drives tumorigenesis and metastasis. *Neoplasia* 2013, **15**(7)**:** 848-862.

285. Pegoraro AF, Janmey P, Weitz DA. Mechanical Properties of the Cytoskeleton and Cells. *Cold Spring Harb Perspect Biol* 2017, **9**(11).

286. Blanchoin L, Boujemaa-Paterski R, Sykes C, Plastino J. Actin dynamics, architecture, and mechanics in cell motility. *Physiol Rev* 2014, **94**(1)**:** 235-263.

287. Booth AJ, Hadley R, Cornett AM, Dreffs AA, Matthes SA, Tsui JL*, et al.* Acellular normal and fibrotic human lung matrices as a culture system for in vitro investigation. *Am J Respir Crit Care Med* 2012, **186**(9)**:** 866-876.

288. Hotulainen P, Lappalainen P. Stress fibers are generated by two distinct actin assembly mechanisms in motile cells. *J Cell Biol* 2006, **173**(3)**:** 383-394.

289. Kostic A, Sheetz MP. Fibronectin rigidity response through Fyn and p130Cas recruitment

to the leading edge. *Mol Biol Cell* 2006, **17**(6)**:** 2684-2695.

290. Wei S, Siegal GP. Metastatic Organotropism: An Intrinsic Property of Breast Cancer Molecular Subtypes. *Adv Anat Pathol* 2017, **24**(2)**:** 78-81.

291. White FM, Gatenby RA, Fischbach C. The Physics of Cancer. *Cancer Res* 2019, **79**(9)**:** 2107-2110.

292. Xu W, Mezencev R, Kim B, Wang L, McDonald J, Sulchek T. Cell stiffness is a biomarker of the metastatic potential of ovarian cancer cells. *PLoS One* 2012, **7**(10)**:** e46609.

293. Nguyen AV, Nyberg KD, Scott MB, Welsh AM, Nguyen AH, Wu N*, et al.* Stiffness of pancreatic cancer cells is associated with increased invasive potential. *Integr Biol (Camb)* 2016, **8**(12)**:** 1232-1245.

294. Xin Y, Chen X, Tang X, Li K, Yang M, Tai WC*, et al.* Mechanics and Actomyosin-Dependent Survival/Chemoresistance of Suspended Tumor Cells in Shear Flow. *Biophys J* 2019, **116**(10)**:** 1803-1814.

295. Kumar S, Weaver VM. Mechanics, malignancy, and metastasis: the force journey of a tumor cell. *Cancer Metastasis Rev* 2009, **28**(1-2)**:** 113-127.

296. Shoucair I, Weber Mello F, Jabalee J, Maleki S, Garnis C. The Role of Cancer-Associated Fibroblasts and Extracellular Vesicles in Tumorigenesis. *Int J Mol Sci* 2020, **21**(18).

297. Solon J, Levental I, Sengupta K, Georges PC, Janmey PA. Fibroblast adaptation and stiffness matching to soft elastic substrates. *Biophys J* 2007, **93**(12)**:** 4453-4461.

298. Rianna C, Radmacher M. Influence of microenvironment topography and stiffness on the mechanics and motility of normal and cancer renal cells. *Nanoscale* 2017, **9**(31)**:** 11222-11230.

299. Vichare S, Sen S, Inamdar MM. Cellular mechanoadaptation to substrate mechanical properties: contributions of substrate stiffness and thickness to cell stiffness measurements using AFM. *Soft Matter* 2014, **10**(8)**:** 1174-1181.

300. Sen S, Kumar S. Cell-Matrix De-Adhesion Dynamics Reflect Contractile Mechanics. *Cell Mol Bioeng* 2009, **2**(2)**:** 218-230.

301. Guo A, Wang B, Lyu C, Li W, Wu Y, Zhu L*, et al.* Consistent apparent Young's modulus of human embryonic stem cells and derived cell types stabilized by substrate stiffness regulation promotes lineage specificity maintenance. *Cell Regen* 2020, **9**(1)**:** 15.

302. Hogrebe NJ, Augsornworawat P, Maxwell KG, Velazco-Cruz L, Millman JR. Targeting the

cytoskeleton to direct pancreatic differentiation of human pluripotent stem cells. *Nat Biotechnol* 2020, **38**(4)**:** 460-470.

303. Peng GE, Wilson SR, Weiner OD. A pharmacological cocktail for arresting actin dynamics in living cells. *Mol Biol Cell* 2011, **22**(21)**:** 3986-3994.

304. Discher DE, Janmey P, Wang YL. Tissue cells feel and respond to the stiffness of their substrate. *Science* 2005, **310**(5751)**:** 1139-1143.